Spring 5-2007

Biochemical and functional characterization of the tapasin/ERp57 conjugate

David Ryan Peaper
Yale University.

Biochemical and functional characterization of the tapasin/ERp57 conjugate

A Dissertation
Presented to the Faculty of the Graduate School
of
Yale University
in Candidacy for the Degree of
Doctor of Philosophy

By
David Ryan Peaper

Dissertation Director: Peter Cresswell

May 2007

Abstract

Biochemical and functional characterization of the tapasin/ERp57 conjugate

David Ryan Peaper

2007

Recognition of MHC class I/peptide complexes is required for the generation of CD8+ T cell responses. Peptide loading onto MHC class I/β_2m dimers occurs in the ER and involves both specific proteins and cellular chaperones. Tapasin is essential for peptide loading onto most MHC class I alleles, and it forms a mixed disulfide with the glycoprotein specific oxidoreductase ERp57. I have characterized the biochemical requirements for tapasin/ERp57 conjugate formation and addressed potential functions for ERp57 in peptide loading. Tapasin specifically recruits ERp57 into a mixed disulfide at the expense of free ERp57 in the ER. Other components of the MHC class I peptide loading complex are not required for conjugate formation, and, in contrast to models of glycoprotein folding, conjugate formation does not require the generation of monoglucosylated glycans.

Once associated, tapasin has evolved to inhibit the reductase activity of the ERp57 *a* domain leading to the retention of ERp57 in the loading complex over the course of normal peptide loading. In contrast, calreticulin undergoes cycles of binding and release, and its presence in the loading complex is dependent upon MHC class I. ERp57 is a core structural component of the MHC class I loading complex, and it is permanently sequestered there by tapasin.

Finally, I have further characterized cells expressing a tapasin mutant unable to form the conjugate. Loading complex assembly is impaired in these cells, and peptide loading is inefficiently catalyzed by this mutant. Additionally, ERp57 binding stabilizes the structural integrity of tapasin. When endogenous ERp57 expression was suppressed using RNAi, all residual ERp57 was bound to tapasin, and both protein disulfide isomerase and ERp72, other ER resident oxidoreductases, formed mixed disulfides with tapasin. When redox mutant ERp57 proteins were over-expressed in these cells, only slight changes were seen in MHC class I trafficking. My data indicate that ERp57 is a key structural component of the MHC class I loading complex and likely does not exhibit any redox activity in this context. The key features of ERp57 responsible for its function remain unknown.

Acknowledgements

My time in the Cresswell lab has been extremely enjoyable, and that is largely due to the atmosphere that Pete has fostered in the lab. His door is always open, and he is always excited to hear your most recent result no matter how mundane it may seem later. He gives his students great freedom to explore their interests and develop their own experiments, but is also there to bounce around ideas. His mentorship style has allowed me to grow and become a much better scientist than I think I could have been in any other lab.

I would like to thank my committee of Jim, Sankar, and Ruslan. They have provided excellent feedback and support throughout graduate school. I would also like to thank the Section of Immunobiology in general and the Medzhitov and Schatz labs in particular for the use of reagents and equipment. Additionally, most of the data in Chapter 5 of this work would not have been possible were it not for Tom Taylor and the cell sorting facility. Finally, the MD/PhD office, Jim, Sue, Cheryl, and Marybeth, has been extremely supportive during all phases of medical and graduate school. I hope that continues until I graduate.

During my five years in the lab, a number of people have come and gone, and they have all had some impact on the work presented here. I must emphasize the roles of Naveen, Tobi, Suk-Jo, KC, Anne, Weiming, Xiuyan, Allesandra, Randy, and Ella for their camaraderie, experimental ideas, and/or guidance during my earlier days. Additionally, Nancy is the rock that holds the lab together, especially while Pete is away. Finally, my bay-mates Pam and Rebecca have provided an invaluable buffering capacity

to the sometimes loud and chaotic nature of the lab in addition to scientific feedback and ideas.

While in New Haven I have had to opportunity to make some life-long friends, and their presence throughout this process has made life a lot more enjoyable. I would like to thank my parents, David and Patricia, and family for their support over the years. Their willingness to encourage my curiosity is largely responsible for where I am today. Thomas and Constance Perry have also acted as surrogate parents when I am not able to make it to Indiana for long stretches of time, and for that I am grateful. Finally, I dedicate this work to Kate for her love and support.

Table of Contents

Table of Figures

Chapter 1: Introduction

1.1: General function of MHC class I complexes

It was recognized in the 1950s that a restricted region of the mouse genome was responsible for mediating rejection of transplanted grafts. Grafts between mice with a common locus were rejected much more slowly, and this genetic region was labeled the major histocompatibility complex (MHC). The human MHC is located on chromosome 6 and encodes a number of different immunologically relevant proteins including the human leukocyte antigens (HLA) that mediate graft rejection. The comparable antigens in mice are derived from the H-2 locus located on mouse chromosome 17. Subsequent work demonstrated that the HLA and H-2 antigens were the basis for recognition by T cells and, as such, integral to the development of a cellular immune response (Germain, 1994; Klein and Sato, 2000).

The HLA complex is traditionally divided into three segments: class I, class II, and class III. The class I segment encodes the classical MHC class I proteins HLA-A, B, and C as well as the non-classical HLA-E, F, and G and MICA and MICB. Likewise, the class II region encodes the MHC class II molecules HLA-DP, DQ, and DR. All of these proteins are displayed on the cell surface for recognition by cells of the immune system. Other genes encoded in the MHC affect the function of MHC class I and II proteins as well as the immune system in general. The MHC also encodes proteins with no known function in the immune system(Klein and Sato, 2000).

MHC class I and II molecules display peptides on the cell surface to CD8- and CD4-positive T cells, respectively. MHC class I and II proteins are structurally related,

but the natural histories of these proteins within the cell are quite distinct. After folding and assembly in the endoplasmic reticulum (ER), MHC class II molecules traffic through the secretory pathway until they reach late endosomes. Here, they become loaded with peptides 12 to 16 amino acids long typically derived from the extracellular space in a process facilitated by other MHC encoded genes (Watts, 2004). MHC class II molecules are essential for the generation of cellular immunity to extracellular pathogens such as bacteria, and their absence also significantly impairs the generation of humoral immunity (Grusby and Glimcher, 1995). MHC class II will not be considered further.

MHC class I complexes are composed of MHC encoded heavy chains (HLA-A, B or C) and the invariant, non-MHC encoded subunit β_2-microglobulin (β_2m). MHC class I assembly and peptide loading occur in the ER, and, after trafficking to the cell surface, antigen specific CD8+ T cells recognize peptides 8 to 10 amino acids long displayed in association with MHC class I/β_2m complexes. The peptides presented by MHC class I complexes are derived from proteins degraded in the cytosol, and, in theory, CD8+ T cells respond to peptides primarily arising from intracellular pathogens such as viruses and some bacteria (**Figure 1.1a**) (Germain, 1994; Klein and Sato, 2000; Pamer and Cresswell, 1998).

1.2: The structure of MHC class I

Both MHC class I heavy chain (HC) and β_2m are members of the immunoglobulin (Ig) superfamily. The exact length and composition of MHC class I HC varies among alleles, but all HLA alleles consist of three domains (α1, α2, and α3) with the α3 chain containing an internal disulfide bond between Cys-203 and Cys-259. The

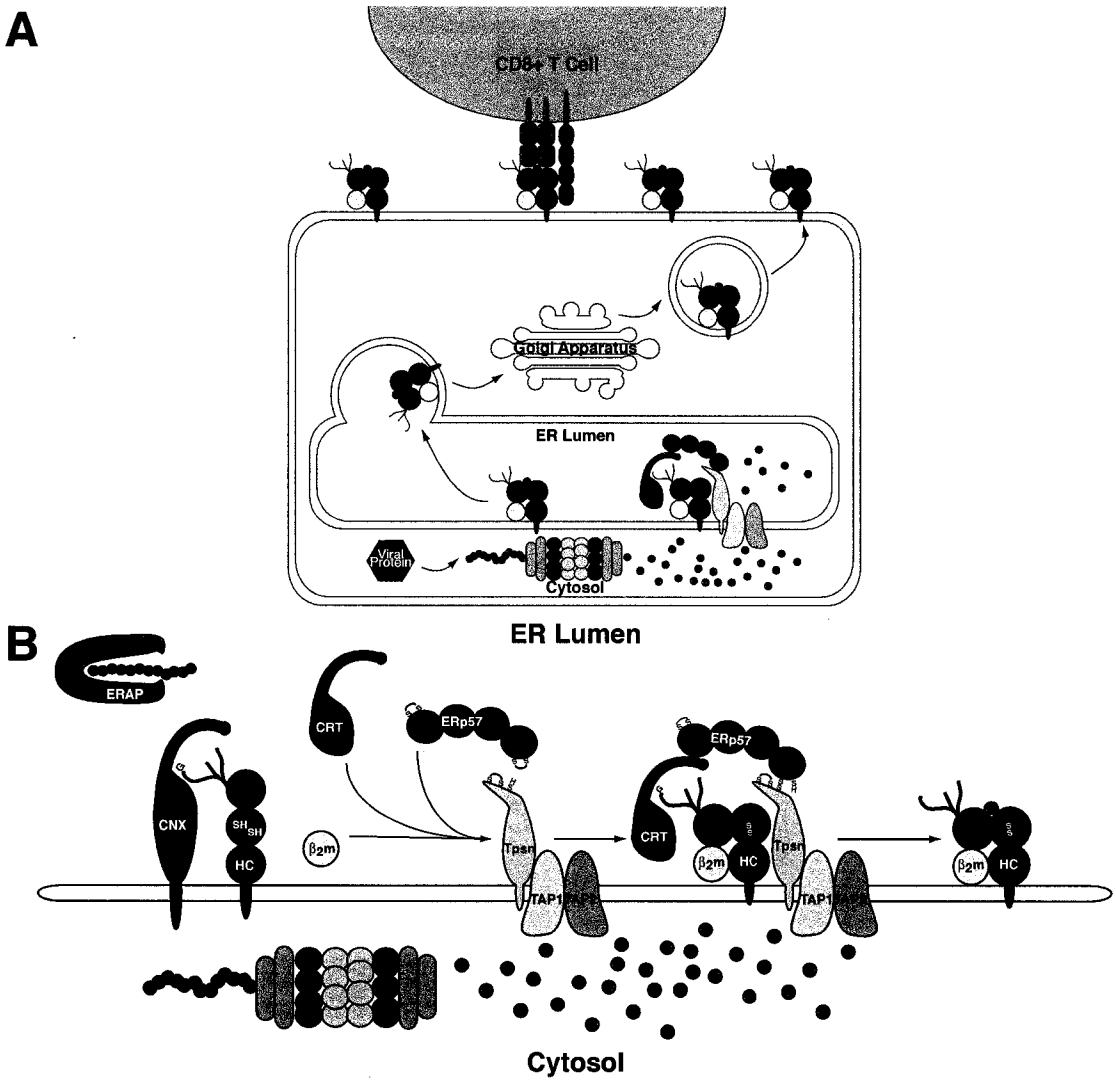

Figure 1.1: MHC class I is loaded with peptide in the ER and presents peptides to CD8+ T cells

A) General scheme of MHC class I antigen processing and presentation. Viral proteins in the cytosol are degraded by the proteasome, and generated peptides are translocated into the ER lumen via the TAP transporter. The peptide loading complex composed of TAP, tapasin, ERp57, and CRT facilitates peptide loading onto MHC class I HC/β_2m dimers. After stably associating with peptide, MHC class I complexes exit the ER and traffic through the Golgi apparatus on their way to the cell surface. Once there, antigen specific $CD8^+$ T cells recognize the presented peptide leading to cell killing and cytokine production.

B) MHC class I folding and assembly takes place in the ER. CNX mediates the early folding stages of MHC class I HC prior to its association with β_2m. Complete heavy chain oxidation occurs during this time, and ERp57 facilitates this process. Once associated and properly oxidized, MHC class I HC/β_2m complexes rapidly associate with CRT, ERp57, and tapasin, which acts as bridge to the TAP heterodimer, to form the MHC class I loading complex. Peptides generated in the cytosol by the proteosome are translocated into the ER by TAP and subsequently are bound to MHC class I through the coordinated action of the loading complex. ERAP trims peptides in the ER to 8 to 10 amino acids, and tapasin is essential for the generation of stable MHC class I/peptide complexes for many HLA alleles. Glucose trimmed, peptide loaded complexes are exported from the ER.

sequence of β_2m does not significantly vary between individuals, and it also contains a disulfide bond between Cys-25 and Cys-80. In humans, MHC class I HCs are glycosylated at Asn-86, while mouse H-2 alleles are glycosylated at residues Asn-86 and Asn-176. β_2m is not glycosylated in either humans or mice (Bjorkman et al., 1987a).

The structure of HLA-A*0201 associated with β_2m and peptide was first solved in 1987, and over 50 different MHC class I/β_2m/peptide structures have been solved encompassing a variety of human and mouse HLA and H-2 alleles (Bjorkman et al., 1987a). These structures share remarkable similarities and explain a variety of observations made prior to that time (Parham, 2005). The α3 domain and β_2m are proximal to the membrane and lie immediately beneath the α2 and α1 domains, respectively. The α1 and α2 domains form the boundaries of the peptide binding groove, and both domains contribute to the β-pleated sheet comprising the floor of the binding groove. The α1 domain forms a continuous α-helix along one side of the peptide, while the α2 domain forms an α-helix in three segments opposite the α1-helix. The helices narrow at the extreme ends of the peptide binding groove restricting the length of peptide that can be bound. A disulfide bond bridges the α2-helix and the β-pleated floor between Cys-101 and Cys-164, respectively (**Figure 1.2a and 1.2b**) (Bjorkman et al., 1987a; Wright et al., 2004).

HLA alleles are the most polymorphic human genes, and the most variable regions of MHC class I heavy chains are the floor and helices of the peptide binding groove (Bjorkman et al., 1987b). Residues in these locations affect peptide and T cell receptor binding (Garboczi et al., 1996). Polymorphisms in the floor of the peptide binding groove are the basis for the different binding specificities of different HLA

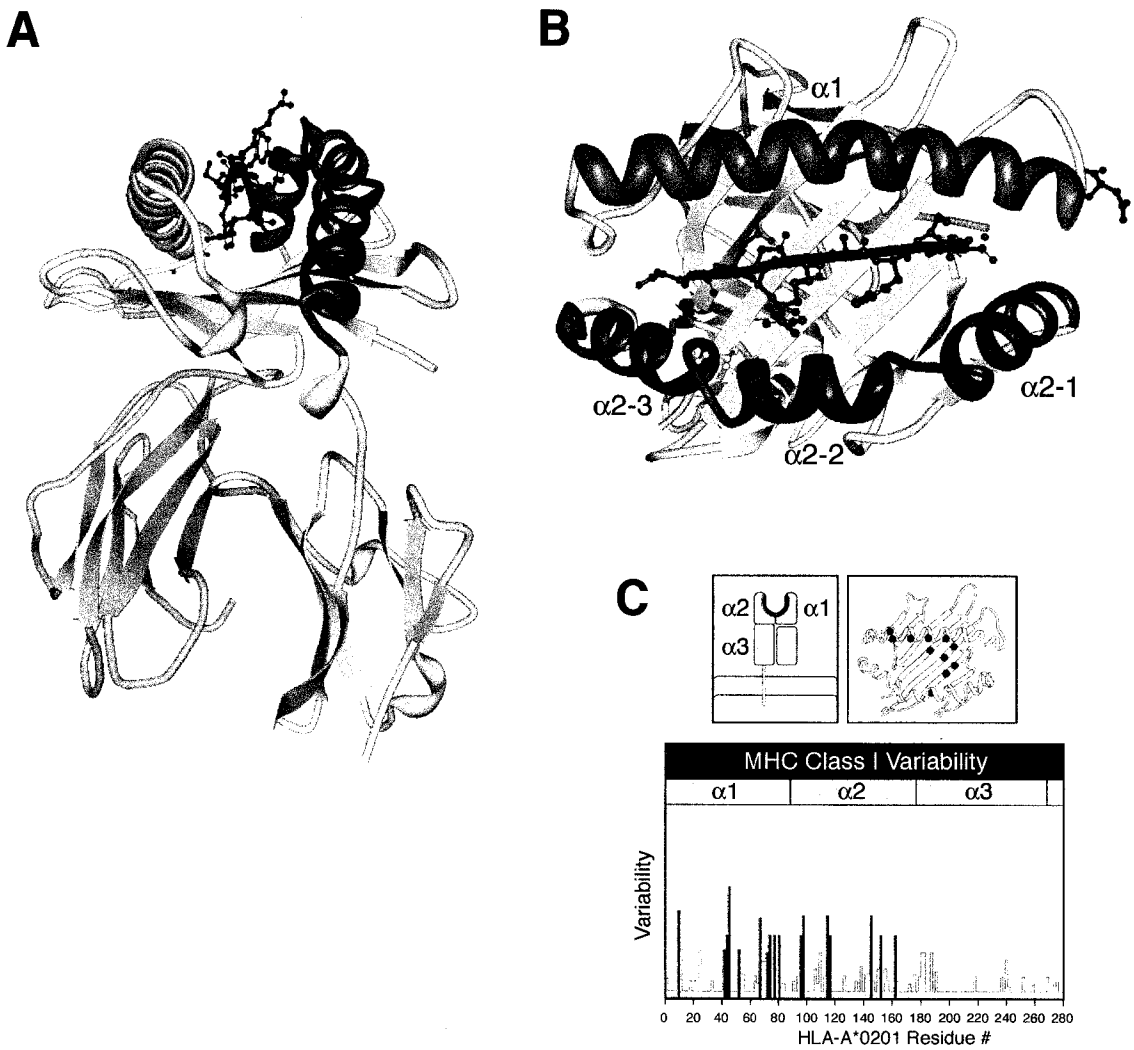

Figure 1.2: MHC class I molecules are comprised of multiple domains and are highly polymorphic.

A and B) The crystal structure of HLA-B*4402 with a peptide derived from HLA-DPA*0201. The MHC class I HC is shown in blue with gray α1 and α2 helices; β_2m is light gray. The bound peptide derived from HLA-DPA*0201 is shown in red. Cys-101 and Cys-164 are shown in yellow, and Asn-86 is shown in blue. The face thought to mediate tapasin binding is shown in (A), and the face recognized by the T-cell receptor is shown in (B).
C) MHC class I polymorphisms are clustered in and around the peptide binding groove. Highly variable residues are shown in red in a cartoon of MHC class I and the crystal structure of HLA-A*0201 (upper panel). The lower panel displays the variability of each residue throughout the length of the MHC class I HC. Figure was adapted from Janeway et al. Immunobiology, 5th edition.

alleles. The peptide binding groove contains six distinct pockets (A – F) that preferentially bind particular amino acids or side chains. For most alleles, two or three residues are highly conserved in all bound peptides (anchor residues), but other peptide residues are more variable. In addition to binding the peptide side chains, MHC class I molecules strongly interact with both the amino- and carboxy-termini. The combination of these interactions determines the overall affinity of a bound peptide (**Figure 1.2c**) (Rammensee, 1995).

1.3: The generation and translocation of MHC class I peptide ligands

MHC class I binding peptides are traditionally derived from protein antigens in the cytosol. The precise source of these peptides is somewhat controversial, but it is clear that the initial step in the generation of MHC class I binding peptides is proteasomal degradation (Strehl et al., 2005; Yewdell and Nicchitta, 2006). Inhibition of proteasome activity using specific inhibitors dramatically decreases the pool of peptides capable of binding MHC class I molecules and leads to their retention in the ER and subsequent degradation (Hughes et al., 1997; Hughes et al., 1996). The 20S proteasome is composed of 28 subunits, and the association of other co-factors that affect its proteolytic activity and specificity gives rise to the 26S proteasome (Strehl et al., 2005). Several proteasome subunits and a specific activator are upregulated by interferon gamma (IFN-γ), and their expression alters the pool of generated peptides to be more compatible with MHC class I binding (Strehl et al., 2005).

Peptide generation occurs in the cytosol, but peptide loading takes place in the ER. The transporter associated with antigen processing (TAP) comprised of TAP1 and

TAP2 provides the link between these two distinct cellular compartments (Spies et al., 1992; Spies and DeMars, 1991). Both TAP1 and TAP2 are members of the large ATP-binding cassette (ABC) family of transporters, and peptide binding induces ATP hydrolysis and translocation (Androlewicz et al., 1993; Neefjes et al., 1993). The TAP heterodimer is promiscuous in its peptide binding and transport activities and can act upon peptides up to 40 amino acids. However, TAP transports peptides of 8 to 12 amino acids most efficiently, and this size is close to ideal for binding MHC class I molecules (Androlewicz and Cresswell, 1994; Momburg et al., 1994). Proteasomal cleavage typically creates a peptide carboxy terminal compatible with MHC class I binding, and peptides are typically extended at their amino terminus (Cascio et al., 2001). The ER amino peptidase (ERAP/ERAAP) trims N-extended peptides to a length appropriate for MHC class I binding (Chang et al., 2005; York et al., 2002).

1.4: Overview of MHC class I assembly

The expression of MHC class I heavy chain/β_2m/peptide complexes at the cell surface is the end result of a process that begins in the ER. Within the ER, MHC class I complexes undergo several folding events involving general cellular chaperones as well as MHC class I specific proteins. The generation of stable MHC class I/peptide complexes depends, in most cases, upon the TAP heterodimer as well as the MHC class I specific chaperone tapasin. TAP transports peptides from the cytosol into the ER lumen, and tapasin in some way promotes the formation of stable MHC class I/peptide complexes (Cresswell, 2000). ERAP/ERAAP plays a further role in trimming peptides after translocation (Saric et al., 2002; Serwold et al., 2002). Additionally, calnexin

(CNX) facilitates the early folding of MHC class I heavy chains, while calreticulin (CRT) and ERp57 are intimately involved in the generation of stable complexes (**Figure 1.1b**). Many factors involved in the generation of stable MHC class I/peptide complexes are upregulated by cell exposure to IFN-γ including TAP1, TAP2, tapasin, MHC class I HC, β_2m, and proteasome components. Additionally, the loading and assembly of MHC class I complexes is considered a specialized case of protein folding, and a more thorough discussion of the general aspects of protein folding and quality control is needed before undertaking a specific discussion of MHC class I.

1.5: Protein folding in the endoplasmic reticulum

The ER has evolved multiple functions, but one of its primary roles is to facilitate the folding of proteins destined for the secretory pathway or extracellular secretion. There are a number of resident proteins within the mammalian ER that act as protein folding chaperones including BiP, GRP94, CNX, and CRT. CNX and CRT are carbohydrate binding proteins (lectins) involved in glycoprotein folding (see below), and BiP and GRP94 are members of the highly conserved heat shock protein 70 (Hsp70) and Hsp90 families, respectively. In conjunction with oxidoreductases of the thioredoxin (Trx) family such as protein disulfide isomerase (PDI), ERp57, and ERp72, these proteins prevent the aggregation of newly synthesized, unfolded polypeptides, facilitate the acquisition of correct disulfide bonding patterns, and/or, for terminally misfolded proteins, initiate protein degradation (Kleizen and Braakman, 2004; Ma and Hendershot, 2004). Additionally, BiP plays an essential role in sensing stress within the ER (Bertolotti et al., 2000).

A common theme of chaperone function is the recognition of hydrophobic residues exposed on the surface of folding polypeptides. The luminal and extracellular environments contain charged molecules including carbohydrates and inorganic ions, and the presence of hydrophobic residues on the surface of proteins is energetically unfavorable (Schroder and Kaufman, 2005). BiP promiscuously binds peptides enriched in hydrophobic residues, and the ultimate determinate of CRT and CNX binding depends upon exposed hydrophobic patches (Gething, 1999; Sousa and Parodi, 1995). In contrast, the recognition substrate for GRP94 remains unclear. GRP94 appears to bind a more limited subset of proteins than BiP, and may prefer partially assembled oligomeric complexes (Argon and Simen, 1999).

Folding proteins tend to utilize either the CNX/CRT/ERp57 or BiP/PDI folding pathways, and the particular chaperones used is determined by the location of the first glycan in the polypeptide chain (Molinari and Helenius, 2000). Some proteins successively interact with BiP and CNX (Hammond and Helenius, 1994), but complexes comprised of BiP/PDI and CNX/CRT/ERp57 are not present at high levels (Meunier et al., 2002). While MHC class I heavy chain may interact with BiP during its early folding stages, the folding and assembly of MHC class I/β_2m/peptide complexes is commonly considered a specialized case of glycoprotein folding mediated by the CNX/CRT/ERp57 pathway(Rudd et al., 2001).

1.6: Glycoprotein folding

Many proteins within the secretory pathway undergo N-linked glycosylation, and one report estimated this population at approximately 45% of the total eukaryotic protein

pool (Apweiler et al., 1999). The core N-linked glycan is synthesized in a series of reactions beginning on the cytosolic face of the ER and ending with the generation of the Glc3Man9GlcNAc2 structure in the ER lumen. This core glycan is associated with the ER membrane through a covalent attachment to dolichol-pyrophosphate (Burda and Aebi, 1999). N-linked glycans are added to proteins co-translationally by the oligosaccharide transferase (OST) complex. The OST is associated with the translocon complex and recognizes the consensus sequence NXS/T in unfolded polypeptides shortly after passage through the translocon. OST adds the core glycan to the Asn residue of the consensus sequence, and this core glycan is quickly trimmed of its terminal glucose residue by the enzyme glucosidase I (Hubbard and Robbins, 1979; Kowarik et al., 2002). Further trimming is performed by glucosidase II to generate a monoglucosylated core N-linked glycan. Glucosidase II also plays a role in the chaperone mediated folding of nascent glycoproteins in the ER. Monoglucosylated glycans serve as the recognition site for the two highly conserved ER resident lectin-like chaperones, CNX and CRT (Hebert et al., 1995; Ware et al., 1995).

CNX is a transmembrane protein of 572 amino acids that is highly conserved from yeast to humans, and CRT is a 400 residue soluble CNX homologue conserved from reptiles to mammals (Fliegel et al., 1989; Tjoelker et al., 1994). Both proteins consist of a lectin-like globular domain that mediates glycan binding and an extended proline-rich P-domain that mediates recruitment of ERp57 to nascent glycoproteins (see below) (Ellgaard et al., 2002; Frickel et al., 2002; Leach et al., 2002). The crystal structure of the CNX globular domain has been solved, and the P-domain of CRT has been examined by nuclear magnetic resonance (**Figure 1.3a**) (Ellgaard et al., 2001a;

Ellgaard et al., 2001b; Schrag et al., 2001). The globular domain of CNX contains the glycan binding pocket, and the P-domain curves away from the globular domain, partially shielding the glycan binding site (Schrag et al., 2001). Based on sequence similarity, CRT is assumed to adopt a similar structure, but the P-domains of these proteins differ in length (Ellgaard and Frickel, 2003). The significance of this difference is unknown, but a soluble version of CNX could not fully compensate for the absence of CRT for some folding substrates, including MHC class I HC (Gao et al., 2002; Molinari et al., 2004).

Like classical chaperones, CNX and CRT prevent the aggregation of folding substrates, retain improperly folded proteins in the ER, and, at least in the case of CNX, facilitate the targeting of terminally misfolded proteins for degradation (Hebert et al., 1996; Jackson et al., 1994; Molinari et al., 2003; Oda et al., 2003). However, CNX and CRT do not directly recognize misfolded polypeptides like BiP and Grp94, but they recognize a single glucose residue exposed on an N-linked glycan (Hebert et al., 1995; Ware et al., 1995). Folding substrates undergo successive rounds of CNX/CRT binding, release, glucose trimming, reglucosylation, and rebinding in what is referred to as the glycoprotein quality control cycle as described below (**Figure 1.3b**) (Helenius and Aebi, 2004).

After translation, translocation, and the generation of a monoglucosylated glycan by the sequential action of glucosidases I and II, CNX and CRT bind nascent glycoproteins (Daniels et al., 2003; Wang et al., 2005). Glucosidase II then trims the remaining glucose residue from the N-linked glycan. This either occurs after substrate release from CNX/CRT or while the substrate is still associated with the lectins (Ellgaard and Frickel, 2003). The elimination of the terminal glucose residue precludes further

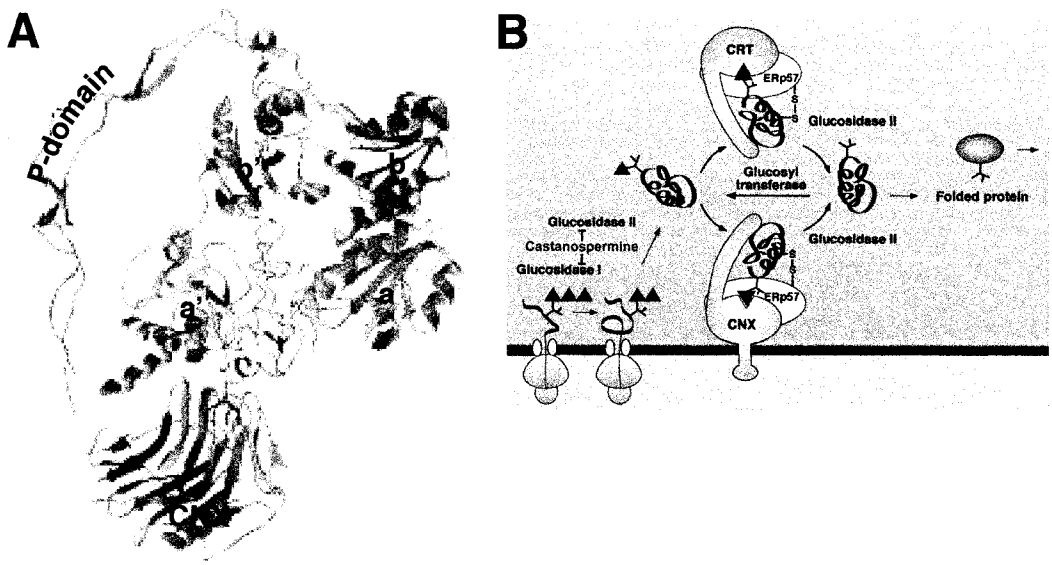

Figure 1.3: CNX, CRT, and ERp57 facilitate glycoprotein folding.

A) Crystal structure of CNX with a hypothetical substrate and extrapolated structure of ERp57. The globular domain of CNX binds the monoglucosylated glycan of a partially folded substrate while ERp57 reduces, oxidizes, and/or isomerizes a disulfide bond. The bb' domains of ERp57 interact with the P-domain of CNX. CNX is shown in yellow, ERp57 is in blue, the folding substrate is yellow, and the monoglucosylated glycan is red.
B) Glycoprotein quality control in the ER. Proteins undergo co-translational glycosylation when the OST transfers a pre-synthesized triply glucosylated core glycan to the NXS/T consensus sequence. Glucosidases I and II quickly trim the core glycan to generate the monoglucosylated glycan capable of binding CRT and CNX. These ER lectins recruit ERp57 to the folding protein to facilitate proper disulfide bond formation. Glucosidase II trims the terminal glucose residue coincident with substrate release. If UGGT detects exposed hydrophobic patches, the substrate is re-glucosylated for successive rounds of CRT/CNX binding. If the substrate adopts its native conformation, it exits the ER. CST inhibits the action of Glucosidases I and II preventing the generation of the monoglucosylated glycan needed for CRT and CNX binding.

lectin binding. The ER resident enzyme UDP-Glc:glycoprotein glucosyltransferase (UGGT) acts as the glycoprotein folding sensor by detecting exposed hydrophobic patches in close proximity to N-linked glycans (Sousa and Parodi, 1995). If such patches are recognized by UGGT, it reglucosylates the folding substrate allowing further interactions with CNX/CRT (Caramelo et al., 2003). Reglucosylation leads to ER retention and re-engagement with CNX and/or CRT (Labriola et al., 1995; Van Leeuwen and Kearse, 1997). This cycle repeats itself until the proper structure is achieved, and the protein is no longer reglucosylated. Alternatively, terminally misfolded proteins are targeted for degradation (Wilson et al., 2000).

A number of different folding substrates have been examined to generate this model of glycoprotein folding including MHC class I, influenza hemagglutinin (HA), and the surface glycoprotein of vesicular stomatitis virus (Hammond and Helenius, 1994; Hebert et al., 1995; Vassilakos et al., 1996). When glucose trimming is inhibited using either castanospermine (CST) or N-Butyldeoxynojirimycin (NB-DMJ), the generation of the lectin binding substrate is prevented and, as predicted, CRT and CNX binding do not occur (Hammond et al., 1994; Hammond and Helenius, 1994; Keller et al., 1998). Additionally, genetic deletion of CRT or CNX differentially affects substrate folding; some proteins absolutely require CNX, while others can fold efficiently with either CNX or CRT (Molinari et al., 2004). The complete disruption of CNX or CRT binding with CST or NB-DMJ reduces folding efficiency and leads to a loss of ER quality control. Under these conditions, enhanced degradation and protein turnover are seen (Hebert et al., 1996; Keller et al., 1998).

The recognition of folding substrates by CNX and CRT has classically been thought to be mediated solely through lectin/glycan interactions. Recent studies have suggested that CNX and CRT are capable of interacting with non-glycosylated substrates and preventing their aggregation (Danilczyk and Williams, 2001; Rizvi et al., 2004). Additionally, the putative polypeptide binding site has been localized to the CNX globular domain (Leach et al., 2002). Most of these studies have examined interactions under conditions of severe cellular and biochemical stress such as elevated temperatures approaching 42° C, however. Thus, while under some conditions CNX and CRT may interact with non-glycosylated proteins or with glycoproteins independent of lectin binding, these interactions are likely not significant for the majority of ER folding substrates.

1.7: Oxidative protein folding

The majority of proteins within the secretory pathway contain disulfide bonds that stabilize the final folded, conformation (Sevier and Kaiser, 2002). The environment of the ER is more oxidizing than the cytosol, and this partially enables spontaneous disulfide bond formation in folding proteins (Hwang et al., 1992). However, not all bonds are formed at this time, and those that do form may not be correct (Darby et al., 1995). Improper disulfide bond formation can lead to protein degradation or aggregation in the ER. Thus, a number of proteins have evolved to generate proper disulfide bonds in folding proteins (Ellgaard and Ruddock, 2005; Ferrari and Soling, 1999).

The sulfhydryl (-SH) side group of cysteine is unique among amino acids, and, when two cysteines are within close proximity a disulfide bond can form. This reaction

requires the deprotonation of one reactive cysteine and the donation of two electrons to an acceptor such as oxygen (Sevier and Kaiser, 2002; Wilkinson and Gilbert, 2004). These processes are dictated by the local redox conditions, and the relative balance between oxidized and reduced glutathione (a tripeptide of glutamic acid, cysteine, and glycine) contributes to the redox state in cells (Hwang et al., 1992). When proteins are incubated in buffers containing physiologic concentrations of oxidized and reduced glutathione, oxidative folding can occur. However, *in vitro* oxidation rates are often much slower than those observed *in vivo*. Within the mammalian ER, a large family of proteins that facilitate the transfer of electrons has evolved, and the addition of the oxidoreductases to *in vitro* folding reactions can greatly accelerate the acquisition of native structures (Weissman and Kim, 1993).

The formation of a disulfide bond between two cysteines is referred to as oxidation, the breaking of a disulfide bond is reduction, and the rearrangement (coupled reduction and oxidation) of a bond within a protein is isomerization (Wilkinson and Gilbert, 2004). All three reactions can be mediated by PDI, the primary enzyme in the ER lumen responsible for controlling disulfide bonding patterns, but PDI primarily acts as an oxidase and isomerase *in vivo* (Frand and Kaiser, 1999; Laboissiere et al., 1995; Pollard et al., 1998). PDI is a member of the larger Trx superfamily with relatively high sequence and structural homology to Trx (Edman et al., 1985). Trx is a cytoplasmic enzyme that mediates reductive events through a well conserved active site consisting of two cysteine residues separated by two amino acids (CXXC motif) (Sevier and Kaiser, 2002). PDI is composed of four Trx-like domains, and the extreme N- and C-terminal domains contain CXXC motifs to generate a molecule with an overall *abb'a'*

arrangement where the *a* and *a'* domains possess redox activity. PDI also contains a KDEL ER-retrieval sequence at its C-terminus (Edman et al., 1985; Tian et al., 2006).

The mechanism of action of PDI has been extensively investigated and is diagrammed in **Figure 1.4a**. During the reduction of a disulfide bond, the N-terminal cysteine of the PDI CXXC motif becomes deprotonated to generate a thiolate anion. This highly reactive moiety attacks a disulfide bond, contributing an electron to a sulfhydryl group in the substrate protein and forming a mixed disulfide between PDI and the substrate. The second cysteine of the now reduced disulfide bond is free to react with another neighboring cysteine residue, as would occur during an isomerization reaction, or to remain in a reduced state (Wilkinson and Gilbert, 2004). The accumulation of PDI/substrate mixed disulfides is undesirable for a number of reasons, and the presence of this mixed disulfide is very transient (Darby and Creighton, 1995). This is due to the presence of the second, C-terminal cysteine of the CXXC motif which becomes deprotonated and attacks the mixed disulfide releasing reduced substrate and oxidized PDI. This is referred to as the Trx motif escape pathway, and elimination of the C-terminal cysteine of the CXXC motif eliminates the escape pathway leading to the accumulation of PDI/substrate mixed disulfides (Walker and Gilbert, 1997; Walker et al., 1996).

The *b'* domain of PDI mediates its interaction with folding substrates, but, within this domain, a number of residues appear responsible for substrate binding. The precise means by which PDI recognizes its substrates is not entirely clear, but it likely involves exposed hydrophobic patches in non-native proteins (Klappa et al., 1998; Pirneskoski et al., 2004). Two recent structural analyses have provided valuable insight into the

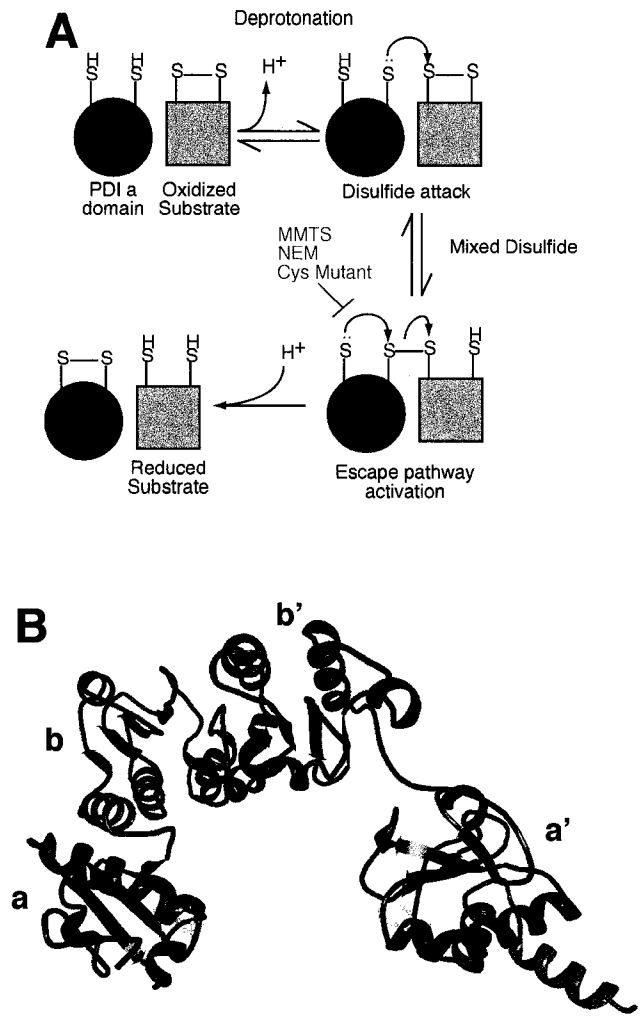

Figure 1.4: PDI is a multifunctional oxidoreductase.

A) Mechanism of PDI action. The N-terminal cysteine of the two thioredoxin (Trx) CXXC motifs of PDI forms a mixed disulfide with folding substrates. The C-terminal cysteine of the CXXC motif attacks the mixed disulfide leading to release of reduced substrate and oxidized enzyme. Pretreatment of cells with the cell permeable sulfhydryl reactive reagents N-Ethylmaleimide (NEM) or methylmethanethiosulfonate (MMTS) or deletion of the C-terminal cysteine theoretically blocks escape pathway activation. The pathway for substrate reduction is shown, and disulfide oxidation is the reverse. Isomerization involves the sequential reduction and oxidation of substrate disulfides.
B) Crystal structure of yeast PDI. The a and a' domains are shown in blue, the b and b' domains are green, and C-terminal tale is orange, consistent with Figure 1.5. Active site cysteines are shown in yellow.

relationship between the substrate binding *b'* domain and the CXXC containing *a* and *a'* domains (Li et al., 2006; Tian et al., 2006). In both the crystal structure of yeast PDI and a small angle X-ray scattering study of its human homologue, PDI appears to adopt a compact, horse-shoe like structure (**Figure 1.4b**). The face of the *b'* domain responsible for substrate binding is oriented towards the innermost surface of the structure, and this arrangement may stabilize enzyme/substrate interactions and facilitate CXXC motif access to disulfide bonds.

Disulfide bond formation is continuously occurring in the ER, and pathways have evolved to maintain the ER redox balance. A genetic screen in yeast revealed that the protein ER oxidoreductin (Ero1) is essential for the generation and maintenance of the ER oxidative capacity, and an Ero1 deficient yeast strain is not viable (Frand and Kaiser, 1998; Pollard et al., 1998). Ero1 is a soluble, membrane associated glycoprotein in the ER lumen, and two human homologues have been identified (hEro1 and hEro2) (Cabibbo et al., 2000; Pagani et al., 2000). The Ero proteins transfer electrons from the cytosol directly to PDI through transient, covalent interactions involving two CXXXC active sites in Ero1 and the Trx motifs of PDI (Benham et al., 2000; Frand and Kaiser, 1999). The factor that transfers electrons from the cytosol across the ER membrane remains unknown. Historically, glutathione was thought to be the primary factor maintaining the relatively oxidative environment of the ER, but, in contrast, glutathione contributes a net reductive effect in the ER (Molteni et al., 2004). Additionally, glutathione directly reduces the active sites of PDI-like molecules (Jessop and Bulleid, 2004). Thus, the Ero1 pathway maintains the oxidative activity of the ER, while reducing equivalents arise from glutathione and its associated transporters and biosynthetic enzymes. Disruption of either

pathway is lethal in yeast due to the unbalanced activity of the remaining pathway, but the growth of Ero1 deficient yeast is restored by the additional disruption of the glutathione pathway (Cuozzo and Kaiser, 1999).

There are a number PDI homologues found in the human genome consisting of various combinations of redox active and inactive domains (**Figure 1.5a and 1.5b**). Some are expressed in a tissue-restricted fashion in highly exocytic tissues (e.g. PDIp in the pancreas), but others, such as ERp72 and ERp57, are broadly expressed (Ellgaard and Ruddock, 2005). These proteins may differ in their ability to interact with Ero1(Pollard et al., 1998). ERp57 is a glycoprotein specific oxidoreductase (see below), and the functional differences between different PDI family members have only recently begun to be addressed. Despite similarities, there may be subtle mechanistic differences between ER Trx family members (Kulp et al., 2006). One report suggests that PDI directs proteins for retrotranslocation, while ERp72 retains substrates in the ER (Forster et al., 2006).

Finally, the importance of pathways facilitating disulfide bond formation is emphasized by the degree of functional, structural, and sequence similarities between mammalian, yeast, and bacterial disulfide pathways. The periplasm of Gram negative bacteria is analogous to the eukaryotic ER and contains a series of proteins responsible for the transfer of electrons from the cytoplasm to the periplamsic space to folding proteins. Bacterial DsbB is a transmembrane protein that accepts electrons from the soluble Trx family member DsbA (Kadokura et al., 2003). DsbB is functionally analogous to Ero1, while DsbA has both sequence and structural similarities with PDI (Sevier and Kaiser, 2002). Additionally, the periplasm also contains DsbC, a two-domain

A

Name	Sol/TM	C-term Tail	# Active domains
PDI	Sol	KDEL	2
ERp57	Sol	QEDL	2
ERp72	Sol	KEEL	3
PDIp	Sol	KEEL	2
ERp65	Sol	KEEL	2
ERp27	Sol	KVEL	0
PDIr	Sol	KEEL	3
ERp28	Sol	KEEL	0
P5	Sol	KDEL	2
ERp18	Sol	EDEL	1
ERp44	Sol	RDEL	1
ERp46	Sol	KDEL	3
TMX	TM	Unknown	1
TMX2	TM	KKDK	1
TMX3	TM	KKKD	1
TMX4	TM	Unknown	1

B

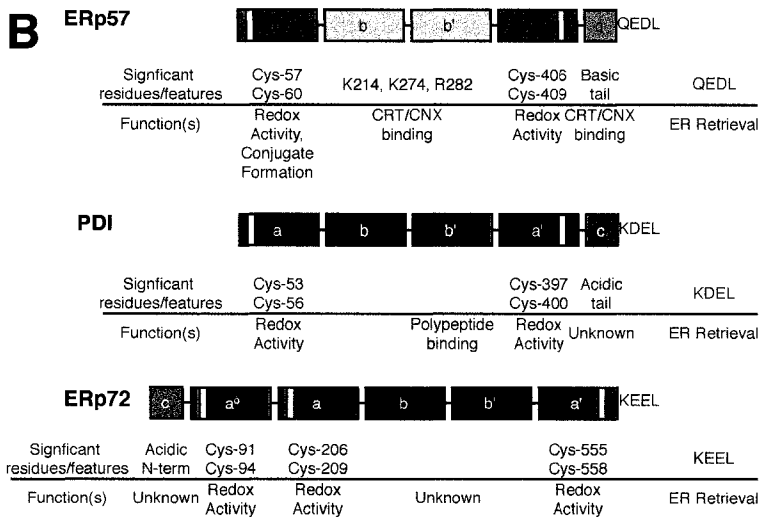

Figure 1.5: The mammalian PDI family is diverse.

A) A sample of mammalian PDI family members. The table indicates whether proteins are soluble (Sol) or transmembrane (TM). If known, the protein ER-retrieval sequence is listed, as are the number of redox active PDI a-like domains. Table is adapted from Elgaard and Ruddock, EMBO Reports, v6 p28.
B) Domain organization of ERp57, PDI, and ERp72. Both ERp57 and PDI possess two redox active a domains and two redox inactive b domains; ERp72 possesses an additional a domain. The a domain of ERp57 forms a mixed disulfide with tapasin, and the b and b' domains mediate CNX and CRT binding. The b' domain of PDI binds hydrophobic residues on substrate proteins. The basic and acidic tails of ERp57 and PDI, respectively, and the acidic N-terminus of ERp72 are of unknown function. All three proteins have KDEL-based ER retrieval motifs.

Trx family member that exhibits isomerase activity. In contrast to eukaryotes, however, the reductive potential of DsbC is directly maintained by DsbD rather than glutathione, which is not found in the periplasm.

1.8: ERp57: a glycoprotein specific oxidoreductase

Human ERp57 was first cloned as GRP58, and a number of different enzymatic functions, including phospholipase, transglutaminase, and protease activity, were ascribed to ERp57 (Hirano et al., 1995; Mazzarella et al., 1994; Murthy and Pande, 1994). What has increasingly become clear, however, is that ERp57 is highly functionally related to PDI and primarily functions in disulfide bond reactions of folding glycoproteins in the ER (Ellgaard and Frickel, 2003). Like PDI, ERp57 is composed of two CXXC containing, redox active Trx domains and two redox inactive Trx domains with an overall arrangement of *abb'a'*(Frickel et al., 2004; Russell et al., 2004; Silvennoinen et al., 2004). ERp57 exhibits reductase, oxidase, and isomerase activity *in vitro*, but the primary *in vivo* function of ERp57 remains unclear (Frickel et al., 2004). ERp57 has not yet been shown to interact with hEro1, but glutathione directly reduces ERp57 regenerating its enzymatic activity (Jessop and Bulleid, 2004; Mezghrani et al., 2001).

ERp57 is specifically recruited to folding glycoproteins through interactions with CNX and CRT (Oliver et al., 1999; Oliver et al., 1997). The P-domains of CNX and CRT primarily bind the *b'* domain of ERp57 analogous to substrate recognition and binding by the *b'* domain of PDI (Frickel et al., 2002; Pollock et al., 2004; Russell et al., 2004). Additional contacts between the ERp57 *b* domain and the P-domain of CNX

stabilize this interaction. The crystal structure of the *bb'* fragment of ERp57 has been solved, and there are several clear differences with PDI in this region. Not surprisingly, these differences correlate to regions of CNX binding (Kozlov et al., 2006).

ERp57 forms mixed disulfides with newly translated glycoproteins, and the disruption of interactions of CNX and CRT with folding substrates using CST or NB-DMJ also prevents substrate interactions with ERp57 (Molinari and Helenius, 1999). Additionally, CST treatment alters the kinetics of oxidative folding for several glycoprotein substrates examined (Kang and Cresswell, 2002; Molinari et al., 2004). The *in vitro* activity of ERp57 towards glycosylated substrates is dramatically enhanced by the presence of CNX or CRT (Zapun et al., 1998). Thus, ERp57 is thought to function specifically with CNX and CRT to promote correct disulfide bond formation in folding glycoproteins. Inhibition of lectin/substrate interactions abolishes the recruitment of ERp57 to folding substrates.

The role of ERp57 in the oxidative folding of glycoproteins was confirmed using ERp57 deficient mouse embryonic fibroblasts (MEFs). In the absence of ERp57, the folding of influenza HA was delayed, and the authors suggest that HA is an obligate ERp57 substrate. In contrast, two Semiliki Forest virus proteins that normally interact with ERp57 were able to fold using alternative oxidative and chaperone pathways, suggesting that they are facultative ERp57 substrates (Solda et al., 2006). Additionally, in this paper RNA-interference (RNAi) was used to knock-down ERp57 expression >90%, but only slight differences were seen in HA oxidative folding. When the work of Solda et al. and Molinari et al. are considered together, it becomes clear that one of the primary functions of CNX and CRT is their recruitment of ERp57. The primary defect

seen in the maturation of viral glycoproteins in the absence of CNX or CRT or in the presence of CST involved altered oxidative folding and the accumulation of high molecular weight disulfide-linked oligomers. In particular, HA translated in cells treated with CST or cells deficient in ERp57 matured and aggregated with remarkable similarities (Molinari et al., 2004; Solda et al., 2006). Thus, glycoprotein folding and oxidative protein folding intersect at ERp57.

1.9: MHC class I: Early folding events

MHC class I heavy chain undergoes co-translational glycosylation at residue Asn-86. Immediately upon translocation, MHC class I HC interacts with BiP followed by CNX (Nossner and Parham, 1995). CNX likely recruits ERp57 to facilitate disulfide bond formation within the α3, Ig-like domain at this time. However, CNX is dispensable for MHC class I HC folding and assembly (Sadasivan et al., 1995). A second disulfide bond between Cys-101 and Cys-164 of the α1 and α2 domains, respectively, subsequently forms, and β_2m association appears required for the stable formation of this bond. In the absence of β_2m, MHC class I HC is found in fully oxidized, partially oxidized, and fully reduced forms (Tector et al., 1997). The overwhelming majority of both human and mouse mutant MHC class I molecules lacking either Cys-101 or Cys-164 do not associate with β_2m and most proteins are rapidly degraded. However, some mutant molecules reach the cell surface, but their ability to stimulate T cells is severely impaired (Warburton et al., 1994). After initial oxidative folding, MHC class I/β_2m complexes dissociate from CNX, but they remain monoglucosylated and associate with CRT.

1.10: Peptide loading in the ER

The early folding of MHC class I molecules and association with β_2m occurs within minutes after synthesis. However, rather than proceed out of the ER, MHC class I/β_2m complexes associate with the peptide loading complex (PLC). In addition to MHC class I HC/β_2m dimers, the PLC is composed of TAP1, TAP2, tapasin, ERp57, and CRT. The transport molecule BAP31 and PDI have also been reported to be associated with the PLC (Ladasky et al., 2006; Paquet et al., 2004; Park et al., 2006; Spiliotis et al., 2000). Several different groups have independently identified the association and function of BAP31, but there is only one report of the involvement of PDI in peptide loading. The TAP heterodimer is the core of the PLC, and four sub-complexes consisting of tapasin, ERp57, CRT and MHC class I/β_2m dimers are associated with each TAP heterodimer (Ortmann et al., 1997). In mice, the association of CNX with MHC class I is maintained within the PLC, but, while CNX can be detected with TAP in human cells, CNX does not appear to directly interact with PLC-associated MHC class I HC (Diedrich et al., 2001; Ortmann et al., 1997; Suh et al., 1996). Cell lines and animals deficient in different components of the MHC class I loading pathway have greatly clarified the particular role for each protein.

First and foremost, β_2m is an obligate partner for MHC class I HC. As discussed above, β_2m association occurs very early during MHC class I folding, and the absence of β_2m virtually precludes all subsequent folding, assembly, and loading steps. Cells lacking β_2m do not express MHC class I complexes on their surface, and mice with the β_2m gene disrupted have severely impaired CD8 T cell mediated immunity (D'Urso et al., 1991; Sege et al., 1981; Williams et al., 1989; Zijlstra et al., 1990).

The stability of MHC class I/β_2m complexes assembled in cells deficient in TAP expression is severely impaired as measured by decreased to absent cell surface expression and their rapid degradation (Salter and Cresswell, 1986; Spies et al., 1992; Spies and DeMars, 1991). Consistent with this, mice genetically disrupted to lack TAP1 have no peripheral CD8+ T cells secondary to absent MHC class I expression on cells of the thymus. The peripheral cells of these mice resemble TAP deficient cell lines in their MHC class I phenotype (Van Kaer et al., 1992). Interestingly, HLA-A*0201 is able to bind signal sequence derived peptides and achieve relatively high surface expression in the absence of a functional TAP transporter. This appears to be unique among HLA molecules examined (Wei and Cresswell, 1992). Thus, peptide transport by TAP is absolutely essential for the generation of stable MHC class I/peptide complexes as well as productive CD8+ T cell immunity. In contrast, more subtle defects were seen in mice deficient in ERAP/ERAAP or the IFN-γ inducible proteasomal subunits LMP2 and LMP7 (Fehling et al., 1994; Hammer et al., 2006; Van Kaer et al., 1994; Yan et al., 2006).

Mice genetically disrupted to lack CRT die shortly after birth, but MHC class I antigen processing and presentation have been examined in cells derived from these animals (Gao et al., 2002). With the exception of CRT, PLC composition appears normal in these cells, but the assembly and transport of MHC class I/peptide complexes were impaired. Unstable, poorly loaded MHC class I complexes exited the ER more rapidly in CRT deficient MEFs compared to wild-type (WT) cells. Additionally, the generation of some CD8 T-cell specific epitopes was impaired in these cells. From the experiments conducted it is impossible to conclude if the defects in MHC class I antigen presentation

seen in CRT deficient cells are due to effects in the PLC or more generally within the ER; it is clear that CRT plays a key role in regulating the export of properly loaded MHC class I molecules to the cell surface.

1.11: Tapasin is an MHC class I specific chaperone

The laboratory of Robert DeMars generated a series of mutant cell lines selected to be deficient in MHC class I surface expression. Genetically, these cell lines all harbored large deletions within the MHC including genes encoding MHC class I HCs and TAP1 and TAP2. One of these cell lines, 721.220, exhibited an allele specific phenotype. The genes encoding endogenous HLA alleles were completely lost, but transfected alleles, including HLA-B*0801, were differentially expressed at the cell surface despite normal mRNA levels(Greenwood et al., 1994). This cell line was later found to lack expression of a novel glycoprotein named tapasin for TAP associated glycoprotein (Sadasivan et al., 1996). Re-expression of tapasin in 721.220 cells restored the surface expression of HLA-B*0801, confirming the importance of tapasin in MHC class I loading (Ortmann et al., 1997). Additional alleles have been examined for their dependence upon tapasin for optimal peptide loading, and HLA-B*4402 is the most "tapasin dependent" allele examined to date (Park et al., 2003).

In the absence of tapasin, MHC class I HC, β_2m, CRT, and ERp57 do not appreciably associate with TAP, and, in the absence of β_2m, tapasin associates with TAP, but CRT and MHC class I HC do not (Hughes and Cresswell, 1998; Sadasivan et al., 1996). Thus, tapasin acts as a bridge between MHC class I/β_2m complexes and TAP. It was originally hypothesized that the primary function of tapasin was to bring MHC class

I/β_2m dimers within close proximity of TAP to facilitate peptide loading. This is clearly not the case, however, as a soluble version of tapasin that does not interact with TAP mediates peptide loading to a great extent, but the generation of a conformation dependent HLA-Bw4 epitope was somewhat impaired in these cells (Lehner et al., 1998; Tan et al., 2002). In contrast, the N-terminus of tapasin is essential for MHC class I association and peptide loading. Tapasin mutants truncated at the N-terminus by 50 or 19 amino acids associate with TAP but poorly recruit MHC class I, and peptide loading in cells expressing these mutants is indistinguishable from cells lacking tapasin altogether (Bangia et al., 1999; Momburg and Tan, 2002). The N-terminus of tapasin appears to constitute a distinct domain from the rest of the molecule (Chen et al., 2002). Tapasin expression also stabilizes TAP, leading to increased steady-state levels compared to tapasin deficient cells (Bangia et al., 1999; Garbi et al., 2003).

Despite numerous studies, tapasin's mechanism of action remains unclear, and these studies have been complicated by the number of alleles examined and the different effects of tapasin on different alleles. In the absence of tapasin, HLA-B*0801 is capable of binding high affinity peptides, but the overall pool of bound peptides is reduced (Zarling et al., 2003). These data suggest that tapasin stabilizes empty MHC class I/β_2m complexes in the ER, facilitating subsequent productive peptide loading events. Alternatively, several studies suggest that tapasin directly optimizes the peptide repertoire bound by MHC class I molecules (Barber et al., 2001; Brocke et al., 2002; Howarth et al., 2004; Purcell et al., 2001; Tan et al., 2002; Williams et al., 2002). Tapasin also exerts a general quality control function in the ER preventing the export of empty or poorly loaded MHC class I complexes (Barnden et al., 2000). The function of tapasin within the

PLC awaits a suitable *in vitro* system analogous to that developed for MHC class II and HLA-DM. Using components purified from cells, a series of studies have demonstrated that the transient interaction of HLA-DM with MHC class II complexes induces the dissociation of CLIP, the MHC class II invariant peptide, stabilizes empty MHC class II complexes, and affects the final pool of peptides presented at the cell surface by MHC class II (Denzin et al., 2005). While it has been hypothesized that tapasin could function directly analogous to HLA-DM, this has yet to be clearly shown (Brocke et al., 2002). Nevertheless, existing data clearly show that the peptide loading of most HLA alleles as measured by cell surface expression, thermostability, turnover, etc. is improved in the presence of tapasin.

1.12: Tapasin and ERp57 form a mixed disulfide within the MHC class I loading complex

From a glycoprotein folding perspective, MHC class I complexes are substrates to be acted upon by the chaperones CRT, ERp57 and tapasin. When ERp57 was identified as a PLC component it was expected to interact directly with MHC class I HC analogous to other glycoprotein folding substrates (Cresswell et al., 1999a; Cresswell et al., 1999b). Thus, the identification of a mixed disulfide between ERp57 and tapasin (the conjugate) within the PLC was surprising (Dick et al., 2002). Cys-95 of tapasin forms a disulfide bond with Cys-57 in the *a* domain of ERp57, and HLA-B*4402 complexes assembled in the presence of a tapasin mutant lacking Cys-95 (C95A) exhibit decreased thermostability and impaired peptide loading. Additionally, the redox state of HLA-B*4402 HCs associated with C95A mutant tapasin is altered; the Cys-101/Cys-164 bond

is reduced after PLC isolation and SDS-PAGE. However, the inability of tapasin to form the conjugate did not affect its ability to promote peptide loading of SIINFEKL (a peptide derived from ovalbumin presented by H2-K^b) and variant peptides (Howarth et al., 2004).

The importance of ERp57 incorporation into the PLC was emphasized by the generation of mice lacking expression of ERp57 in B cells. In these cells, surface H2-K^b expression was reduced and displayed enhanced turnover compared to ERp57 competent cells. Additionally, the recruitment of H2-K^b into the PLC was altered, and its trafficking through the Golgi apparatus was accelerated. ERp57-deficient fibroblasts had slightly decreased presentation of the SIINFEKL epitope, but no alterations in the redox state of PLC-associated H2-K^b were seen in these cells (Garbi et al., 2006).

1.13: Outstanding questions

Despite the generation of mice with ERp57-deficient B cells and murine cell lines completely deficient in ERp57 expression, the role of ERp57 in MHC class I peptide loading remains unclear. There are several discrepancies between data generated using human cells expressing HLA-B*4402 and C95A tapasin and murine B cells lacking ERp57 and expressing H2-K^b. These differences could arise from species or allelic differences or, alternatively, could be a consequence of the systems used. In particular, while the complete absence of ERp57 provides some insight into its function in the PLC, studies examining mutants deficient in one of several possible ERp57 functions would be more informative.

More generally, however, the presence of ERp57 in the PLC was thought to further support the glycoprotein folding model of MHC class I loading. The fact that

ERp57 forms a mixed disulfide with tapasin rather than MHC class I heavy chain deviates somewhat from this model, and further differences may exist. Additionally, it has proven difficult to detect oxidoreductases containing mixed disulfides under normal conditions. Thus, the involvement of ERp57 in MHC class I loading may be exceptional in several aspects. In the following dissertation, I will address these two issues to generate a more complete understanding of the role of ERp57 in MHC class I loading.

Chapter 2: Specific recruitment of ERp57 into the MHC class I loading complex by tapasin.

Optimal peptide loading onto MHC class I molecules depends on the complete assembly of the MHC class I loading complex, consisting of TAP1, TAP2, tapasin, ERp57, CRT, MHC class I HC, and β_2m (Cresswell, 2000). The mixed disulfide between ERp57 and tapasin has only recently been described, and the cellular and immunologic conditions required for conjugate formation remain somewhat unclear (Antoniou and Powis, 2003; Dick et al., 2002). Variations in tapasin conjugation could be related to a number of processes relevant to peptide loading, including the peptide occupancy of MHC class I/β_2m dimers, PLC composition, or others. Finally, if MHC class I peptide loading is a specialized case of glycoprotein folding, the recruitment of ERp57 into the PLC should be consistent with its interactions with other folding substrates. Thus, I initially examined the conditions required for ERp57 incorporation into the MHC class I loading complex and conjugate formation. By using methyl methanethiosulfonate (MMTS) instead of N-ethylmaleimide (NEM), I show that tapasin alone preferentially recruits ERp57 into the conjugate, and this recruitment is independent of glycan binding by ER lectins.

2.1: Tapasin expression determines free ERp57 levels

We previously showed that in NEM-treated B cell lines, a substantial but unquantitated fraction of cellular ERp57 exists in a mixed disulfide with tapasin (Dick et al., 2002), but a population of free tapasin was always observed in these experiments. Thus, different cellular conditions could dictate the extent of tapasin conjugation and potentially affect the efficiency of MHC class I peptide loading. To determine whether free versus tapasin-associated ERp57 levels were dictated by cellular folding requirements or by the levels of tapasin in the ER, I treated HeLa-M cells with IFN-γ to increase expression of tapasin and other components of the MHC class I pathway. We recently found that MMTS is superior to NEM in preserving the tapasin/ERp57 conjugate (P.C., unpublished observation), and cells were treated with MMTS prior to detergent extraction. Based on non-reducing SDS-PAGE and quantitative Western blotting, I observed that overall ERp57 levels did not change with IFN-γ treatment, but the pool of free ERp57 was dramatically reduced (**Figure 2.1a** and **2.1b**). Tapasin expression was increased 8-fold by IFN-γ, and conjugate levels increased by the same amount (**Figure 2.1c**). In untreated cells, nearly 85% of the cellular ERp57 pool was free and available to assist glycoprotein folding. In contrast, in HeLa-M cells treated with IFN-γ, 80% of the ERp57 was disulfide-linked with tapasin, as confirmed by immunoprecipitating for tapasin and blotting for ERp57 (**Figure 2.1d**). Additionally, no free tapasin was seen under non-reducing conditions, but, due to the experimental design, I could not fully rule out the presence of free, unconjugated tapasin in these cells. Interestingly, in both IFN-γ treated and untreated cells, free ERp57 was found in at least two different redox states based on its mobility in SDS-PAGE under non-reducing conditions. Thus, stimulation of

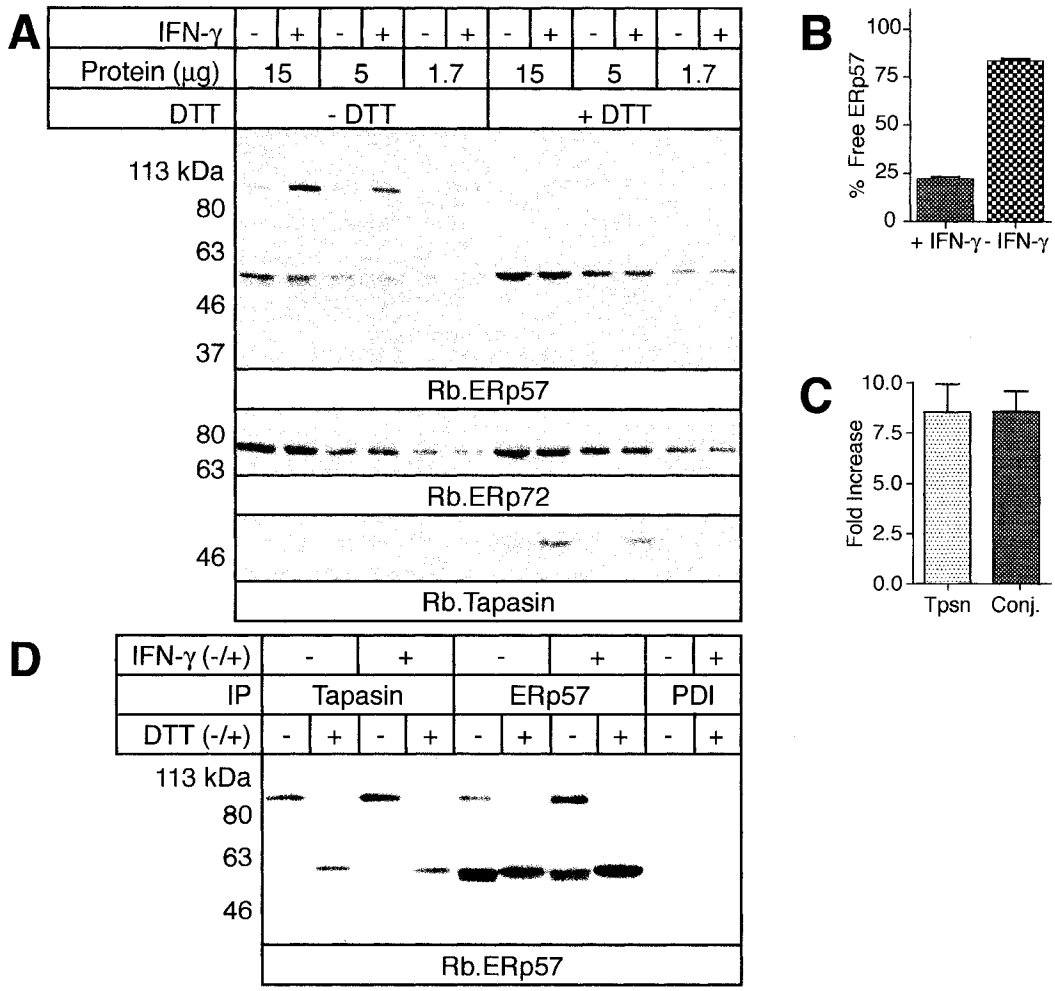

Figure 2.1: IFN-γ treatment drives tapasin association and decreases the pool of free ERp57

A) IFN-γ reduces the pool of free ERp57. HeLa-M cells were treated with IFN-γ for two days prior to harvesting and MMTS treatment. Three fold serial dilutions of cell extracts were resolved by SDS-PAGE under reducing or non-reducing conditions and blotted with rabbit anti-ERp57 raised against a C-terminal peptide (R.ERp57-C). After probing for ERp57, membranes were stripped, cut, and re-probed for tapasin with R.gp48N or for ERp72 with Rb.ERp72 as a loading control.
B) IFN-γ reduces the pool of free ERp57. Bands in (A) corresponding to conjugated and free ERp57 under non-reducing conditions were quantitated, and the percent of free ERp57 was calculated. Data shown are the average ± SEM of three dilutions from two separate experiments.
C) IFN-γ increases conjugate levels to the same extent as tapasin expression. Bands in (A) corresponding to tapasin and conjugated ERp57 with and without IFN-γ treatment were quantitated, and the fold increase in expression was calculated. Data shown are the average ± SEM of three dilutions from two separate experiments.
D) IFN-γ induction of tapasin reduces the pool of free ERp57. Lysates from (A) were precleared and precipitated with mouse anti-tapasin (PaSta1), -ERp57 (MaP.ERp57), or -PDI (M.PDI) and protein G-sepharose. Samples were resolved under reducing or non-reducing conditions as indicated and blotted with rabbit anti-peptide R.ERp57-C. The upper molecular weight species contains both tapasin and ERp57, and ERp57 exists in at least two oxidation states.

tapasin expression by IFN-γ dramatically reduces the level of non-tapasin associated ERp57 available to assist glycoprotein folding.

2.2: Conjugate formation is independent of β_2m, MHC class I HC, TAP1, and TAP2

In the absence of NEM treatment, no ERp57 was found associated with TAP or tapasin in the β_2m deficient B-LCL Daudi, and only a small fraction of total tapasin was detected in a disulfide-linked conjugate with ERp57 when these cells were treated with NEM (Dick et al., 2002; Hughes and Cresswell, 1998). Additionally, no conjugate was seen in the β_2m-deficient melanoma cell line FO-1 under similar conditions. Expression of β_2m in these cells by transfection led to increased steady state levels of the tapasin/ERp57 conjugate (Dick et al., 2002). The expression of tapasin in FO-1 cells is relatively low and can be increased by IFN-γ treatment. To determine whether increased tapasin expression in the absence of β_2m could promote greater conjugate formation, or if defective conjugate formation was due to the absence of β_2m, I stimulated FO-1 and FO-1.β_2m, a β_2m-expressing transfectant, with IFN-γ. The cells were then treated with MMTS prior to solubilization in digitonin, which preserves the TAP/tapasin interaction, or Triton X-100, which does not. By a combination of immunoprecipitations, reducing and non-reducing SDS-PAGE, and Western blotting, I observed that all detectable TAP-associated and total intracellular tapasin was conjugated to ERp57, regardless of β_2m expression (**Figure 2.2a**). These findings confirm the preliminary data above suggesting that, under steady-state conditions, all tapasin is conjugated to ERp57. Unlike **Figure 2.1a** however, the design of this experiment allows me to reliably draw this conclusion.

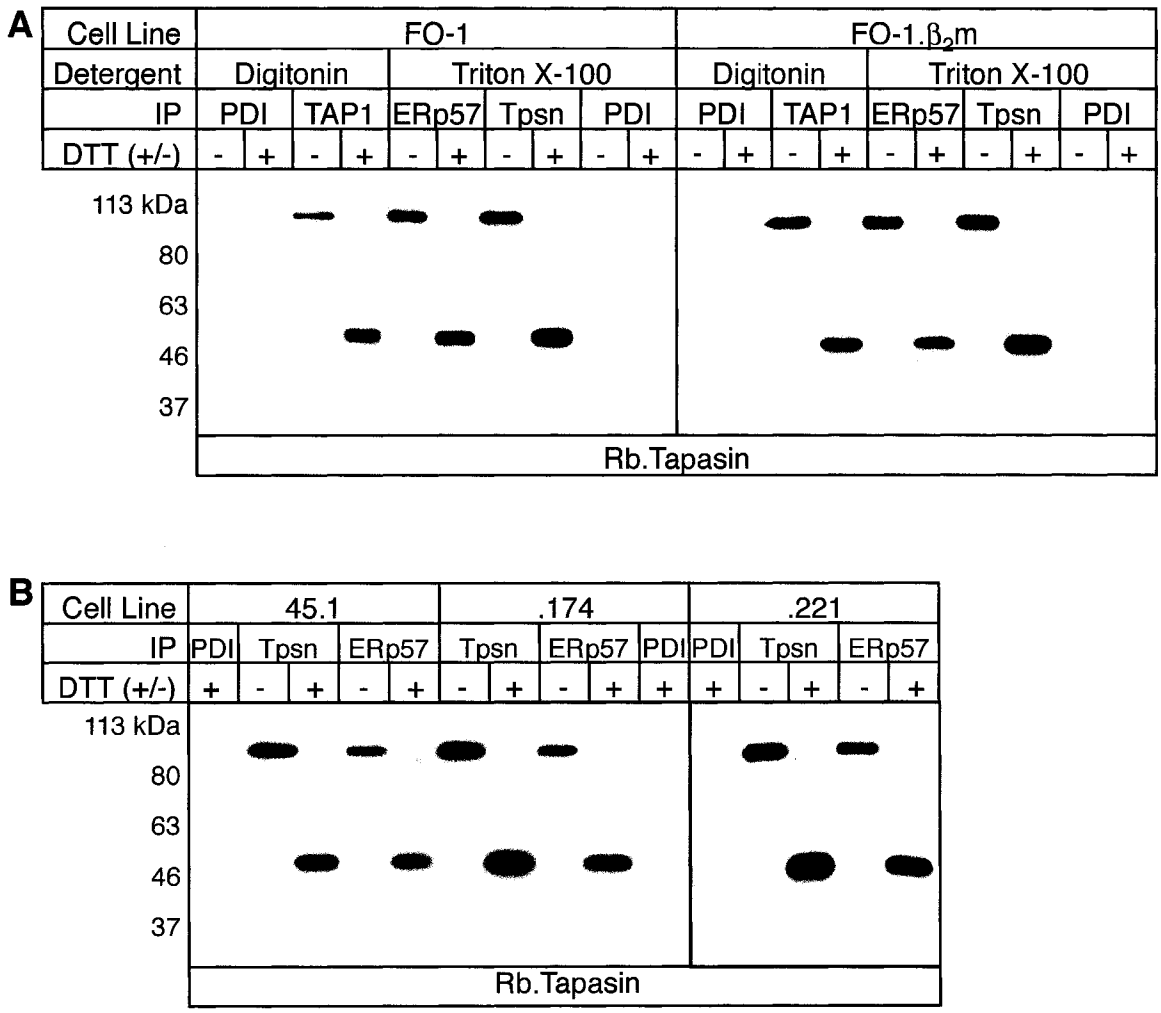

Figure 2.2: All tapasin is conjugated to ERp57 in the absence of β_2m, TAP1, TAP2, or MHC class I HC

A) All TAP associated and cellular tapasin is conjugated to ERp57 in the presence or absence of β_2m. Post-nuclear supernatants from IFN-γ treated FO-1 or FO-1.β_2m cells solubilized in the indicated detergents were precipitated with mouse anti-TAP1 (148.3), -ERp57 (MaP.ERp57), -tapasin (PaSta-1), or -PDI (M.PDI) and protein G-sepharose. SDS-PAGE was performed under reducing or non-reducing conditions and probed for tapasin with R.gp48C.
B) Full conjugate formation occurs in the absence of TAP1 and TAP2 as well as HLA-A, B, and C. The indicated derivatives of the B-LCL 721 were solubilized in Triton X-100 and post-nuclear supernatants were precipitated with mouse anti-ERp57 (MaP.ERp57) or -tapasin (PaSta1) coupled to A15m agarose or mouse anti-PDI (M.PDI) and protein G-sepharose. Samples were incubated in the presence or absence of DTT as indicated. Following separation and transfer, tapasin was detected by probing with R.gp48C.

Identical results were obtained with Daudi and its β_2m-expressing derivative Daudi.β_2m (data not shown).

We previously observed conjugate formation in the TAP1 and TAP2 negative cell line 721.174, but, as with β_2m deficient cells, the extent of conjugate formation varied somewhat leading to speculation that the conjugation state of tapasin could be related to the relative peptide occupancy or loading state of associated MHC class I/β_2m dimers (Dick et al., 2002; Wright et al., 2004). Therefore, I next examined the extent of conjugate formation under steady-state conditions in cells expressing minimal amounts of MHC class I HC (721.221), cells lacking TAP1 and TAP2 expression (721.174), and a related cell line that is fully competent for MHC class I antigen loading (721.45.1). Once again, in cells pretreated with MMTS, all cellular and TAP-associated tapasin was disulfide bound to ERp57 regardless of the presence of MHC class I HC, TAP1 or TAP2 (**Figure 2.2b**). Thus, there appears to be no relationship between the ability of the cell to generate MHC class I HC/β_2m complexes, with or without TAP translocated peptides, and full conjugate formation.

2.3: The kinetics of conjugate formation are unaffected by β_2m expression

We previously showed that tapasin and ERp57 rapidly associate with TAP shortly after synthesis (Diedrich et al., 2001). These experiments were conducted without NEM or MMTS treatment, however, so formation of the disulfide-linked conjugate could not be assessed. Additionally, if the kinetics of conjugate formation are related to the incorporation of MHC class I heavy chain or other loading complex components, the rate or order of loading complex assembly may be altered in cells lacking β_2m. Only minimal

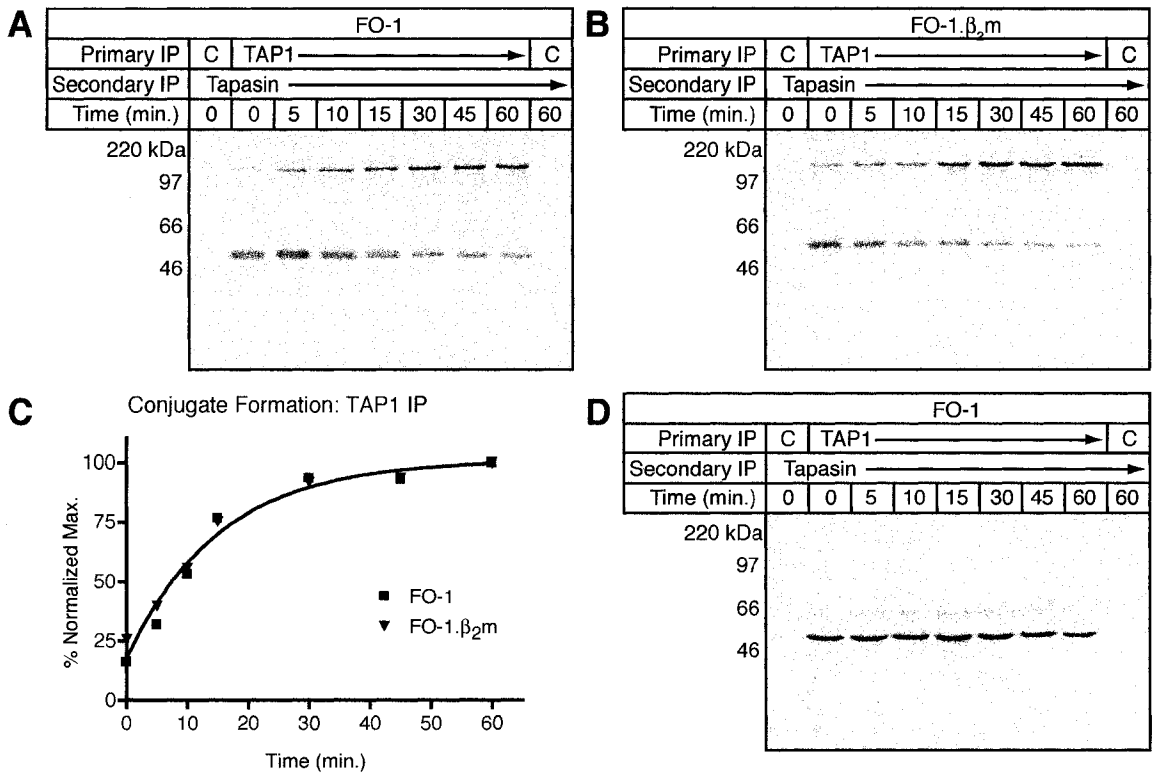

Figure 2.3: β_2m expression does not affect the rate of conjugate formation

A and B) IFN-γ treated FO-1 or FO-1.β_2m cells pulsed with [^{35}S]-methionine and cysteine for five minutes were chased for the indicated periods prior to solubilization in digitonin. Post-nuclear supernatants were precipitated with the anti-TAP1 mAb 148.3 or mouse IgG coupled to agarose beads (C = Ctrl). Associated proteins were stripped in 1% SDS and tapasin and its conjugate with ERp57 were reprecipitated with R.gp48C and protein A-sepharose.
C) Data from panels A and B presented as a percentage of the maximum ERp57-tapasin conjugate signal throughout the chase period.
D) Newly synthesized tapasin represents most of the radioactivity incorporated into the conjugate. Samples were prepared as in A and B, but gels were run under reducing conditions.

amounts of MHC class I HC are associated with TAP in the absence of β_2m, and in these cells no TAP-associated CRT is seen. Thus, the altered incorporation of these key PLC components could affect the *kinetics* of conjugate formation without largely perturbing the *extent* of conjugate formation. To examine these questions, I looked at the kinetics of conjugate formation in IFN-γ-treated FO-1 and FO-1.β_2m cells using pulse-chase analyses. After a 5 min pulse with [^{35}S]-methionine and cysteine some TAP1-associated tapasin-ERp57 conjugate was already detectable, regardless of β_2m expression (**Lane 1** in **Figures 2.3a** and **2.3b**). Conjugate formation then increased with identical kinetics in FO-1 and FO-1. β_2m cells (**Figure 2.3c**). When samples were run under reducing conditions, the signals from both ERp57 and tapasin were unchanged with time but tapasin was more strongly labeled, arguing that the majority of the dimer signal under non-reducing conditions arises from newly synthesized tapasin and resident ERp57 (**Figure 2.3d**). Identical results were obtained when the primary immunoprecipitations were performed with a monoclonal antibody (mAb) specific for ERp57 (**Figure 2.4a-d**).

2.4: Complete tapasin oxidation can occur after TAP association

Comparing **Figure 2.3a** with **Figure 2.3d**, the band corresponding to free tapasin became noticeably sharper at later chase points under non-reducing conditions. Under reducing conditions, however, tapasin clearly resolved as a single band. These data suggested that tapasin may initially associate with TAP in a partially oxidized state. To test this hypothesis, I examined the biosynthesis of the ERp57-tapasin conjugate in a pulse chase analysis by first immunoprecipitating for TAP1, releasing associated tapasin under non-reducing conditions with SDS, and resolving free and conjugated tapasin by

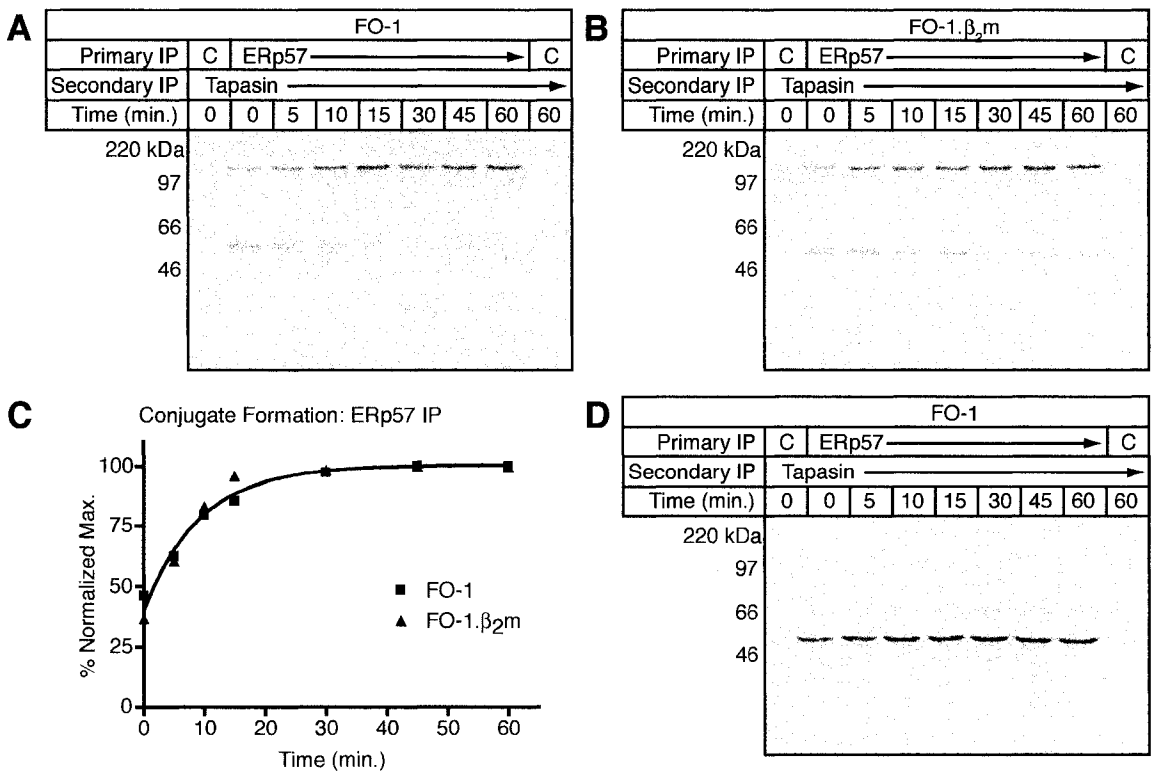

Figure 2.4: β_2m expression does not affect the rate of conjugate formation

A and B) IFN-γ treated FO-1 or FO-1.β_2m cells pulsed with [^{35}S]-methionine and cysteine for five minutes were chased for the indicated periods prior to solubilization in digitonin. Post-nuclear supernatants were precipitated with the anti-ERp57 mAb MaP.ERp57 or mouse IgG coupled to agarose beads (C = Ctrl). Associated proteins were stripped in 1% SDS and tapasin and its conjugate with ERp57 were reprecipitated with R.gp48C and protein A-sepharose.
C) Data from panels A and B presented as a percentage of the maximum ERp57-tapasin conjugate signal throughout the chase period.
D) Newly synthesized tapasin represents most of the radioactivity incorporated into the conjugate. Samples were prepared as in A and B, but gels were run under reducing conditions.

SDS-PAGE under both reducing and non-reducing conditions. Tapasin initially associates with TAP as a monomer in two oxidation states (**Figure 2.5**). Tapasin contains two luminal disulfide bonds, between Cys-295 and Cys-362 in the membrane-proximal immunoglobulin-like domain and between Cys-7 and Cys-71 in the N-terminal region. Ig domains fold relatively freely and independently, and a human tapasin Cys-295 mutant fails to associate with TAP (Dick et al., 2002; Isenman et al., 1979; Turnquist et al., 2004). It is highly likely, therefore, that upon TAP association tapasin contains an oxidized disulfide bond within the Ig domain, but the Cys-7-Cys-71 bond is initially reduced (upper band in Lane 2). Within 30 min of TAP association, all tapasin resolves as a single band of increased mobility consistent with full oxidation. The rate of ERp57/tapasin dimer formation is inversely related to the rate of disappearance of the upper band that putatively lacks the Cys-7-Cys-71 disulfide.

ERp57 can form a mixed disulfide with tapasin mutants lacking the Cys-7-Cys-71 disulfide bond (Dick et al., 2002), and it is therefore conceivable that the tapasin/ERp57 conjugate could form during the early folding stages of tapasin and persist after TAP association. Alternatively, the conjugate could form concurrently with or rapidly following complete tapasin oxidation. My experiments do not differentiate between these possibilities. Nevertheless, while ERp57 may play a role in tapasin folding after assembly with TAP, in contrast to the behavior expected for a protein disulfide isomerase, the association persists after tapasin has acquired the characteristics of a native protein, including full oxidation, functional activity and reactivity with conformation specific antibodies.

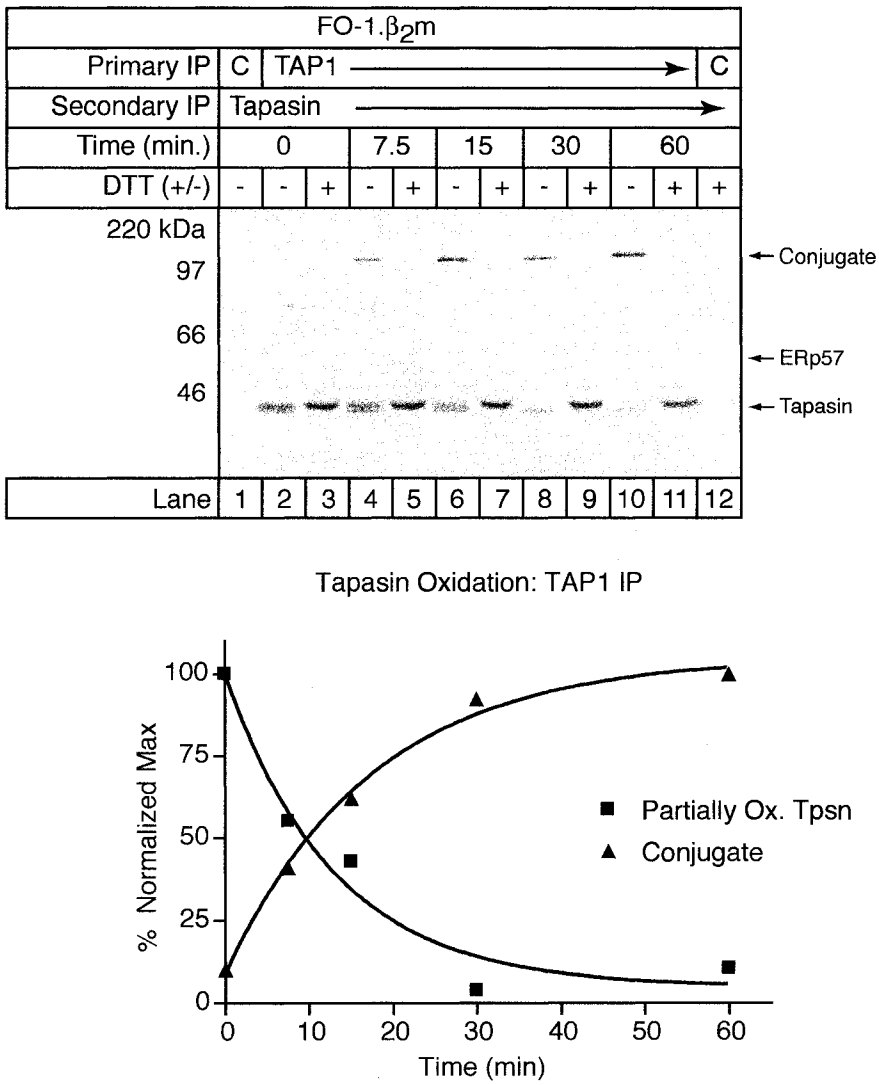

Figure 2.5: Tapasin completes oxidative folding after TAP association

IFN-γ-stimulated FO-1.β_2m cells pulsed with [^{35}S]-methionine and cysteine for 5 min were chased for the indicated times prior to solubilization in digitonin. Post-nuclear supernatants were precipitated with an anti-TAP1 mAb (148.3) or mouse IgG coupled to agarose beads (C=Ctrl), stripped, and reprecipitated with R.gp48C recognizing tapasin and protein A-sepharose. Samples were incubated with DTT before SDS-PAGE where indicated. The upper band in non-DTT treated samples represents partially oxidized monomeric tapasin, and the lower band corresponds to fully oxidized tapasin. The lower panel shows quantitation of the partially oxidized upper band and the conjugate throughout the chase period.

2.5: Conjugate formation is independent of tapasin glycosylation

I showed above that the mixed disulfide between tapasin and ERp57 can form in the absence of TAP-associated MHC class I HC/β_2m dimers, and these were the presumed source of glycans responsible for recruiting ERp57 into the PLC. However, tapasin is also a glycoprotein, and it remained possible that interactions between the lectin chaperones and glycosylated tapasin could promote ERp57 recruitment and conjugate formation (Ortmann et al., 1997; Sadasivan et al., 1996). To exclude this possibility, I used site directed mutagenesis to substitute an alanine residue for Asn-233, the residue that undergoes N-linked glycosylation in tapasin. This mutated construct was introduced into tapasin deficient 721.220 cells expressing HLA-B*4402 that were subsequently selected and cloned by limiting dilution. Tapasin expression was somewhat reduced in these cells, and expressed tapasin migrated somewhat faster, consistent with the loss of a single glycan (**Figure 2.6a, b**). Given the well-known role of N-linked glycans in stabilizing protein secondary and tertiary structure, it is likely that N233A mutant tapasin exhibits some local misfolding that adversely affects its steady-state expression. Despite this, however, N233A tapasin associated with TAP and recruited MHC class I and CRT into the PLC (**Figure 2.6c**). Consistent with this normal recruitment, HLA-B*4402 expressed in these cells achieved cell surface expression levels comparable to cells expressing WT-tapasin (**Figure 2.6d**). Finally, in cells pretreated with MMTS, N233A-tapasin formed high levels of the tapasin/ERp57 conjugate (**Figure 2.6c**). Some free tapasin was consistently seen in cells expressing mutant tapasin, and this is likely due to some degree of misfolding. Nevertheless, the

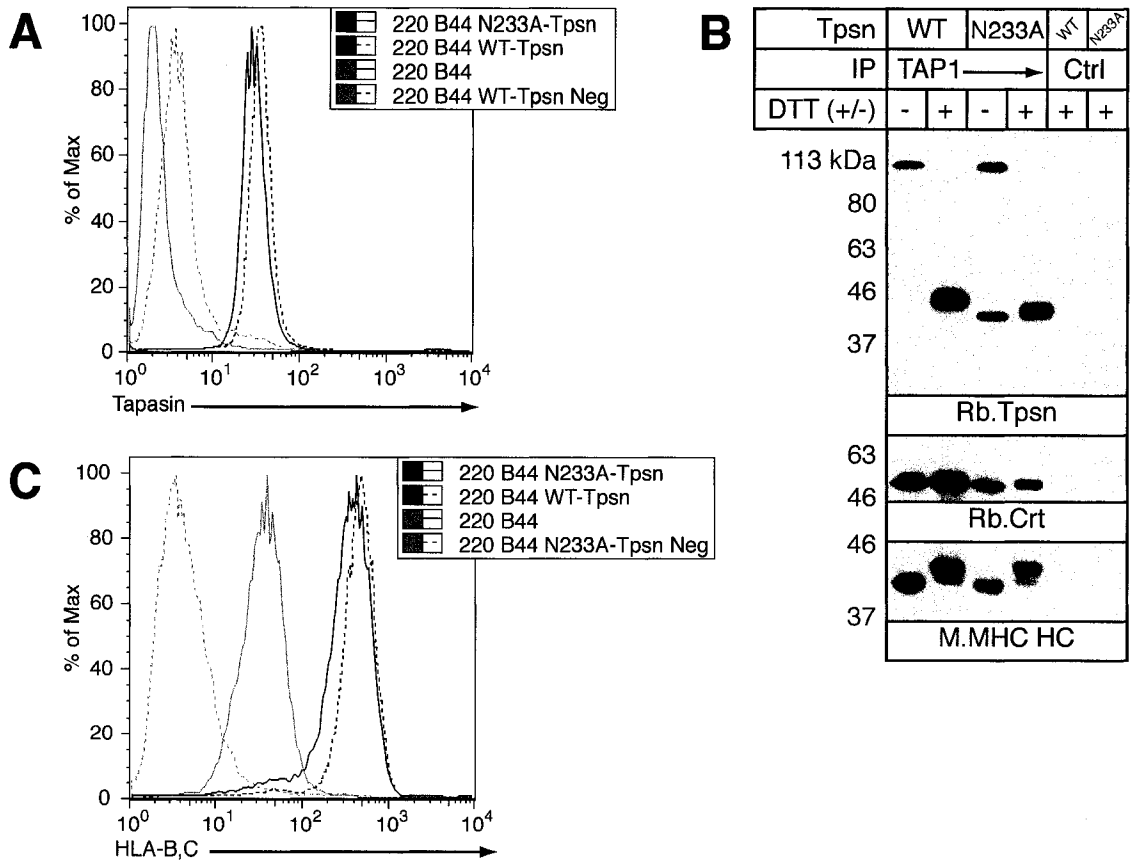

Figure 2.6: Conjugate formation is independent of tapasin glycosylation.

A) Generation of a glycan-deficient tapasin mutant. 721.220 cells expressing HLA-B*4402 with or without WT or N233A tapasin were fixed with 3.7% formaldehyde and permeabilized with 0.1% Triton X-100 in FACS buffer. Permeabilized cells were stained with mouse anti-tapasin (PaSta1) or anti-HLA-A*0201 (BB7.2) as a negative control for 30 minutes, washed, and incubated with a 1:100 dilution of goat anti-mouse-FITC secondary.

B) N233A tapasin forms the conjugate and recruits MHC class I HC and CRT into the PLC. 220.B4402 cells expressing either WT or N233A tapasin were treated with MMTS prior to solubilization in 1% digitonin. Post-nuclear supernatants were precipitated with the mouse anti-TAP1 antibody 148.3 or the mouse anti-HLA-DP antibody B7 coupled to agarose beads. After washing, immunoprecipitated material was resolved by SDS-PAGE under reducing or non-reducing conditions as indicated. Following transfer and blocking, membranes were incubated with a rabbit anti-serum raised against the C-terminus of tapasin(R.gp48C), rabbit anti-calreticulin, or mouse anti-MHC class I HC (HC10). Membranes were then incubated with species appropriate secondary antisera coupled to HRP, incubated with ECL substrate, and detected by exposure to film.

C) Normal MHC class I surface expression in N233A expressing cells. 721.220 cells expressing HLA-B*4402 with or without WT or N233A tapasin were incubated in 100 µL of 4E tissue culture supernatant, washed with FACS buffer, and incubated with 100 µL of 1:100 dilution of goat anti-mouse FITC. All steps were performed on ice.

glycan of tapasin is clearly not required for MHC class I, CRT, or ERp57 recruitment and conjugate formation.

2.6: Conjugate formation occurs in the absence of CNX or CRT

I showed above that, amongst MHC class I specific proteins, only tapasin is needed to recruit ERp57 normally. However, ERp57 is traditionally thought to be recruited to folding substrates through interactions with CRT and/or CNX (Oliver et al., 1999), and one model of loading complex assembly predicts that CNX is responsible for bringing ERp57 into the loading complex (Diedrich et al., 2001). To test this model, I examined conjugate formation in CEM.NKR cells deficient in CNX expression and their CNX expressing transfectants. These cells were treated with MMTS prior to solubilization in Triton X-100 and immunoprecipitation with the anti-tapasin mAb PaSta1. After reducing/non-reducing SDS-PAGE, membranes were blotted for tapasin using the antiserum R.gp48C. CNX was clearly not required for conjugate formation, however, as equal amounts of conjugate were seen in CNX deficient and competent cells (**Figure 2.7a**).

Human cell lines deficient in CRT expression have not been described. Gao et al. reported that in CRT deficient MEFs, ERp57 was associated with the loading complex, but they did not assess conjugate formation (Gao et al., 2002). These experiments are complicated by the fact that mouse MHC class I molecules possess at least one additional N-linked glycan, and a greater role for loading complex-associated CNX has been suggested for mouse cells (Suh et al., 1996). We obtained CRT deficient MEFs and their WT counterparts, and I treated IFN-γ induced

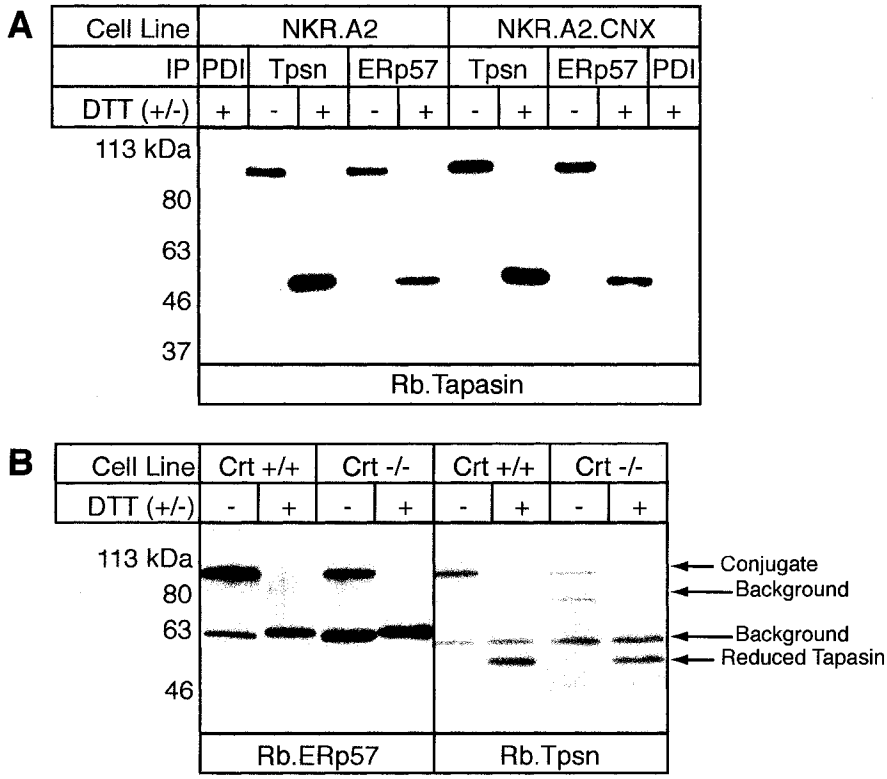

Figure 2.7: Calnexin and calreticulin are individually dispensable for conjugate formation.

A) CNX is dispensable for conjugate formation. CNX-negative CEM.NKR cells expressing HLA-A*0201 or HLA-A*0201 and CNX were treated with MMTS, solubilized in Triton X-100, and post-nuclear supernatants were precipitated with M.PDI, PaSta1 (anti-tapasin mAb), or MaP.ERp57 and protein G-sepharose. SDS-PAGE was performed under reducing or non-reducing conditions, and, following transfer, membranes were probed for tapasin with R.gp48C.
B) CRT is dispensable for conjugate formation. CRT deficient MEFs and their WT counterparts were induced with mouse IFN-γ for 48 hours prior to MMTS treatment and solubilization in 1% Triton X-100. Post-nuclear supernatants were resolved by SDS-PAGE under reducing or non-reducing conditions, and, following transfer, membranes were blotted with rabbit antisera raised against full-length recombinant human ERp57 (R.ERp57) or tapasin (R.SinA). The conjugate, reduced tapasin, and background bands are indicated by arrows in the R.SinA blot.

MEFs with MMTS prior to solubilization and blotting with anti-tapasin and anti-ERp57 antisera raised against full-length human versions of these proteins. Given the high degree of conservation of both ERp57 and tapasin between mice and humans, I reasoned that these reagents would likely cross-react with their murine orthologues. Indeed, despite the absence of ideal antibody reagents, I found that regardless of the expression of CRT all tapasin was conjugated to ERp57, and a substantial portion of ERp57 was conjugated to tapasin in IFN-γ induced MEFs (**Figure 2.7b**). Thus, I have individually eliminated the contribution of CRT, CNX, the MHC class I HC glycan, and the tapasin glycan for conjugate formation.

2.7: Conjugate formation is independent of monoglucosylated N-linked glycans

ERp57 is thought to assist glycoprotein folding exclusively through glycan-dependent interactions with CRT and CNX. These interactions depend on the generation of monoglucosylated glycans by the sequential removal of glucose residues by glucosidases I and II from the triply glucosylated core N-linked oligosaccharide ($Glc_3Man_9GlcNAc_2$). Incubation of cells with CST, a glucosidase inhibitor, blocks the glycan-dependent interactions of glycoproteins with CRT and CNX and prevents the recruitment of ERp57 to all folding substrates examined thus far (Hammond et al., 1994; Kang and Cresswell, 2002; Molinari and Helenius, 1999).

To ascertain the requirement for the generation of mono-glucosylated N-linked glycans, I examined the effects of CST on the formation of the ERp57-tapasin conjugate. When cells were starved, labeled and chased in the presence of 2 mM CST, the rate of conjugate formation was unaffected (**Figure 2.8**). The CST treatment was effective in

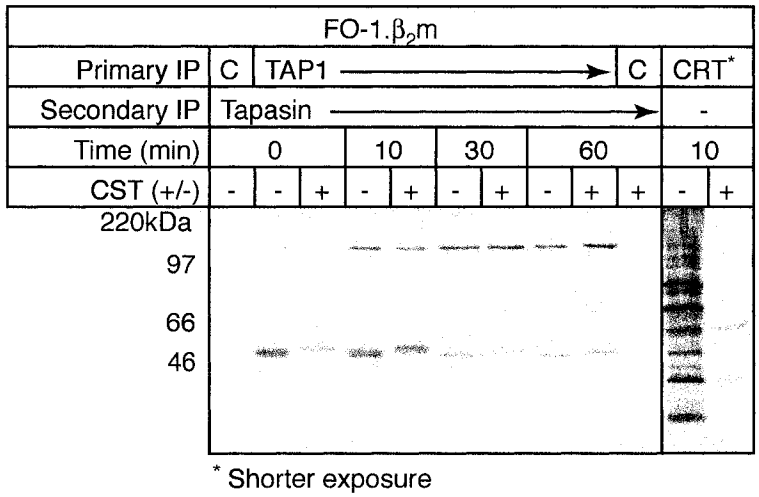

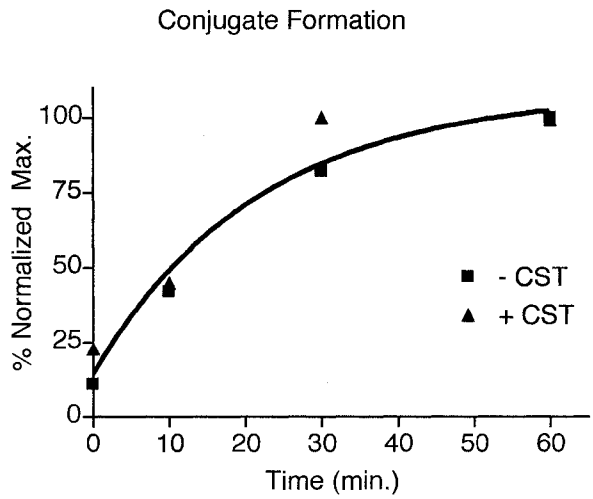

Figure 2.8: Mono-glucosylated N-linked glycans are not required for conjugate formation

IFN-γ-induced FO-1.β_2m cells were incubated with or without 2 mM castanospermine (CST) throughout starvation, pulse-labeling for 5 min. with [^{35}S]-methionine and cysteine, and chase. Post-nuclear supernatants of digitonin lysates were precipitated with an anti-TAP1 mAb (148.3) or mouse IgG coupled to agarose beads (C=Ctrl), stripped, and reprecipitated with R.gp48C recognizing tapasin and protein A-sepharose. Immunoprecipitated tapasin and its conjugate with ERp57 were subjected to SDS-PAGE without reduction. The lower panel depicts the percent maximum conjugate signal throughout the chase period. Post-nuclear supernatants from cells chased for 10 minutes were precipitated with rabbit anti-calreticulin (Rb.CRT) and protein A-sepharose to confirm the successful inhibition of glucose trimming following treatment with CST.

that it inhibited the bulk of CRT-substrate interactions (right lane). Additionally, the mobility of monomeric tapasin isolated from CST-treated cells was slightly lower than that from untreated cells. The increased molecular weight likely corresponds to the additional, untrimmed glucose residues resulting from CST treatment.

2.8: Discussion

The events surrounding the assembly of the MHC class I loading complex have been extensively examined, but most studies were completed prior to the observation that tapasin and ERp57 form a mixed disulfide within the loading complex (Bangia et al., 1999; Diedrich et al., 2001; Gao et al., 2002; Hughes and Cresswell, 1998). Because a tapasin mutant unable to form the conjugate with ERp57 is impaired in its ability to promote peptide loading, I examined the kinetics and characteristics of conjugate formation in greater detail to better understand the biochemical events leading to the formation of this important component of the MHC class I loading complex (Dick et al., 2002).

My data provide new insight into MHC class I peptide loading complex formation. Previously, TAP with non-covalently associated tapasin was thought to comprise the core functional unit of the loading complex (Momburg and Tan, 2002), but my data indicate that ERp57 conjugated to tapasin is also a core component. Conjugate formation does not correlate with the incorporation of MHC class I/β_2m heterodimers into the loading complex, arguing against a role for MHC class I in recruiting ERp57. It was previously suggested that CNX could fulfill this role, but cells deficient in CNX are fully competent for conjugate formation (Diedrich et al., 2001). A role for CRT in

recruiting ERp57 to TAP is unlikely because CRT is not found associated with TAP or tapasin in the absence of β_2m, a condition I now find compatible with full conjugate formation (Diedrich et al., 2001; Sadasivan et al., 1996), and cells deficient in CRT are able to form the conjugate to the same extent as WT cells. Additionally, the kinetics of conjugate formation and ERp57 recruitment to TAP are not affected when the generation of CRT and CNX binding sites is blocked by CST. The covalent linkage of tapasin and ERp57 may facilitate the assembly of the peptide loading complex by stabilizing the much weaker non-covalent interactions between tapasin and MHC class I heavy chain, CRT and ERp57, and the MHC class I heavy chain glycan and CRT.

Our previous inability to detect the ERp57-tapasin conjugate in β_2m-deficient FO-1 cells was likely due to a combination of factors, including less efficient conjugate preservation with NEM compared to MMTS and reduced tapasin expression without IFN-γ treatment. It is possible that Cys-60 of ERp57, which is required for activation of the escape pathway and release of tapasin, is less accessible to NEM in the absence of β_2m while MMTS is able to react equally well in its presence or absence. Tapasin may also exist in slightly different conformations within the loading complex that could affect the accessibility of Cys-60. More experiments are needed to resolve this issue, but it is clear from the experiments in **Figure 2.2** that at steady state all the cellular tapasin is disulfide linked to ERp57, and that this is not affected by the presence or absence of β_2m, TAP1, TAP2, or MHC class I HC.

The tapasin/ERp57 conjugate was previously detected in cells deficient in β_2m (Antoniou and Powis, 2003; Dick et al., 2002). This was under steady state conditions, however, and the low levels of conjugate observed could be explained by its transient

formation and rapid reduction in the absence of other stabilizing factors within the MHC class I loading complex. In the absence of β_2m, virtually no CRT and very little free MHC class I heavy chain is found associated with TAP (Harris et al., 2001; Hughes and Cresswell, 1998; Sadasivan et al., 1996). My data argue that the rate of formation and steady-state level are not affected by β_2m expression nor by the presence of other factors recruited into the loading complex by MHC class I heavy chain/β_2m dimers.

In the pulse-chase analysis, some free tapasin was seen at all chase points, in contrast to the results obtained by Western blotting. I have no explanation for these differences, but I have limited my conclusions from each set of experiments to those appropriate for the technique employed. That is to say, Western blotting most accurately represents the steady-state conditions, and pulse-chase analyses are the only means to assess the kinetics of assembly of the loading complex.

While there are implications of my findings specific to loading complex formation, the data are also significant in the general context of glycoprotein folding. The nature of the interaction of ERp57 with tapasin and the loading complex is quite different from that with other substrates. The interaction between the MHC class I heavy chain and CRT is abolished in the presence of CST, and CST inhibits the interaction of ERp57 with all substrates examined to date (Elliott et al., 1997; Kang and Cresswell, 2002; Molinari and Helenius, 1999; Oliver et al., 1997; Sadasivan et al., 1996; Van der Wal et al., 1998). The mixed disulfide formed with tapasin is the only identified exception. Additionally, conjugate formation occurs equally well in the presence or absence of CNX in human cells or CRT in MEFs. Doubly deficient cells would be needed to fully address the requirement of CNX and CRT for conjugate formation, but

the CST experiments clearly indicate that conjugate formation is independent of the presence of a monoglucosylated N-linked glycan on tapasin or within the loading complex.

My data indicate that the behavior of ERp57 with respect to conjugate formation and the MHC class I loading complex differs dramatically from its normal activity associated with glycoprotein folding. Protein-protein interactions between ERp57 and tapasin alone are sufficient to promote conjugate formation, and, under normal conditions, tapasin does not form mixed disulfides with other ER resident oxidoreductases despite the high degree of conservation and expression equal to or greater than ERp57. Thus, tapasin specifically recruits ERp57 into the MHC class I loading complex, and this likely at least partially explains our ability to biochemically detect the conjugate with sulfhydryl reactive reagents. However, additional mechanisms may stabilize the tapasin/ERp57 conjugate *in vivo*.

Chapter 3: Biochemical events following peptide loading

The high levels of the tapasin/ERp57 conjugate achieved through the specific recruitment of ERp57 by tapasin no doubt facilitate the detection of this mixed disulfide. However, oxidoreductase/substrate interactions are typically transient and exist in equilibrium between free and mixed-disulfide forms prior to the acquisition of native structure. The absence of free tapasin under all conditions examined indicates this equilibrium is dramatically shifted towards the conjugate, suggesting that the redox activity of tapasin-associated ERp57 may be altered. I first examined the ability of tapasin to modulate the redox activity of ERp57 within the PLC, and non-covalent interactions between tapasin and ERp57 inhibit the escape pathway normally associated with disulfide bond reduction. This was observed under steady-state conditions, but peptide loading onto MHC class I molecules is an active event. The key time during this process is likely the period that MHC class I/β_2m dimers are engaged with the PLC, and the events surrounding peptide loading in the ER and PLC remain somewhat of a "black box." To clarify the dynamics of MHC class I complex assembly, I showed that reduction of the conjugate does not occur during peptide loading, reinforcing my hypothesis that the conjugate plays a structural role in the PLC. I next examined the interaction of CRT with the PLC. By specifically inhibiting the incorporation of newly synthesized MHC class I/β_2m dimers into the PLC using RNAi against β_2m, I was able to follow changes in PLC composition following the release of peptide loaded MHC class I molecules. As expected, levels of MHC class I HC associated with the PLC decreased following transfection of β_2m-specific siRNA duplexes. In these cells, conjugate levels did not

change with time, but PLC-associated CRT decreased with similar kinetics as MHC class I HC. Incorporating the data from Chapters 2 and 3, I have constructed a new model of MHC class I loading complex formation and cycling.

3.1: Exposure to cytoplasmic contents, dilution, and time do not lead to conjugate reduction

Trapping mutants of ERp57 can form stable mixed disulfides with a variety of undefined substrates (Dick and Cresswell, 2002), but chemical crosslinking reagents are required for the detection of substrate interactions with WT ERp57, with the exception of viral glycoproteins in virally infected cells (Molinari and Helenius, 1999). In such cells, host protein translation is inhibited and viral proteins are highly expressed. Current models of oxidative protein folding predict the transient existence of mixed disulfides due to the rapid activation of the Trx escape pathway and enzymatic reduction (Sevier and Kaiser, 2002). When particular substrates are abundant, mixed disulfides may exceed the minimal levels needed for detection. This most likely explains the findings in virally infected cells, and is consistent with our ability to detect the tapasin-ERp57 conjugate following the 8-fold increase in tapasin expression induced by IFN-γ and its subsequent recruitment of ERp57. However, the absence of free tapasin in these cells suggests that the normal cycles of mixed disulfide formation and reduction may be slowed or eliminated for tapasin-associated ERp57.

ERp57 is non-covalently associated with the complete MHC class I loading complex isolated from cells which have not been treated with NEM or MMTS, arguing that reduction of the disulfide bond with tapasin occurs at some point during the isolation process (Hughes and Cresswell, 1998; Lindquist et al., 1998; Morrice and Powis, 1998). Biochemical isolation from the lumen of the ER involves several steps that could lead to the reduction of the tapasin-ERp57 conjugate and dissociation of free ERp57, including exposure to elevated cytosolic levels of glutathione, extended time periods not

compatible with conjugate preservation, and detergent effects both during solubilization and SDS-PAGE. To better characterize the conditions that lead to conjugate reduction, I prepared membranes from cells treated or untreated with MMTS. The membrane isolation process requires several hours and involves both the dilution of cellular material as well as the mixing of cytosolic and luminal contents, but it takes place in the absence of detergents until the addition of SDS sample buffer. Once membranes were separated from the soluble cellular components, they were subsequently treated or untreated with MMTS. If conjugate reduction is a consequence of mixing, dilution, or the duration of isolation, free tapasin should be seen in isolated membranes treated with MMTS. However, all tapasin remained conjugated to ERp57 in MMTS treated membranes, suggesting that other factors lead to conjugate reduction (**Figure 3.1**).

3.2: Tapasin inhibits the ERp57 escape pathway

The preservation of the conjugate during membrane isolation in the absence of detergent suggests that non-covalent interactions between ERp57 and tapasin were responsible for the preservation of the conjugate, and the disruption of these interactions by detergent during isolation and analysis promoted reduction of the mixed disulfide. Immunoisolation of tapasin from cells solubilized in the non-denaturing detergents digitonin and Triton X-100 and subsequent incubation of material with the denaturing detergent SDS prior to SDS-PAGE leads to conjugate reduction (Dick et al., 2002). To differentiate between detergent effects occurring during isolation or during sample preparation for SDS-PAGE, I prepared membranes from cells not treated with MMTS and resuspended the membranes in buffer alone, 1.0% Triton X-100, or 0.1% SDS. The

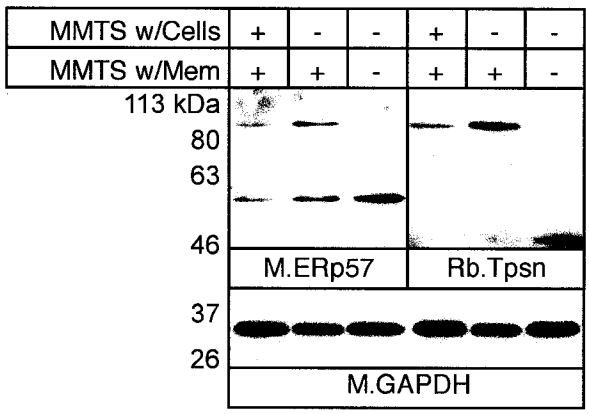

Figure 3.1: The tapasin/ERp57 conjugate is stable after exposure to cytoplasmic contents, dilution, and extended biochemical purification.

IFN-γ induced FO-1.β_2m cells were treated with MMTS as indicated prior to freeze thaw lysis and membrane preparation by ultracentrifugation. Membranes were resuspended in TBS with or without MMTS for five minutes prior to the addition of Triton X-100. All membranes were solubilized for 30 minutes in detergent prior to centrifugation. After non-reducing SDS-PAGE and transfer, blots were cut into three pieces and probed with mouse anti-ERp57 (MaP.ERp57), rabbit anti-tapasin (R.SinA), or mouse anti-GAPDH (M.GAPDH) as a loading control.

samples were then incubated with or without MMTS prior to heating to 95° C for 5 minutes in 1% SDS, conditions that lead to complete protein denaturation, and precipitated with a conformation independent anti-tapasin antiserum. As can be seen in **Figure 3.2**, the complete disruption of native non-covalent interactions by heating in SDS promoted conjugate reduction in membranes not treated with MMTS (Lane 1), but the conjugate was preserved when MMTS was added before SDS addition (Lane 3). Note that these lanes were run under non-reducing conditions. Simple membrane solubilization in Triton X-100 (Lane 5) or 0.1% SDS (Lane 7) promoted conjugate reduction to some extent, but only when all non-covalent interactions were disrupted by heating in 1% SDS did full conjugate reduction occur. Thus, within intact membranes under native conditions, non-covalent interactions between tapasin and ERp57 appear to inhibit escape pathway activation and preserve the conjugate, and my current model of this process is depicted in **Figure 3.3**.

The tapasin-ERp57 conjugate exists within the peptide loading complex, which contains multiple non-covalently interacting proteins (Wright et al., 2004). I performed the experiments in **Figure 3.2** with 721.221 cells that do not express HLA-A, B, or C alleles to limit possibly confounding effects arising from cooperative interactions within the MHC class I loading complex, but identical results were obtained with IFN-γ treated HeLa-M and FO-1.β_2m cells fully competent for MHC class I loading (data not shown).

3.3: Conjugate reduction does not occur during the course of peptide loading

Our ability to biochemically observe the tapasin-ERp57 mixed disulfide is likely a result of two independent factors, the high conjugate levels achieved secondary to the

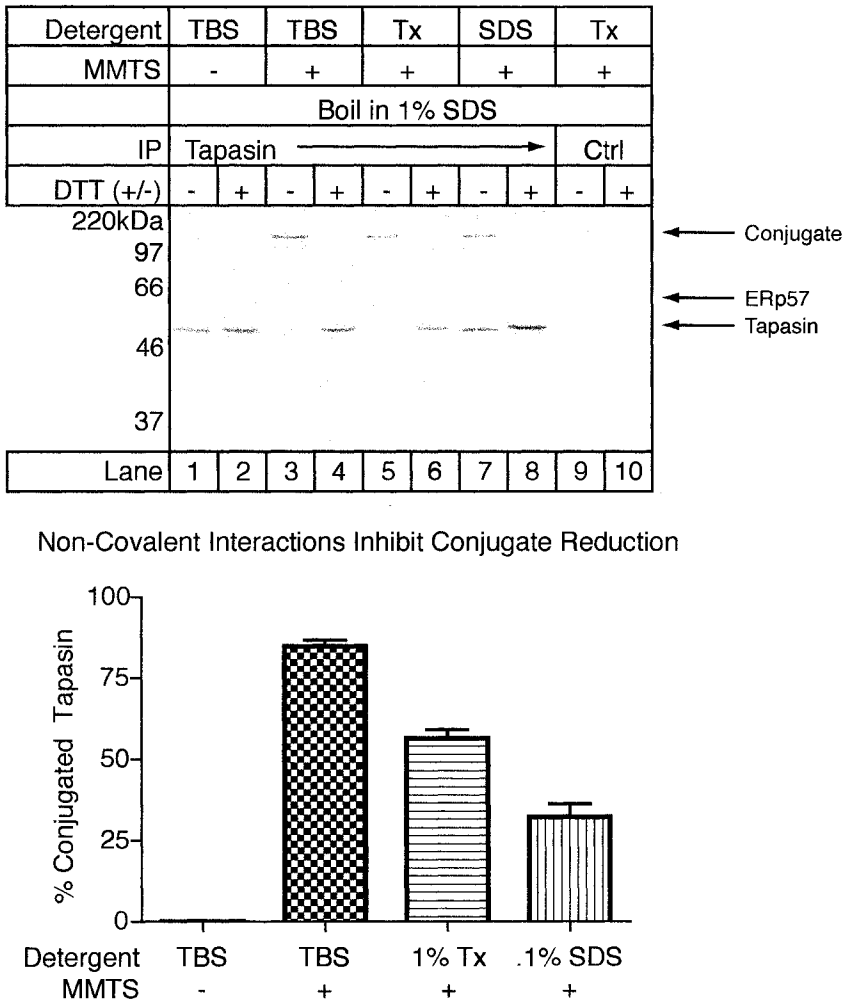

Figure 3.2: Non-covalent interactions prevent conjugate reduction

Non-covalent interactions within the MHC class I loading complex inhibit ERp57 escape pathway activation. HLA-A, B and C-negative 721.221 cells were labeled with [^{35}S]-methionine and cysteine for 30 min and chased for an additional 30 min before membrane preparation. Membranes were resuspended in TBS, 1% Triton X-100, or 0.1% SDS in TBS with 1mM $CaCl_2$ for 1 hr on ice before MMTS addition where indicated. All samples were then heated at 95° C for 5 min in 1% SDS, brought to 1 ml with 1% Triton X-100 in TBS with 2 mM MMTS, and immunoprecipitated with rabbit anti-tapasin (R.SinA) or normal rabbit serum (Ctrl) and protein A-sepharose. SDS-PAGE was performed under non-reducing or reducing conditions as indicated, and percent conjugated tapasin was calculated. Data shown are the mean ± SEM of two independent experiments.

specific recruitment of ERp57 into the loading complex and the preservation of this mixed disulfide through the inhibition of the ERp57 escape pathway. I examined conjugate stability and composition under steady-state conditions in **Figures 3.1** and **3.2**, but conjugate reduction could be dynamically regulated by tapasin. Given the preferential recruitment of ERp57 into the PLC by tapasin, unconjugated tapasin would likely rapidly reform a mixed disulfide with ERp57, and a substantial population of unconjugated tapasin would not likely be detectable under these conditions. To examine the kinetics of conjugate formation and reduction during the course of peptide loading, I used cells expressing either FLAG-tagged WT or C60A mutant ERp57 in addition to endogenous ERp57 (Dick et al., 2002). I hypothesized that if tapasin is regulating the activity of the ERp57 escape pathway, released ERp57 could be replaced in the loading complex by either endogenous ERp57 or the exogenously expressed, FLAG-tagged WT or C60A trapping mutant. Because the escape pathway is inactivated by mutagenesis in C60A-FLAG mutant ERp57, reduction of conjugates containing this mutant would not occur. Thus, if there is free exchange of ERp57 between loading complex associated and free ERp57 pools, C60A-FLAG ERp57 should accumulate in the loading complex with time. It should act as a "dominant negative" mutant with respect to conjugate reduction. The presence of C60A-FLAG ERp57 within the loading complex can be detected by boiling non-MMTS treated samples in SDS. Tapasin-ERp57 conjugates containing WT-FLAG or endogenous ERp57 will become reduced upon denaturation, but C60A-FLAG containing conjugates will remain in a mixed disulfide (**Figure 3.4a**).

I first examined the steady-state composition of the conjugate in C1R cells expressing HLA-A*0201 and either FLAG-tagged WT or C60A ERp57 (**Figure 3.4b**).

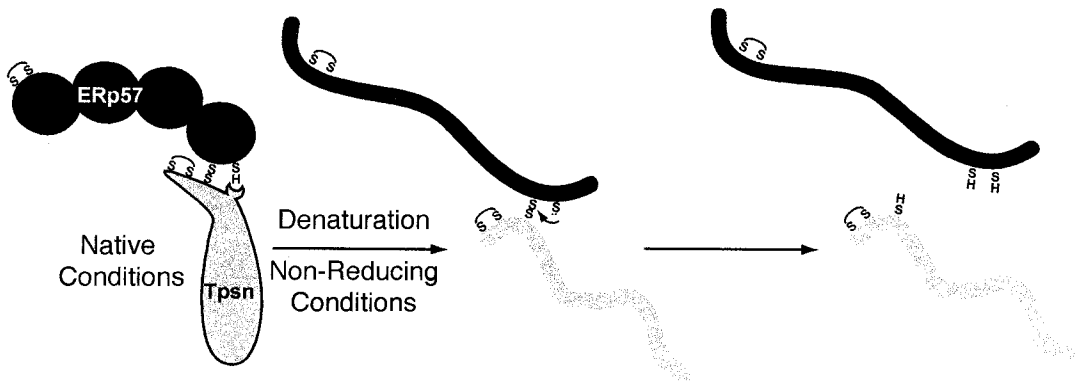

Figure 3.3: Non-covalent interactions between tapasin and ERp57 prevent escape pathway activation

Under native conditions, non-covalent interactions between tapasin and ERp57 eliminate the ability of the sulfhydryl of Cys-60 of ERp57 to attack the mixed disulfide between tapasin and ERp57. I hypothesize that tapasin reduces the access of Cys-60 to the mixed disulfide and/or alters the local redox environment to prevent Cys-60 deprotonation. When denatured, the interactions of tapasin with ERp57 are disrupted, and the sulfhydryl of Cys-60 is now able to attack the mixed disulfide leading to conjugate reduction. I speculate that the mixed disulfide with tapasin serves a structural rather than enzymatic function.

As expected, all tapasin in either cell line treated with MMTS was detected in the conjugate (Lanes 1 and 7). Cells expressing WT-FLAG ERp57 in addition to endogenous ERp57 had no detectable conjugate after immunoprecipitation and blotting in the absence of MMTS (Lane 3). In contrast, cells expressing C60A-FLAG ERp57 contained a mixture of unconjugated and conjugated tapasin in the absence of MMTS treatment, indicating that the loading complexes of these cells contain a mixture of endogenous and exogenously expressed ERp57 (Lane 9).

The loading complexes of cells expressing C60A-FLAG ERp57 contain a mixture of tapasin conjugated to endogenous or exogenous ERp57, but the experiment shown in **Figure 3.4b** only represents a "snap shot" of the peptide loading complex composition. To examine changes in loading complex composition dynamically, I labeled and chased WT- or C60A-FLAG ERp57 expressing cells (**Figure 3.5**). Cells, not treated with MMTS unless indicated, were solubilized in digitonin and precipitated for tapasin prior to boiling in SDS sample buffer. Eluted material was then resolved by SDS-PAGE under reducing or non-reducing conditions. As expected, in the cells expressing WT-FLAG ERp57, no conjugate was seen in cells untreated with MMTS after boiling in SDS without DTT (Lanes 2, 4, 6, 8, and 10, upper panel), but MMTS treatment at the 1 hour chase point led to conjugate preservation (Lane 13). In contrast, cells expressing both endogenous ERp57 and C60A-FLAG ERp57 had substantial amounts of detectable conjugate in the absence of MMTS treatment (Lanes 2, 4, 6, 8, and 10, lower panel). More significantly, the total proportion of reduced tapasin did not change over the course of the experiment, arguing that C60A-ERp57 does not accumulate in the loading complex with time (Lane 2 v. Lane 10, for example). The time-scale of this pulse-chase is

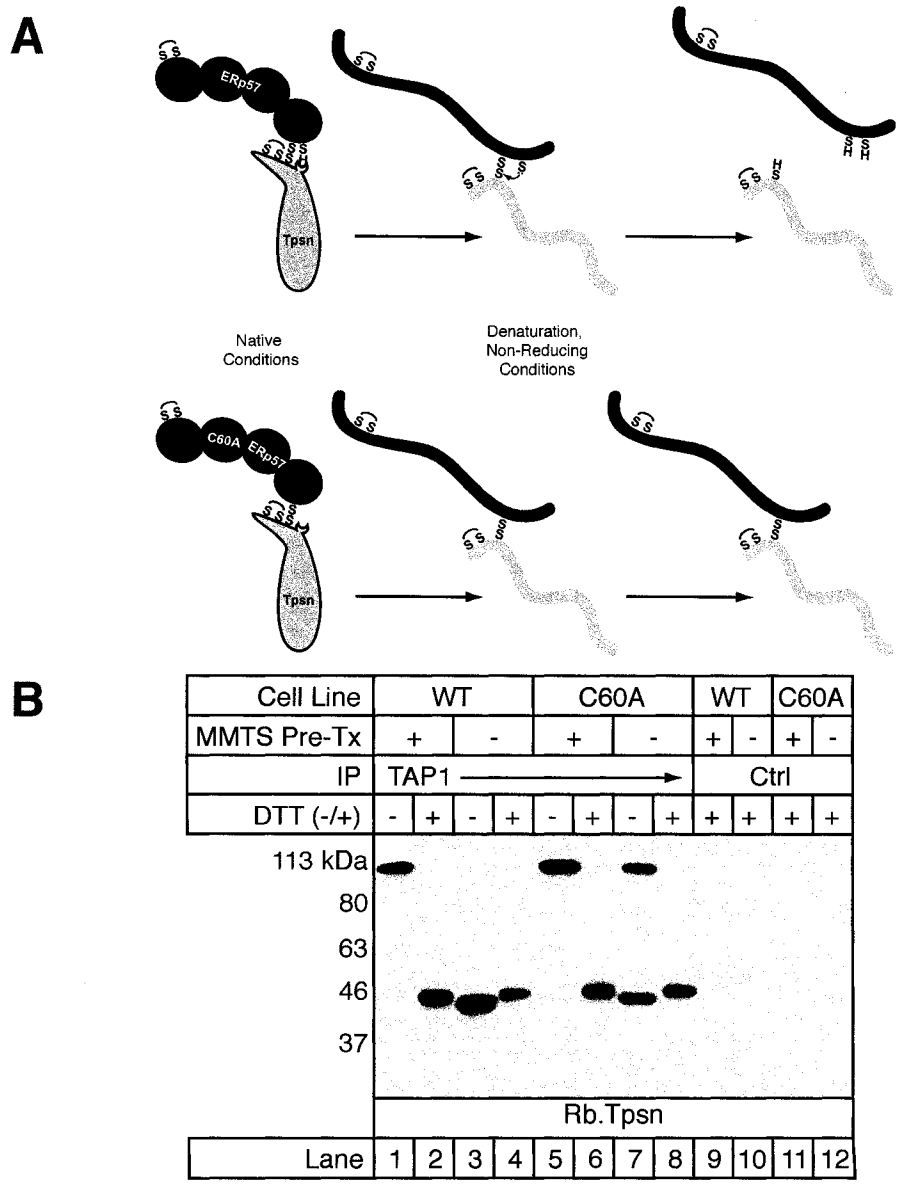

Figure 3.4: PLCs contain a mixture of endogenous and C60A ERp57 under steady-state conditions.

A) C60A containing conjugates are resistant to denaturation-induced reduction. Upon boiling in SDS, denaturation relieves the inhibition of the ERp57 escape pathway leading to the reduction of conjugates containing WT ERp57. Conjugates containing the C60A escape pathway mutant are resistant to denaturation-induced reduction.
B) PLCs contain a mixture of endogenous and C60A ERp57 under steady-state conditions. C1R cells expressing HLA-A*0201 and WT or C60A ERp57 in addition to endogenous ERp57 were treated with MMTS as indicated prior to solubilization in 1% digitonin. Post-nuclear supernatants were precipitated with the mouse anti-TAP1 antibody 148.3 or the mouse anti-HLA DP antibody B7 (Ctrl) coupled to agarose beads. After washing, immunoprecipitated material was resolved by SDS-PAGE under reducing or non-reducing conditions as indicated. Following transfer and blocking, tapasin was detected by probing with R.gp48C.

compatible with peptide loading as evidenced by the decrease in tapasin-associated MHC class I HC. Thus, regulated conjugate reduction does not appear to occur during peptide loading. Once incorporated into the MHC class I loading complex, ERp57 is permanently sequestered.

3.4: β_2m RNAi decreases PLC-associated MHC class I HC and CRT, but conjugate levels are not affected

MHC class I is predicted to associate with the peptide loading complex, become loaded with high affinity peptides, and depart the loading complex and ER for eventual presentation to CD8+ T cells at the cell surface (Cresswell, 2000). In order to study the events that take place surrounding peptide loading and the departure of MHC class I/β_2m/peptide complexes from the loading complex, I needed to devise a way to specifically prevent the incorporation of newly synthesized MHC class I/β_2m complexes from entering the PLC without disrupting the loading and departure of previously assembled complexes. These stringent criteria eliminated the use of commonly used chemical inhibitors because they would tend to globally affect protein folding and/or the generation of peptide ligands. However, the inhibition of β_2m translation by RNAi should specifically inhibit the generation of new MHC class I/β_2m dimers without affecting other aspects of cellular physiology.

I determined the optimal β_2m specific siRNA oligonucleotides mediating the greatest extent of β_2m knock-down by examining cell surface MHC class I levels after transfection (data not shown). Once identified, I transiently transfected 721.220 cells expressing HLA-B*0801 and tapasin with either β_2m specific or control siRNA

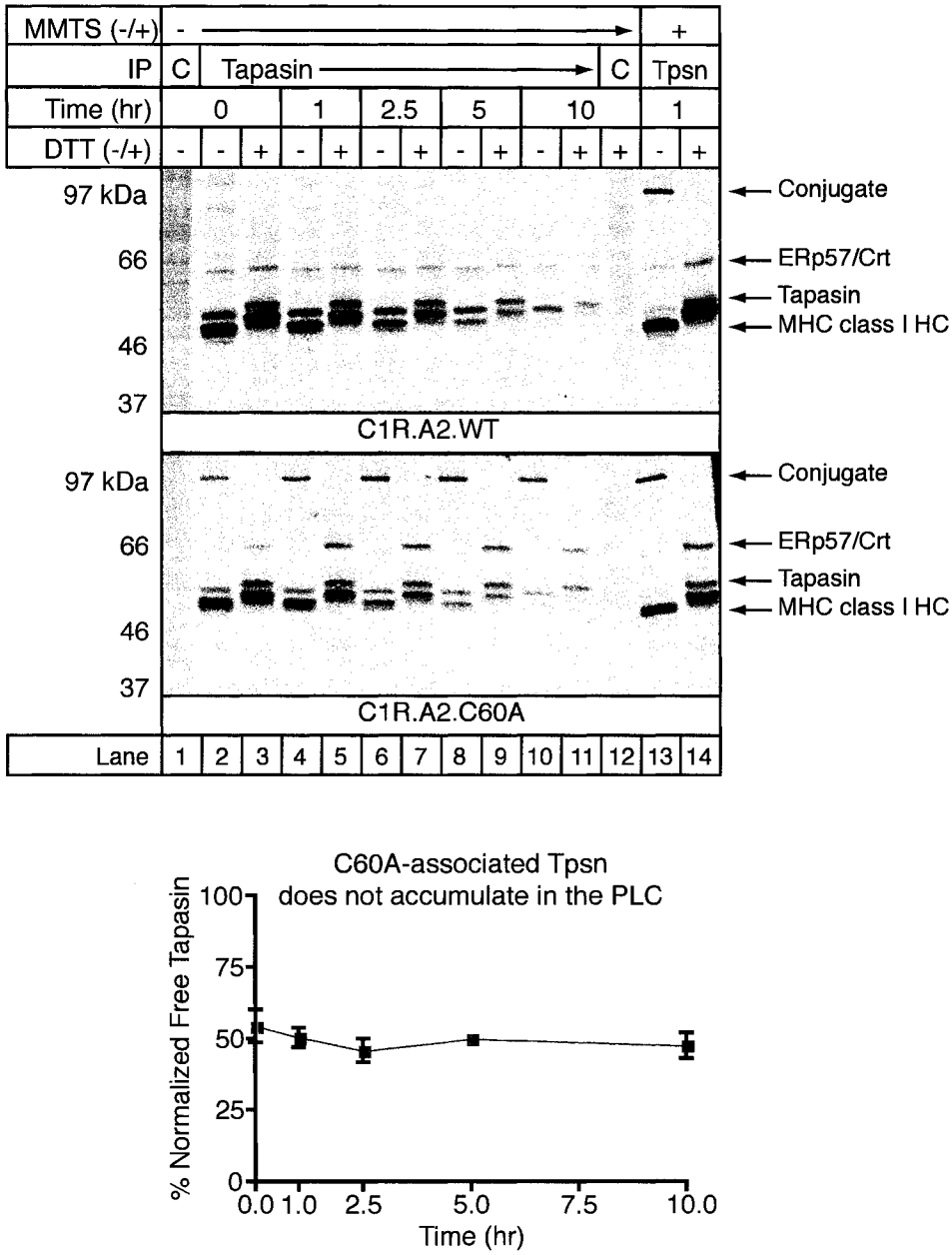

Figure 3.5: The conjugate does not undergo escape pathway mediated reduction during peptide loading.

C1R cells expressing HLA-A*0201 and FLAG-tagged WT or C60A ERp57 were labeled with [^{35}S]-methionine and cysteine for 45 min. and chased for the indicated periods of time prior to treatment with or without MMTS as indicated. Frozen cell pellets were solubilized in 1% digitonin and pre-cleared post nuclear supernatants were immunoprecipitated with the anti-tapasin mAb PaSta1 or anti-OX-68 (Ctrl) coupled to agarose beads. Samples were washed with 0.1% Triton X-100 and resolved by SDS-PAGE under reducing or non-reducing conditions as indicated. Bands corresponding to tapasin were quantitated, and the amount of free tapasin under non-reducing conditions was normalized to the total amount of tapasin present after reduction. The chart depicts the mean +/- SEM of two independent experiments.

oligonucleotides. Cells were harvested at different times after transfection and treated with MMTS. Digitonin lysates were immunoprecipitated for TAP1, and, following non-reducing SDS-PAGE, the relative amounts of PLC-associated tapasin-ERp57 conjugate, TAP1, CRT, and MHC class I HC were examined. As can be seen in **Figure 3.6**, transfection of cells did not affect the levels of TAP1 or TAP1-associated conjugate. As expected, the amount of loading complex-associated MHC class I HC decreased with time following β_2m knock-down. Additionally, loading complex associated CRT decreased with similar kinetics and to a similar extent as MHC class I HC. Thus, MHC class I HC is needed to recruit CRT into the loading complex, but the departure of (presumably) peptide loaded MHC class I/β_2m complexes and CRT from the PLC are closely related (Sadasivan et al., 1995).

3.5: Discussion

Oxidative folding in the ER is an extremely important process, and aberrant disulfide formation can negatively affect protein expression, normal cellular physiology, and ultimately organism viability. To facilitate oxidative folding, a complex system of enzymes that transfer electrons between the cytosol and recipient proteins has evolved in bacteria and eukaryotes (Ellgaard and Ruddock, 2005; Kadokura et al., 2003). A common motif present in most of these enzymes is the Trx N-CXXC-C motif frequently contained in the highly conserved Trx domain (Sevier and Kaiser, 2002). During an oxidation reaction, the N-terminal cysteine residue forms a mixed disulfide with the substrate protein, and the deprotonated C-terminal cysteine residue attacks this mixed disulfide leading to substrate release and intramotif disulfide formation. This disulfide

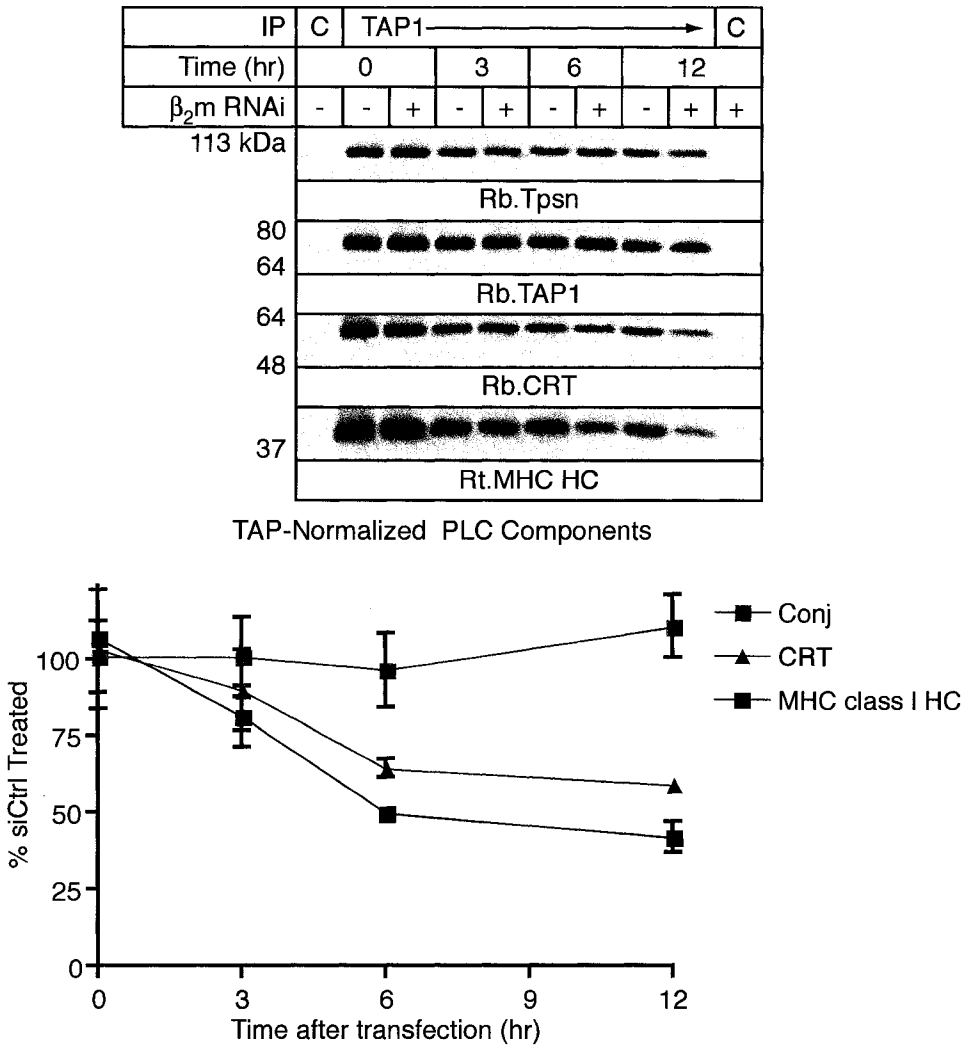

Figure 3.6: Calreticulin departs the loading complex following peptide loading.

721.220 cells expressing HLA-B*0801 and WT tapasin were transfected with β_2m-specific or nonspecific siRNA oligonucleotides using the Amaxa nucleofector device. Cells were harvested at the indicated times, treated with MMTS, and frozen. Digitonin solubilized cell pellets were precipitated with the anti-TAP1 mAb 148.3 or mIgG coupled to agarose beads and resolved by non-reducing SDS-PAGE. After transfer, membranes were cut into four pieces and blotted with rabbit anti-tapasin (R.gp48C), anti-TAP1 (RING.4C), anti-CRT, and rat anti-MHC class I HC (3B10.7). Samples were quantitated using a Storm 860 imaging system and Imagequant software. PLC components were normalized to the signal for TAP1, and the chart depicts the mean +/- SEM of three independent experiments.

bond can be reduced directly by glutathione, and Ero1 is responsible for generating the oxidizing potential of the ER (Jessop and Bulleid, 2004; Mezghrani et al., 2001). The enzymatic mechanism of PDI is the best studied amongst eukaryotic and mammalian Trx-family ER resident oxidoreductases. Activation of the Trx motif escape pathway within PDI is an extremely rapid process that occurs in both native and denatured proteins, and the rate constant for formation of the intradomain disulfide bond within the PDI *a* domain is $10 - 30\ s^{-1}$ (Darby and Creighton, 1995; Walker and Gilbert, 1997). Thus, the Trx domain active site has evolved to rapidly and efficiently release bound substrates for subsequent rounds of oxidative folding. The accumulation of substrate-enzyme mixed disulfides or misfolded proteins containing aberrant disulfide bonds could overwhelm the folding capacity of the ER leading to the release of misfolded and dysfunctional proteins, the cessation of protein translation, or the induction of apoptosis, the end result of a chronic unfolded protein response (Schroder and Kaufman, 2005).

My data indicate that the normal enzymatic activity of the ERp57 *a* domain does not occur when it is associated with tapasin, but the elimination of non-covalent interactions by the denaturation of ERp57 and/or tapasin relieves the inhibition and allows reduction to proceed normally, as it would for a typical ERp57 substrate. Additionally, we have shown that tapasin alone is capable of mediating this inhibition using purified recombinant proteins (Peaper et al., 2005). Thus, tapasin has evolved to specifically recruit and stabilize ERp57 within the MHC class I loading complex.

Our understanding of the events surrounding MHC class I peptide loading has evolved. With the discovery of the tapasin-ERp57 conjugate, models were proposed wherein the conjugation state of tapasin could be related to peptide loading. One model

predicted that preassembled complexes of CRT, ERp57, MHC class I HC, and β_2m were incorporated into the loading complex through associations with tapasin (Antoniou et al., 2003). A non-mutually exclusive model predicted that conjugate reduction precedes the release of peptide loaded MHC class I molecules (Dick, 2004; Wright et al., 2004). The absence of large amounts of non-conjugated tapasin associated with the loading complex argues against these models (**Figure 2.2**), but steady-state analyses may not accurately reflect the active process of peptide loading.

To better understand the dynamics of peptide loading, I used two complementary approaches. First, using reagents existing in the lab, I analyzed the reduction and oxidation of the tapasin-ERp57 conjugate during peptide loading. These experiments demonstrated that escape pathway mediated conjugate reduction does not occur within the loading complex over the course of 10 hours, a period during which peptide loading was clearly occurring. It remains possible that the conjugate is reduced independently of escape pathway activity, but this is unlikely. My findings are contrary to the model of Wright et al. and support a static, structural role for ERp57 within the loading complex. The precise role of ERp57 in peptide loading remains elusive, but I have conducted experiments toward resolving this function (See Chapter 4).

Once associated, ERp57 appears to be permanently sequestered within the loading complex. Thus, replacement of PLC-associated ERp57 by ERp57 associated with CRT/MHC class I HC/β_2m complexes does not appear to take place. However, CRT is found associated with MHC class I HC/β_2m dimers in both the presence and absence of tapasin ((Turnquist et al., 2002) and Pamela Wearsch, manuscript in preparation), and it remained possible that complexes lacking ERp57 could incorporate into the PLC upon

the departure of peptide loaded MHC class I/β_2m dimers. In order for this to occur, PLC-associated CRT would have to dissociate to allow for the incorporation of newly synthesized, empty MHC class I HC/β_2m dimers associated with CRT. When this was examined by preventing the assembly of new MHC class I/β_2m dimers through inhibiting the translation of β_2m using RNAi, CRT departed the loading complex with similar kinetics and to a similar extent as MHC class I HC. Thus, despite the ability of CRT to interact with ERp57, the continued presence of CRT in the loading complex depends on the incorporation of newly synthesized MHC class I HC/β_2m dimers. When the data from the literature and Chapters 2 and 3 are considered together, I generated the model of conjugate and MHC class I loading complex formation and action depicted in **Figure 3.7**.

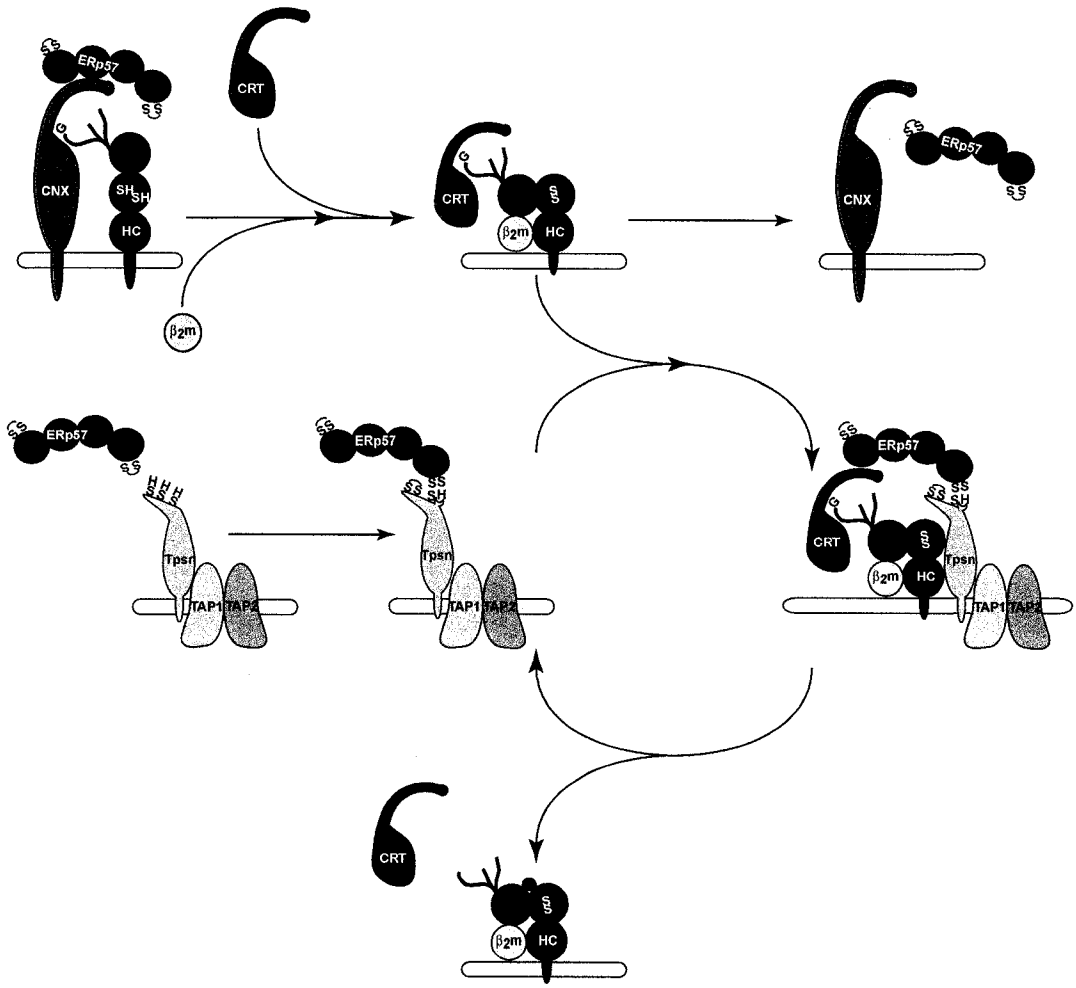

Figure 3.7: The folding and assembly of MHC class I loading complex components.

CNX mediates the early folding stages of MHC class I heavy chain prior to its association with β_2m. Complete heavy chain oxidation occurs during this time, and ERp57 facilitates this process. Once associated and properly oxidized, MHC class I HC/β_2m complexes rapidly associate with CRT. In parallel, newly synthesized tapasin associates with TAP with a reduced Cys7-Cys71 disulfide bond; this bond becomes oxidized at some point during complex assembly. Conjugate formation with ERp57 proceeds rapidly after TAP association independently of lectin binding by CRT or CNX. CRT/HC/β_2m sub-complexes rapidly associate with the TAP/tapasin/ERp57 sub-complex. Through unknown mechanisms in a tapasin-dependent manner, the loading complex facilitates the generation of highly stable MHC class I/peptide complexes leading to the release of loaded MHC class I molecules and CRT. The core subcomplex of TAP/tapasin/ERp57 is then able to facilitate peptide loading onto additional MHC class I molecules.

Chapter 4: Altered PLC structure and function in the absence of ERp57

Although initially identified in the PLC in 1998, the role of ERp57 in peptide loading remains unclear eight years later. Two key studies have addressed the functional significance of ERp57 within the PLC, but they examined different systems that make universal conclusions difficult. Dick et al. used a tapasin mutant unable to form the mixed disulfide with ERp57 to determine the role of conjugate formation in HLA-B*4402 peptide loading (Dick et al., 2002). In contrast, Garbi et al. used ERp57-deficient mouse B cells to primarily study H2-K^b loading (Garbi et al., 2006). Both of these studies used NEM to preserve the conjugate, but the increased efficiency of conjugate preservation with MMTS may allow for more accurate data to be obtained. Thus, I sought to expand the initial work of Dick et al. using 721.220 cells expressing HLA-B*4402 and WT or C95A tapasin, emphasizing the contrasting conclusions reached by Garbi et al. As expected, some aspects of peptide loading differed between these systems, but broadly applicable conclusions can be drawn about the role of ERp57 in peptide loading. Specifically, the recruitment of MHC class I HC into the PLC appears to depend upon conjugate formation in a species-independent manner, but changes in the maturation and stability of MHC class I complexes varied between HLA-B*4402 and H2-K^b. Additionally, I show that conjugate formation alters the conformational stability of tapasin, suggesting a possible mechanism for the altered recruitment of MHC class I and CRT into the PLC in the absence of ERp57.

4.1: Impaired loading complex formation in cells expressing a tapasin mutant unable to form the conjugate

Tapasin in which Cys-95 is mutated to Ala (C95A) is unable to form the conjugate with ERp57, and the initial characterization of cells expressing HLA-B*4402 and this mutant emphasized qualitative differences in PLC composition compared to cells expressing WT tapasin. In particular, C95A-tapasin containing PLCs were able to recruit both MHC class I HC and CRT to some extent, and mutant tapasin was recognized by the conformation specific anti-tapasin mAb PaSta1 (Dick et al., 2002). In contrast, a tapasin mutant in which the N-terminal 50 amino acids were deleted did not recruit CRT or ERp57 into the PLC, and MHC class I was recruited much less efficiently. This mutant also did not react with either PaSta1 or PaSta2, an additional conformation specific anti-tapasin antibody (data not shown and (Bangia et al., 1999)). Additionally, mouse B cells deficient in ERp57 expression had altered PLC recruitment of MHC class I HC and CRT (Garbi et al., 2006).

There could be a number of reasons why differences were observed between mouse cells lacking ERp57 expression and human cells expressing a tapasin mutant that does not form a mixed disulfide with ERp57. Thus, I wished to reexamine the PLC composition in C95A-tapasin expressing cells using a more quantitative approach to more fully determine the phenotype of these cells in relation to ERp57-deficient cells. Additionally, MMTS has proven more effective at preserving the tapasin/ERp57 conjugate than NEM, and this could reveal more pronounced differences between WT- and C95A-expressing cells.

MMTS treated 721.220 cells expressing HLA-B*4402 and either WT or C95A tapasin were treated with MMTS, and the PLC was immunoprecipitated from digitonin lysates using the anti-TAP1 mAb 148.3. Serial dilutions representing a 10-fold difference were resolved by reducing SDS-PAGE, and the individual loading complex components were blotted with appropriate reagents for fluorimetry and quantitation (**Figure 4.1**). As expected, TAP1 and tapasin levels were identical in TAP1 immunoprecipitates from cells expressing WT and C95A tapasin. Additionally, no ERp57 was associated with C95A-containing PLCs. Consistent with previous reports, both CRT and MHC class I HC were recruited to TAP1 by C95A mutant tapasin, but the extent of recruitment in these cells was much less than that seen in cells expressing WT tapasin. PLCs from C95A-expressing cells contained only 25% of the CRT and MHC class I HC compared with WT-expressing cells.

4.2: Delayed maturation and impaired stability of MHC class I complexes assembled in 220.B4402.C95A-Tapasin cells

After their synthesis and loading in the ER, MHC class I/β_2m complexes travel through the Golgi apparatus on their way to the cell surface. Within the Golgi, further glycan processing takes place, and, after passage through the medial Golgi, glycans become resistant to cleavage by Endoglycosidase-H (EndoH). Monitoring the rate at which MHC class I/β_2m complexes acquire EndoH resistance is a traditional method for assessing the rate of MHC class I peptide loading and maturation.

H2-K^b molecules assembled in ERp57-deficient B cells acquired EndoH resistance more rapidly than in cells expressing ERp57. Additionally, these complexes

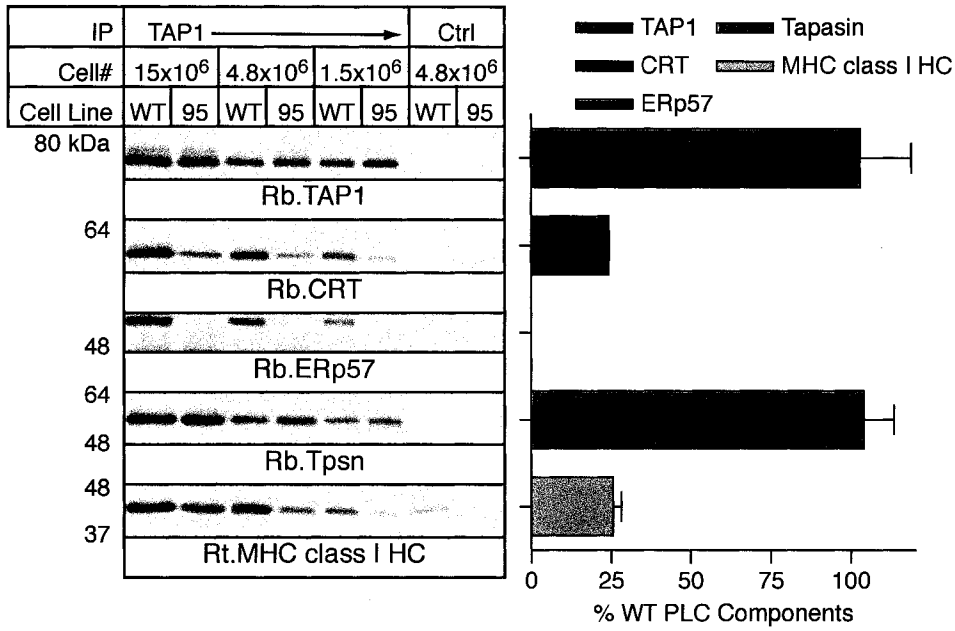

Figure 4.1: MHC class I HC and CRT are inefficiently incorporated into conjugate-deficient PLCs.

721.220 cells expressing HLA-B*4402 and either WT or C95A tapasin were treated with MMTS prior to solubilization in 1% digitonin. Post-nuclear supernatants were immunoprecipitated with the mouse anti-TAP1 antibody 148.3 or the mouse anti-HLA-DP antibody B7 coupled to agarose beads as a control (Ctrl). After washing, immunoprecipitated material was eluted under reducing conditions and separated by SDS-PAGE. Following transfer and blocking, membranes were cut and individually probed with rabbit antisera raised against the C-terminal peptide of TAP1 (RING.4C), CRT, the C-terminal peptide of ERp57 (R.ERp57-C), the N-terminal peptide of tapasin (R.gp48N), or rat anti-MHC class I HC (3B10.7). Samples were quantitated using a Storm 860 imaging system and Imagequant software. Signals corresponding to PLC components precipitated from C95A cells were normalized to those from WT-tapasin expressing cells. Values are the mean +/- SEM for the dilutions, and this is representative of three independent experiments.

were less stable as measured by their more rapid internalization from the cell surface (Garbi et al., 2006). When the thermostability and $t_{1/2}$ of HLA-B*4402/β_2m complexes assembled in C95A-expressing cells were examined, these complexes were also less stable than those from WT-expressing cells (Dick et al., 2002). However, the initial characterization of these cells emphasized the long-term stability of MHC class I/ β_2m complexes. Therefore, I wished to examine the rate of short-term maturation of HLA-B*4402 assembled in C95A-expressing cells.

721.220 cells expressing HLA-B*4402 and either WT or C95A tapasin were pulse-labeled with [^{35}S]-methionine and cysteine for 15 minutes and chased for different lengths of time in the presence of excess cold methionine and cysteine. Cells were solubilized in digitonin prior to immunoprecipitation with the conformation specific anti-MHC class I/β_2m antibody W6/32. Digitonin preserves the interactions of the PLC, but W6/32 does not precipitate PLC-associated MHC class I complexes. Thus, only free MHC class I/β_2m dimers were precipitated in this experiment. Precipitated material was then incubated with EndoH overnight and resolved by SDS-PAGE (**Figure 4.2**). Surprisingly, the rate at which MHC class I/β_2m complexes acquired EndoH resistance was only slightly, but significantly, delayed in C95A-expressing cells. However, consistent with previous reports, substantially fewer W6/32 complexes survived for the four hours of the experiment. Those complexes that acquired EndoH resistance were relatively long-lived, however. Taken together, these results suggest that C95A mutant tapasin supports peptide loading to a lesser extent that WT tapasin, but a sub-set of complexes assembled in these cells is somewhat stable.

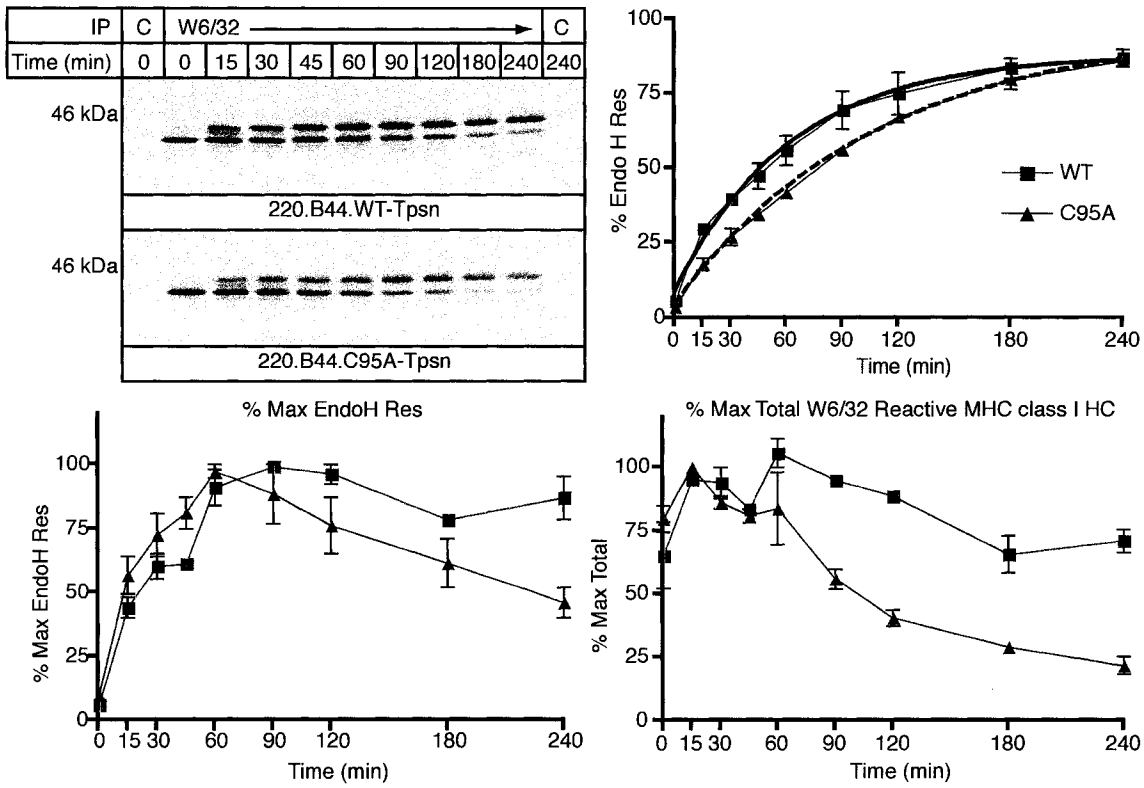

Figure 4.2: Delayed maturation and enhanced dissociation of MHC class I/β_2m complexes assembled in the presence of conjugate-deficient tapasin.

721.220 cells expressing HLA-B*4402 and either WT or C95A tapasin were pulse-labeled with [^{35}S]-methionine and cysteine for 15 minutes and chased for the indicated periods of time. Frozen cell pellets were solubilized in 1% digitonin, and post-nuclear supernatants were immunoprecipitated with the anti-MHC class I HC/β_2m conformation specific antibody W6/32 or the CD1d specific antibody 51.1.3 as a control and protein A-sepharose. Samples were washed with 0.1% Triton X-100 in TBS, eluted in 2x EndoH buffer with heating to 95° C, and incubated with 1 mU EndoH overnight at 37° C. Digested material was then resolved by reducing SDS-PAGE. Bands corresponding to EndoH resistant (upper band) and sensitive (lower band) MHC class I HC were quantitated, and the % EndoH resistant MHC class I HC was calculated (upper right panel). Signals were further expressed as % Max EndoH Res MHC class I HC (lower left panel) and % Max Total MHC class I HC (lower right panel) as a measure of the overall stability of W6/32 reactive complexes throughout the chase period. The mean +/- SEM of two independent experiments is shown.

4.3: Impaired recruitment and retention of MHC class I HC by C95A tapasin

Under steady-state conditions in the presence of C95A mutant tapasin, less MHC class I HC and CRT were associated with the PLC than in the presence of WT tapasin. This could be explained by the dissociation of these components during biochemical isolation. The coordinating interaction of CRT with ERp57 in these complexes could be essential for the stability of the PLC in detergent extracts, but, *in vivo*, MHC class I HC and CRT could be recruited normally. To differentiate between these possibilities, I performed a pulse-chase analysis to examine the kinetics of MHC class I HC association with the PLC. I hypothesized that if the loss of MHC class I HC from TAP1 immunoprecipitates is an artifact of detergent solubilization the same proportion of MHC class I HC should be lost from the PLC at each time point. In this model, the absolute amount of MHC class I HC associated with C95A tapasin containing PLCs would be less, but the relative amount of PLC-associated MHC class I HC should be constant. Additionally, the rate of MHC class I egress from the PLC would be the same for both C95A and WT tapasin containing PLCs. Alternatively, if there truly is a defect in the recruitment and/or stabilization of MHC class I HC in mutant PLCs, then both the absolute and relative amount of PLC-associated MHC class I HC should be different in WT- and C95A-expressing cells.

I labeled 721.220 cells expressing HLA-B*4402 and either WT or C95A tapasin with [^{35}S]-methionine and cysteine for 15 minutes and chased them in the presence of an excess of cold methionine and cysteine for up to four hours. The PLC was immunoprecipitated from MMTS-treated cells using a rabbit antiserum raised against TAP1, and Triton X-100 was used to dissociate subcomplexes containing tapasin, ERp57,

CRT, MHC class I HC, and β_2m from the TAP heterodimer. After reducing SDS-PAGE, the bands corresponding to MHC class I HC were quantitated, and the %Maximum TAP-associated MHC class I HC was calculated for each time point (**Figure 4.3**). As expected, the intensity of the MHC class I HC band associated with C95A tapasin was much less than that from WT PLCs despite similar tapasin labeling. The rate at which labeled MHC class I departed the loading complex also differed substantially between these two cell lines. Thus, the differences in steady-state MHC class I association with the PLC are at least partially attributable to decreased recruitment and retention by C95A tapasin. These experiments cannot exclude the contributions of the interaction of CRT with ERp57, but this will be addressed in the future.

4.4: Conjugation alters the conformational stability of tapasin

The absence of ERp57 from the PLC clearly adversely affects the recruitment of MHC class I and CRT. There are a number of non-mutually exclusive explanations for this observation. Garbi et al. proposed that ERp57 recruits MHC class I HC into the PLC, but they did not speculate about the mechanism(s) controlling this recruitment (Garbi et al., 2006). It is possible that interactions between the ERp57 *b* and *b'* domains and the CRT P-domain indirectly recruit MHC class I HC into the PLC, and, once incorporated, additional interactions between tapasin and MHC class I HC would stabilize the mature subcomplex. The recruitment of MHC class I through direct interactions with ERp57 seems unlikely. Alternatively, conjugate formation could generate an additional binding site for MHC class I on tapasin itself. In the absence of ERp57, low affinity interactions between tapasin and MHC class I HC could mediate the degree of recruitment and

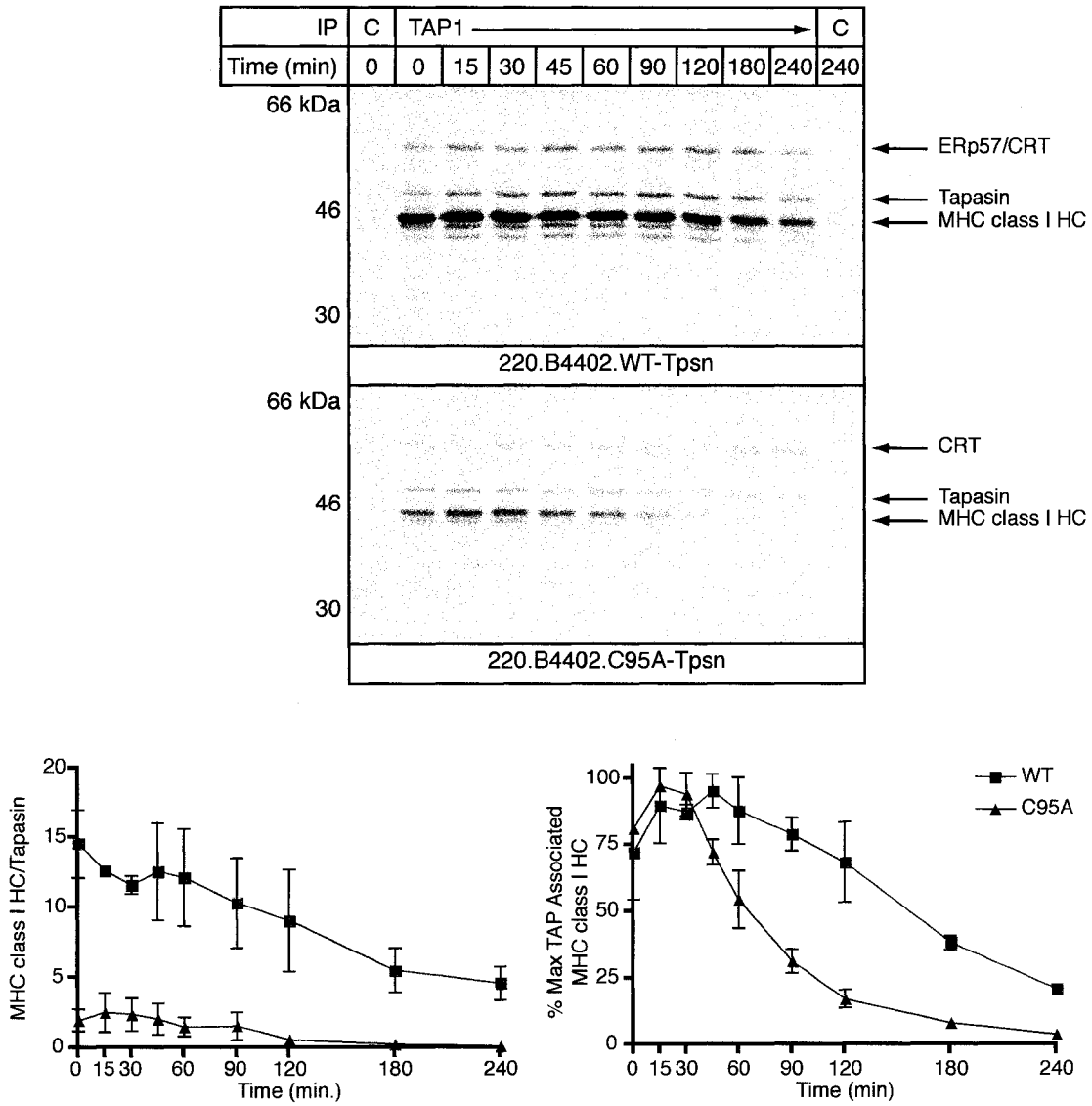

Figure 4.3: Decreased association and more rapid MHC class I egress from conjugate deficient PLCs.

721.220 cells expressing HLA-B*4402 and either WT or C95A tapasin were pulse-labeled with [^{35}S]-methionine and cysteine for 15 minutes and chased for the indicated periods of time. MMTS treated frozen cell pellets were solubilized in 1% digitonin, and post-nuclear supernatants were pprecipitated with rabbit anti-TAP1 (RING4C) or NRS (C=Ctrl) and protein A-sepharose. Precipitated material was washed with 0.1% digitonin in TBS prior to elution in 0.1% Triton X-100 in TBS for 5 min at 4° C. Eluted material was incubated with reducing sample buffer and resolved by SDS-PAGE. The bands corresponding to MHC class I HC and tapasin were quantitated and expressed as the % Maximum TAP associated MHC class I HC (lower right panel), and the MHC class I HC/tapasin ratio was also calculated (lower left panel). The mean +/- SEM of two independent experiments is shown.

peptide loading observed in C95A-expressing cells, but the absence of a conjugate-dependent high affinity binding site would prevent peptide loading comparable to WT cells.

I hypothesized that conjugate formation could affect the tertiary structure of tapasin in some way. C95A tapasin reacts with the conformation specific antibodies PaSta1 and PaSta2 and is able to support some degree of peptide loading (data not shown and (Dick et al., 2002). However, WT and C95A tapasin could respond differently to detergent and/or heating. To examine this possibility, I radio-labeled 721.220 cells expressing HLA-B*4402 and WT or C95A tapasin with [^{35}S]-methionine and cysteine for one hour and chased them for one hour in the presence of excess cold methionine and cysteine to allow the cells to reach some degree of steady-state conditions with respect to conjugate formation. MMTS treated cell lysates were immunoprecipitated with the anti-TAP1 antiserum RING4C, and tapasin and associated components were eluted with 0.1% Triton X-100. Triton eluates were split and incubated for 30 minutes at different temperatures. Aggregated material was removed by centrifugation, and supernatants were immunoprecipitated with either PaSta1 or R.gp48C, a conformation independent rabbit antiserum (**Figure 4.4**). As expected, the amount of tapasin immunoprecipitated with R.gp48C was not affected by heating. In contrast, heating to 40° C caused the amount of PaSta1-precipitable WT tapasin to decrease by 30%, and only 10% of the level of unheated WT tapasin was precipitated with PaSta1 after heating to 45° C. Surprisingly, incubation at both 4° C and 24° C did not affect the PaSta1 reactivity of C95A tapasin, but only 15% of C95A tapasin remained PaSta1 reactive after only 30 minutes at 37° C. Virtually no C95A tapasin was precipitated by PaSta1 after heating to

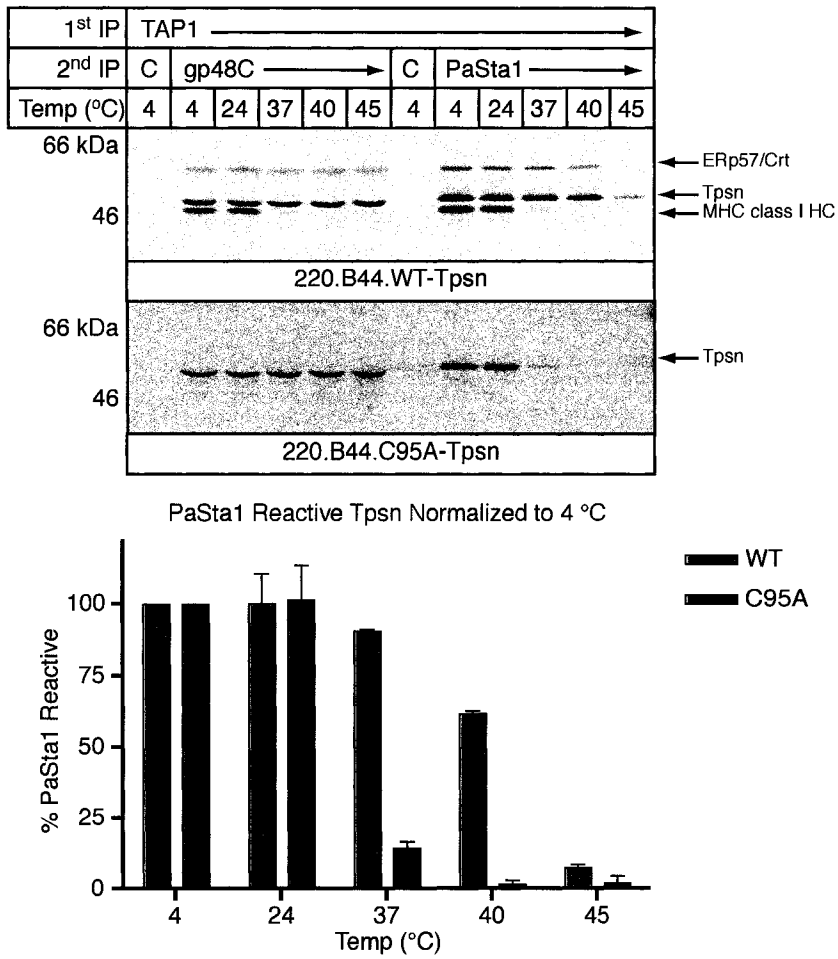

Figure 4.4: The conformational stability of C95A tapasin is decreased.

721.220 cells expressing HLA-B*4402 and WT or C95A tapasin were labeled with [^{35}S]-methionine and cysteine for 1 hr and chased for 1 hr prior to MMTS treatment. Cells were solubilized in 1% digitonin, and precleared post-nuclear supernatants were immunoprecipitated with mouse anti-TAP1 (148.3) coupled to agarose beads. After washing in 0.1% digitonin, samples were eluted in 0.1% Triton X-100 in TBS for 5 min on ice. Eluted material was incubated for 30 minutes at the indicated temperature, allowed to sit on ice for 10 min, and aggregates were pelleted by spinning at 14,000 RPM in a microcentrifuge at 4° C. Supernatants were then precipitated with a conformation independent rabbit anti-tapasin antiserum (R.gp48C) or NRS and protein A-sepharose or the conformation specific mouse anti-tapasin mAb PaSta1 or mouse anti-OX68 as a control coupled to agarose beads. Samples were separated by reducing SDS-PAGE. Precipitated material was visualized after exposure to a phosphor screen and bands corresponding to tapasin were quantitated using a Storm 820 imaging system and Imagequant software. Tapasin bands were normalized to that specifically immunoprecipitated from unheated (4° C) samples, and the mean +/- SEM of two independent experiments is shown.

40° C or 45° C. Thus, the conformational stability of C95A tapasin is lower than that of WT tapasin.

4.5: Unconjugated, WT tapasin is less thermostable than conjugated, WT tapasin

Cys-95 of tapasin is clearly needed to form a mixed disulfide with ERp57, and mutation of this residue to Ala altered the susceptibility of tapasin to a heating induced conformational change. However, the loss of PaSta1 reactivity following heating of C95A tapasin could be unrelated to the conjugation state and instead arise due to direct effects of this mutation. To exclude this possibility, I used a cell line expressing WT tapasin in which ERp57 expression was knocked-down by 90% using RNA interference (RNAi). These cells will be described in greater detail in Chapter 5, but there is an increased population of unconjugated WT tapasin associated with the PLC.

721.220 cells expressing HLA-B*4402 and WT tapasin with suppressed expression of ERp57 were labeled and chased as described above. Triton X-100 eluates from TAP1 immunoprecipitations were incubated on ice or at 37° C for 30 minutes prior to centrifugation and re-precipitation with either R.gp48C or PaSta1 (**Figure 4.5**). The bands corresponding to conjugated and unconjugated tapasin were quantitated and normalized to material precipitated by PaSta1 incubated at 4° C. As seen above, heating to 37° C did not affect the ability of R.gp48C to precipitate free or conjugated tapasin (Lanes 1 and 2). Additionally, PaSta1 precipitated nearly 100% of conjugated tapasin after incubation at 37° C (Conj band, lanes 3 and 4). In contrast, only 10% of unconjugated tapasin remained PaSta1 reactive after incubating at 37° C (tapasin band,

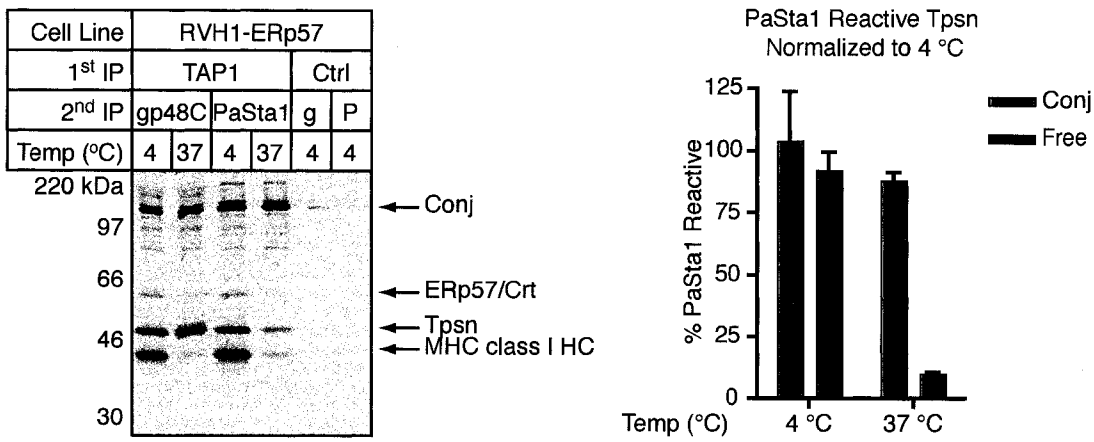

Figure 4.5: WT, unconjugated tapasin is less thermostable than WT, conjugated tapasin.

721.220 cells expressing HLA-B*4402 and WT tapasin with suppressed ERp57 were labeled with [^{35}S]-methionine and cysteine for 1 hr and chased for 1 hr prior to MMTS treatment. Cells were solubilized in 1% digitonin, and precleared post-nuclear supernatants were immunoprecipitated with mouse anti-TAP1 (148.3) or mouse anti-OX68 as a control coupled to agarose beads. After washing in 0.1% digitonin, samples were eluted in 0.1% Triton X-100 in TBS for 5 min on ice. Eluted material was incubated for 30 minutes at the indicated temperature, allowed to sit on ice for 10 min, and aggregates were pelleted by spinning at 14,000 RPM in a microcentrifuge at 4° C. Supernatants were then precipitated with a conformation independent rabbit anti-tapasin antiserum (R.gp48C, g) and protein A-sepharose or the conformation specific mouse anti-tapasin monoclonal antibody PaSta1 (P) coupled to agarose beads. Samples were resolved by non-reducing SDS-PAGE. Precipitated material was visualized after exposure to a phosphor screen and bands corresponding to free and conjugated tapasin were quantitated using a Storm 820 imaging system and Imagequant software. Signals were normalized to that specifically immunoprecipitated from unheated (4° C) samples, and the mean +/- SEM of two independent experiments is shown.

lanes 3 and 4). Thus, the altered conformational stability of unconjugated tapasin is a direct consequence of its failure to form a mixed disulfide with ERp57.

4.6: Tapasin and ERp57 alone are responsible for determining the thermostability of tapasin

I showed above that a conformation specific epitope was differentially susceptible to heating in a tapasin mutant unable to form a mixed disulfide with ERp57 and unconjugated WT tapasin in cells in which ERp57 expression was suppressed. However, the overall PLC composition in C95A-expressing cells is altered, and, as is clear from **Figure 4.4**, MHC class I HC and presumably CRT dissociate from tapasin upon heating. These components are not associated with C95A tapasin after Triton X-100 elution even at 4° C. I wished to clearly show that only tapasin and ERp57 were responsible for controlling the conformational stability of tapasin in response to heating, and recombinant, insect cell expressed free and conjugated tapasin were kindly provided by Pamela Wearsch to examine this possibility.

Insect cells co-expressing soluble, 6xHis-tagged tapasin and human ERp57 were treated with MMTS prior to detergent extraction. Conjugated and free tapasin were co-purified using cobalt resin, but these were then separated by gel filtration. Equal amounts of conjugated and free tapasin in the absence of detergent were incubated at different temperatures for 30 minutes, aggregates were pelleted, and supernatants were immunoprecipitated with PaSta1. After non-reducing SDS-PAGE and staining with Coomassie brilliant blue, I quantitated the amount of PaSta1 precipitated tapasin using densitometry. To ensure that the signals obtained were within the linear range of

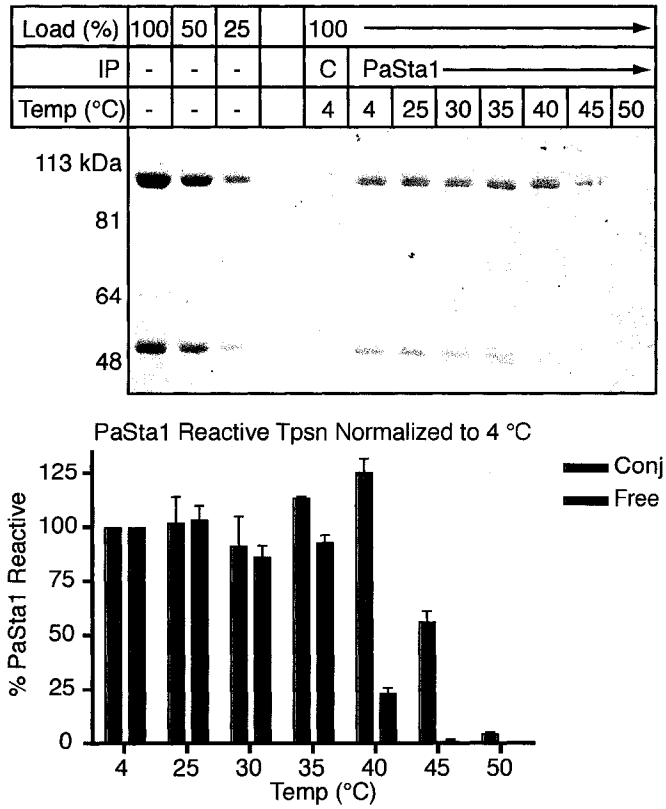

Figure 4.6: Other PLC components are not responsible for conjugate thermostability.

ERp57 conjugated and free tapasin isolated from MMTS-treated insect cells was purified and incubated at the indicated temperatures for 30 minutes. Samples were cooled on ice for 10 minutes prior to centrifugation at 14,000 RPM for 10 minutes at 4° C. Supernatants were precipitated with the conformation specific mouse anti-tapasin antibody PaSta1 or mouse anti-OX68 as a control coupled to agarose beads and resolved by non-reducing SDS-PAGE. Gels were stained with Coomassie brilliant blue, destained, and quantitated by densiometry. The left three lanes of the gel were non-immunoprecipitated samples to generate a standard curve. Bands corresponding to free and conjugated tapasin were normalized to signals precipitated at 4° C. The mean +/- SEM of two independent experiments is shown.

detection, I also ran serial dilutions of non-immunoprecipitated samples (**Figure 4.6**). PaSta1 reactivity was maintained in both conjugated and free tapasin after heating to 35° C. At 40° C, the amount of PaSta1-precipitated ERp57-conjugated tapasin was the same as that seen at 4° C, while only 25% of the free tapasin was pulled down. This difference was exacerbated after heating to 45° C. Neither conjugated nor free tapasin retained PaSta1 reactivity after heating to 50° C. This experiment clearly shows that the conformational stability of tapasin is dependent only upon ERp57 and does not require other PLC components.

4.7: Discussion

Within the PLC, a number of different interactions take place between PLC components. The transmembrane and/or cytoplasmic domain of tapasin is essential for its interaction with TAP, but the interaction of MHC class I with tapasin is somewhat more complicated (Lehner et al., 1998). There are at least two sites of interaction between MHC class I HC and tapasin (Wright et al., 2004). The membrane proximal Ig domain of tapasin interacts with the MHC class I α3 domain, and mutants in these domains interfere with MHC class I recruitment into the PLC (Kulig et al., 1998; Suh et al., 1999; Turnquist et al., 2004; Turnquist et al., 2001). Additionally, there is an interaction between the N-terminal domain of tapasin and the α2 domain of MHC class I HC (Bangia et al., 1999; Lewis and Elliott, 1998; Peace-Brewer et al., 1996). The studies characterizing these mutants are difficult to interpret, however, as most were conducted prior to the advent of NEM or MMTS treatment. Indeed, in my hands a D337A mutation in tapasin that completely prevents H-2 L^d association with the PLC had only minimal

effects on HLA-B*0801 and HLA-B*4402 PLC incorporation (data not shown). However, while the differences between different MHC class I and tapasin mutants are likely not as absolute as originally described, the consistency of the data suggests that the general two site binding model is correct.

In addition to binding MHC class I HC, tapasin also catalyzes peptide loading. This activity appears to require an intact N-terminus, as N-terminal deletion mutants do not support peptide loading (Bangia et al., 1999; Momburg and Tan, 2002). A proteolysis study of tapasin also indicated that the N-terminus of tapasin is an independent domain, but this study did not examine conjugated tapasin (Chen et al., 2002). It seems likely that an intact N-terminus is required for both ERp57 recruitment and the catalysis of peptide loading, but conjugate formation is not required for peptide loading. Rather than impaired peptide loading, the defects seen in C95A cells likely arise from the decreased recruitment and stabilization of MHC class I in the PLC secondary to poor binding between the $\alpha 2$ domain and the N-terminal binding site of tapasin. The combination of Ig/$\alpha 3$ and low-affinity N-terminus/$\alpha 2$ interactions are sufficient to mediate peptide loading to some extent. The mechanism by which mutation of Cys-95 affects this binding site is unclear. Presumably ERp57 binding is responsible for this phenotype, and this is supported by the similarities in MHC class I recruitment between mouse B cells lacking ERp57 and a human B cell line expressing C95A tapasin. It is interesting to speculate that conjugate formation induces a conformational change in tapasin to generate a high affinity binding site for MHC class I.

In addition to the interactions between tapasin and MHC class I, CRT also binds the monoglucosylated glycan of MHC class I HC with an affinity of approximately 1 μM

(Wearsch et al., 2004). The binding characteristics of the MHC class I/tapasin interaction have not been worked out. ERp57 almost certainly acts as a bridge between tapasin and CRT, and the P-domain of CRT binds ERp57 with a Kd $\approx$ 9 μM (Frickel et al., 2002). The combination of these weak interactions could stabilize the PLC. The decreased levels of CRT seen in C95A tapasin containing PLCs is consistent with this hypothesis, but it is impossible to determine at this time whether this is a direct result of the decreased MHC class I recruitment or the absence of ERp57 from the PLC. It seems most likely that some combination of factors will ultimately be found responsible for this phenotype.

It is difficult to examine structural changes of small amounts of proteins in crude cell extracts, but I used a conformation specific antibody available in the lab to probe changes in the structure of tapasin following heating. Incubation of cell-expressed or recombinant unconjugated WT tapasin or the C95A mutant at or near physiologic temperatures dramatically destabilized the PaSta1 binding site. For cell-expressed tapasin, this was likely exacerbated by the presence of detergents, but recombinant tapasin was incubated in TBS alone. The amount of degradation of C95A tapasin was not substantially different from WT tapasin over the course of 8 hrs suggesting that the overall stability of this mutant is not impaired (Dick et al., 2002). It is possible that there are subtle conformational differences between conjugated and unconjugated tapasin *in vivo* that do not affect protein half-life but adversely affect MHC class I recruitment. A detailed structural analysis of free and conjugated tapasin with and without MHC class I HC/β_2m complexes is needed to fully resolve this hypothesis.

It is interesting to consider my experiments in conjunction with those of Garbi et al. to generate a universal model of the role of ERp57 in peptide loading. Indeed, H2-K^b and HLA-B*4402 are amongst the most different MHC class I molecules studied. First and foremost, the recruitment and stabilization of MHC class I HC into the PLC is dramatically reduced in an allele- and species-independent manner. In contrast, the trafficking and maturation of these two alleles is quite different when assembled in the absence of ERp57. H2-K^b passed through the Golgi much more quickly in the absence of ERp57, but HLA-B*4402 was slightly delayed in acquiring EndoH resistance. In tapasin-deficient mice, empty H2-K^b molecules reach the cell surface but are quickly internalized. The surface expression of these molecules is stabilized by the presence of exogenous peptide (Grandea et al., 2000). Cell surface expression of H2-K^b expressed in 721.220 cells is the same in the presence or absence of tapasin, and H2-K^b trafficking is accelerated in these cells comparable to tapasin deficient mouse B cells (Barnden et al., 2000). Additionally, H2-K^b is expressed on the cell surface in human cells deficient in TAP expression at 37° C (Anderson et al., 1993). In contrast, in the absence of tapasin, HLA-B*4402 surface levels are greatly reduced, and very few MHC class I/β_2m complexes reach the Golgi apparatus (Dick et al., 2002; Peh et al., 1998). It is likely that H2-K^b assembled with or without low affinity peptides is able to pass the quality control checkpoints in the ER, but these unstable complexes dissociate in post-ER compartments. HLA-B*4402 assembled with or without low affinity peptides does not appear capable of exiting the ER and likely undergoes ER associated degradation (ERAD).

Chapter 5: Absence of ERp57 redox activity within the PLC

The complete absence of ERp57 from the PLC is detrimental to the acquisition of high affinity peptides by both HLA-B*4402 and H2-K^b. In chapter 4, I discussed some of the potential mechanisms by which ERp57 could be affecting peptide loading, but these experiments and those using ERp57-deficient B cells could not differentiate between a direct role for ERp57 in peptide loading and the indirect consequences arising from the absence of conjugate formation. In particular, the redox difference seen in HLA-B*4402 associated with the PLC in C95A-expressing cells could be due to the absence of ERp57 oxidase activity. I used a combination of RNAi and mutagenesis to examine these questions. When ERp57 expression was stably suppressed, all residual ERp57 was associated with tapasin leading to minimal changes in PLC composition. Accordingly, peptide loading of HLA-B*4402 was not affected. Interestingly, both PDI and ERp72 were able form mixed disulfides with tapasin in the absence of ERp57. Exogenous WT or mutant FLAG-tagged ERp57 were efficiently incorporated into the PLC in the absence of endogenous ERp57, but peptide loading was not affected by mutation of Cys-60 responsible for the *a*-domain escape pathway or the complete inactivation of *a'* domain redox activity. Finally, the redox state of HLA-B*4402 associated with a C60/406/409A redox inactive mutant was normal, arguing against a role for ERp57 mediated disulfide bond oxidation in the PLC.

5.1: Successful generation of ERp57-suppressed 721.220.B4402.WT-tapasin cells

One factor complicating the MHC class I antigen processing field is the variety of cell lines and alleles studied. When direct comparisons between alleles expressed in 721.220 cells with and without tapasin have been made, HLA-B*4402 has consistently exhibited the greatest increase in surface expression following tapasin transfection (Park et al., 2003; Peh et al., 1998). Additionally, 721.220 cells expressing HLA-B*4402 were used to characterize the functional defects of the C95A tapasin mutant (Dick et al., 2002). Thus, to be most consistent with the literature as well as to facilitate comparisons between the C95A cells, I wished to stably knock-down ERp57 expression in 721.220 cells expressing HLA-B*4402 and WT tapasin.

Initial experiments were conducted using HeLa-M cells transiently transfected with small inhibitory RNA duplexes (siRNA) specific for the coding region and 3'-untranslated region (UTR) of ERp57 (data not shown). From these experiments it became clear that both siRNA duplexes effectively knocked-down ERp57 expression, but probably because of the high expression and stability of ERp57, two separate transfections were required for efficient knock-down. Because of these technical difficulties, combined with the lack of characterization of HeLa-M expressed HLA alleles, I decided to generate cells stably suppressing ERp57 expression. Additionally, given that 721.220 cells are somewhat refractory to traditional lipid transfection and electroporation, an RNAi retrovirus system was employed (Barton and Medzhitov, 2002). Finally, I used the 3' UTR to target ERp57 mRNA for degradation to allow the re-expression of WT and mutant ERp57 constructs.

Complementary oligonucleotides specific for the 3' UTR of ERp57 or a non-specific sequence were ligated into the RVH1 retroviral vector. This vector also contains a truncated, non-signaling version of human CD4 under the control of the CMV immediate early promoter to allow the identification and sorting of transduced cells. CD4 expression was previously shown to correlate with genomic integration and RNAi-mediated suppression (Barton and Medzhitov, 2002). Retrovirus was produced by co-transfection of 293T cells with RVH1-ERp57 or RVH1-Ctrl with the amphotrophic retroviral packaging vector pCL-Ampho. 721.220 cells expressing HLA-B*4402 and WT tapasin were then transduced by three rounds of "spinfection" at 2500 RPM for 90 minutes at 32° C. Cells were then sorted three times for high CD4 expression.

Transduced and sorted cells were solubilized in Triton X-100, and 3.16-fold serial dilutions representing a 10-fold difference in loaded lysate were separated by reducing SDS-PAGE prior to quantitative Western blotting. These samples were then blotted using a rabbit antiserum raised against the C-terminal peptide of ERp57 or rat anti-GRP94 as a loading control (**Figure 5.1a**). Cells transduced with RVH1-Ctrl retrovirus maintained high levels of ERp57 expression as expected, but ERp57 expression in RVH1-ERp57 transduced cells was decreased by approximately 90%. The differences seen in ERp57 expression in this experiment are not the result of decreased loading because GRP94 levels were identical between these two cell lines. These levels of ERp57 suppression have been maintained for greater than six months (data not shown).

Cells typically have an excess of ERp57 over tapasin, and increasing tapasin expression by IFN-γ treatment decreases the pool of free ERp57 (**Figure 2.1**). Having established a cell line with decreased ERp57 expression, I next wished to examine the

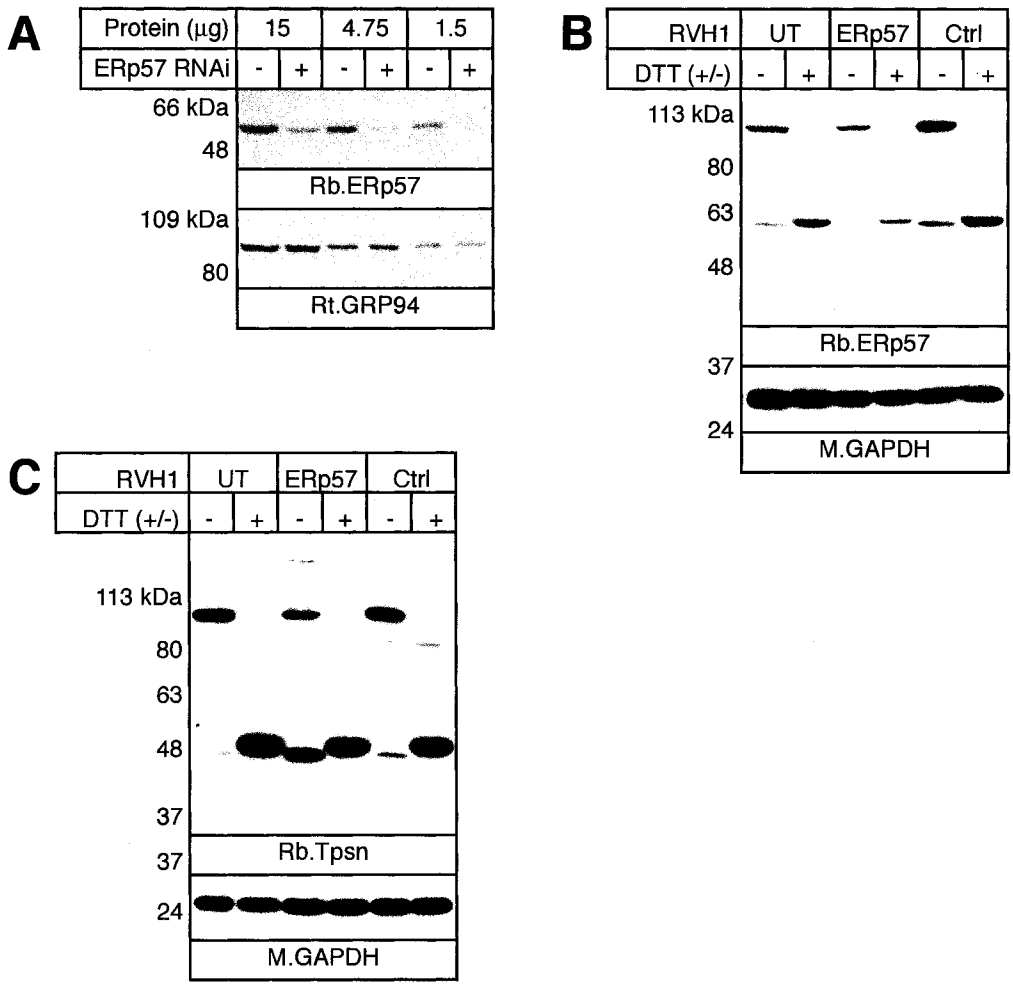

Figure 5.1: Successful knock-down of ERp57 in 220.B44.Tpsn cells.

A) Generation of ERp57-suppressed cell lines. 721.220 cells expressing HLA-B*4402 and WT tapasin transduced with retroviruses encoding short-hairpin RNAs specific for ERp57 or a non-specific sequence were solubilized in 1% Triton X-100. Serial dilutions of ERp57 suppressed (+ RNAi) or control cells (-RNAi) were resolved by reducing SDS-PAGE. Following transfer and blocking, membranes were cut and probed with a rabbit antiserum raised against the C-terminus of ERp57 (R.ERp57-C) and monoclonal rat anti-GRP94. Samples were quantitated using a Storm 860 imaging system and Imagequant software. ERp57 knock-down was approximately 90%.
B) All remaining ERp57 is conjugated to tapasin. 721.220 cells expressing HLA-B*4402 and tapasin transduced with RVH1-ERp57 or RVH1-Ctrl or untransduced (UT) were treated with 10 mM MMTS and solubilized in 1% Triton X-100. Post-nuclear supernatants were resolved by reducing/non-reducing SDS-PAGE. After transfer and blocking, membranes were probed with rabbit anti-ERp57-C or mouse anti-GAPDH.
C) Conjugate levels are slightly decreased in ERp57-suppressed cells. Cells were prepared as in (B), but blotted with a rabbit anti-serum raised against full length, insect cell expressed tapasin (R.SinE) or mouse anti-GAPDH.

distribution of the residual ERp57 between conjugated and non-conjugated pools. Consistent with the effects of IFN-γ, all of the residual ERp57 expressed in RVH1-ERp57 transduced cells forms a mixed disulfide with tapasin in MMTS treated cells (**Figure 5.1b**). Accordingly, the amount of conjugated tapasin was only somewhat decreased in these cells compared with untransduced 721.220.B4402.WT-Tpsn or RVH1-Ctrl transduced cells (**Figure 5.1c**). These data clearly show that ERp57 is preferentially recruited into a mixed disulfide by tapasin and emphasize the data presented in Chapters 2 and 3.

5.2: Tapasin conjugation with PDI and ERp72 in ERp57-suppressed cells

In HeLa, HeLa-M, and 721.220.B4402.WT-Tpsn cells in which ERp57 expression was transiently or stably suppressed, higher molecular weight bands were consistently seen in whole cell extracts blotted for tapasin under non-reducing conditions (data not shown and **Figure 5.1b**). These bands were not present after reduction or when blotting for ERp57. This observation suggests that, in the absence of ERp57, tapasin may form mixed disulfides with other proteins.

Given the high degree of sequence, structural, and functional homology between PDI family members, I examined whether PDI and/or ERp72 were components of these higher molecular species. This experiment was complicated by the limitations of the available reagents. Specifically, the only commercially available mouse anti-ERp72 mAb does not immunoprecipitate under native conditions; it only recognizes denatured protein. Additionally, the anti-ERp72 antisera used cross-react with other proteins of approximately 57 kDa, and it is possible that these proteins are ERp57. Finally, until

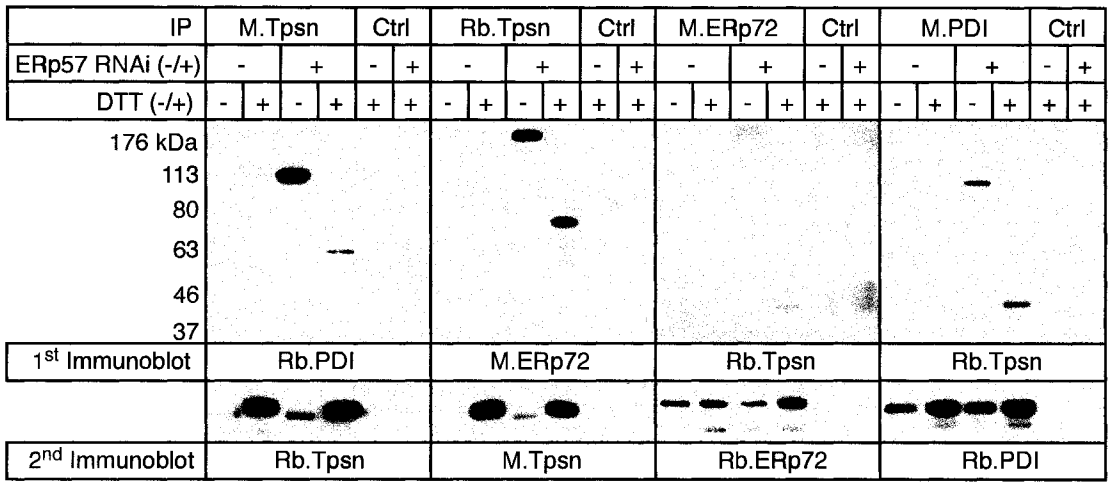

Figure 5.2: Other Trx family members form mixed disulfides with tapasin in ERp57 suppressed cells.

PDI and ERp72 form mixed disulfides with tapasin in the absence of ERp57. 721.220 cells expressing HLA-B*4402 and WT tapasin with or without ERp57 RNAi were treated with MMTS prior to solubilization in 1% Triton X-100. SDS was added to a final concentration of 1% to ¼ of the post-nuclear supernatants destined for mouse anti-ERp72 immunoprecipitation. These samples were heated to 95° C for 5 minutes and diluted in 1% Triton X-100 to a final SDS concentration of 0.05%. All samples were then pre-cleared with protein G- or protein A-sepharose for immunoprecipitations with mouse monoclonal antibodies or rabbit antisera or coupled beads, respectively. Samples were then precipitated with PaSta1 or anti-HLA-DP coupled to agarose beads, rabbit anti-tapasin (R.gp48C) or rabbit anti-HLA-DR (R.DRAB) and protein A-sepharose, or mouse anti-ERp72 (M.ERp72), mouse anti-PDI (M.PDI), or mouse anti-HLA-DM (MaP.DM) as a control (Ctrl) and protein G-sepharose. Samples were resolved by reducing/non-reducing SDS-PAGE as indicated, transferred to PVDF membranes, and blocked. Membranes were then probed with rabbit anti-PDI (Rb.PDI), mouse anti-ERp72 (M.ERp72), or rabbit anti-tapasin (R.SinE for M.ERp72 or R.gp48C for M.PDI). Following initial blotting, membranes were stripped in 1% SDS, washed, and re-probed with rabbit anti-tapasin (R.gp48C), mouse anti-tapasin (M.Tpsn-C), rabbit anti-ERp72 (Rb.ERp72), or rabbit anti-PDI (Rb.PDI) to confirm efficient immunoprecipitation.

recently we did not have an anti-tapasin mAb that blotted effectively. However, once optimal conditions were worked out, I treated 721.220.B4402.WT-Tpsn cells with or without stably suppressed ERp57 with MMTS prior to detergent extraction. One-quarter of the lysate was boiled in the presence of SDS to generate the appropriate anti-ERp72 epitope, and this sample was then diluted into Triton X-100 to minimize the effects of SDS on antibody binding. The remaining lysate was precipitated with mouse anti-tapasin, rabbit anti-tapasin, or mouse anti-PDI followed by reducing/non-reducing SDS-PAGE. Following transfer and blocking, membranes were blotted for PDI, ERp72, or tapasin (**Figure 5.2**). In RVH1-Ctrl transduced cells, no PDI or ERp72 was precipitated with tapasin and no tapasin was precipitated with PDI or ERp72, despite efficient pull-down as indicated by the presence of the appropriate protein after re-blotting (lower panel). However, mixed disulfides containing both PDI and ERp72 were precipitated with anti-tapasin reagents in ERp57-suppressed cells. Additionally, tapasin was immunoprecipitated with anti-PDI and anti-ERp72 mAbs. The amount of precipitated protein was similar between RVH1-ERp57 and RVH1-Ctrl transduced cells when the membranes were re-blotted for the immunogens (lower panel). Thus, only when the expression of ERp57 is suppressed are other PDI family members including PDI and ERp72 capable of forming mixed disulfides with tapasin. These data further argue that tapasin specifically recruits ERp57 to the PLC, but the ability of tapasin to inhibit the Trx-motif escape pathway is likely universal.

5.3: Slightly altered PLC composition and normal surface MHC class I expression in RVH1-ERp57 transduced cells.

Despite achieving ERp57 knock-down of approximately 90%, a substantial amount of tapasin was conjugated to the residual ERp57. The differences in PLC composition between 721.220.B4402 cells expressing WT or C95A tapasin were profound, however, and I wished to determine whether the increase in unconjugated tapasin in ERp57-suppressed cells was sufficient to alter the overall PLC composition. Cells transduced with RVH1-ERp57 or –Ctrl were treated with MMTS prior to extraction in digitonin, and PLCs were immunoprecipitated using an anti-TAP1 mAb. Precipitated material was eluted under reducing conditions, and serial dilutions were run across a 10-fold concentration range. Membranes were then blotted for individual PLC components using appropriate reagents for fluorimetry and quantitation (**Figure 5.3a**). Consistent with the results from WT- and C95A-expressing cells, the amounts of TAP1 and tapasin incorporated into the PLC did not differ between ERp57-suppressed and competent cells. The presence of ERp57 in the PLC was decreased by approximately 30% in RVH1-ERp57 transduced cells, consistent with the non-quantitative HRP blots shown in **Figure 5.1**. Additionally, incorporation of both CRT and MHC class I HC was decreased by 30% in ERp57-suppressed cells. However, these differences in PLC composition were not sufficient to cause a decrease in the surface expression of HLA-B*4402 (**Figure 5.3b**).

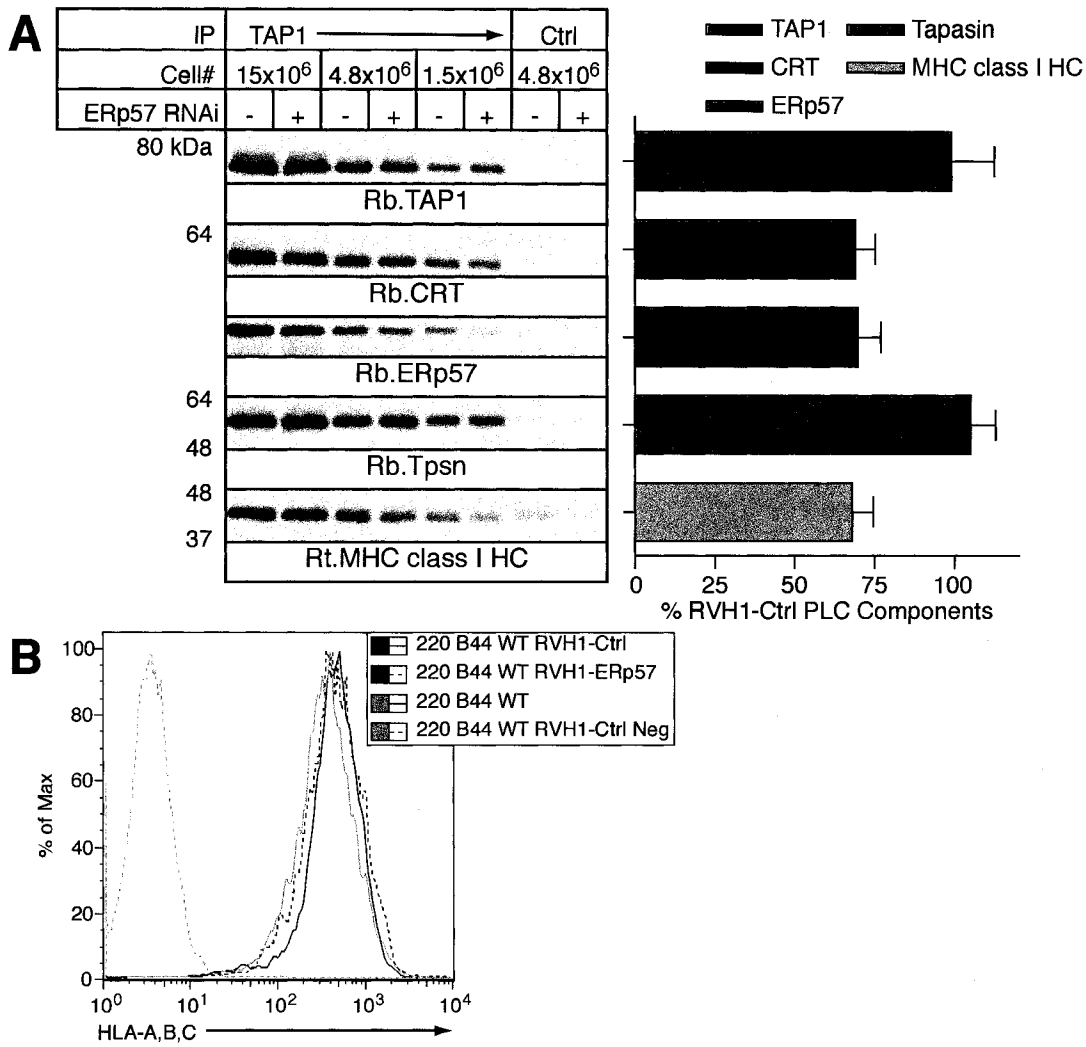

Figure 5.3: Suppression of ERp57 expression does not dramatically alter PLC composition.

A) Slightly altered PLC composition in ERp57-suppressed cells. 721.220 cells expressing HLA-B*4402 and WT tapasin with or without ERp57 suppression (-/+ RNAi) were treated with MMTS prior to digitonin solubilization. Post-nuclear supernatants were immunoprecipitated with the mouse anti-TAP1 antibody 148.3 (M.TAP1) or the mouse anti-HLA-DP antibody B7 coupled to agarose beads as a control (Ctrl). After washing, immunoprecipitated material was eluted under reducing conditions and separated by SDS-PAGE. Following transfer and blocking, membranes were cut and individually probed with rabbit antisera raised against the C-terminal peptide of TAP1 (RING.4C), CRT, the C-terminal peptide of ERp57 (Rb.ERp57-C), the N-terminal peptide of tapasin (R.gp48N), or rat anti-MHC class I HC (3B10.7). Samples were quantitated using a Storm 860 imaging system and Imagequant software. Signals corresponding to PLC components precipitated from RVH1-ERp57 transduced cells were normalized to those from RVH1-Ctrl transduced cells. Values are the mean +/- SEM for the dilutions, and this is representative of three independent experiments.

B) Normal MHC class I surface expression in ERp57-suppressed cells. 721.220 cells expressing HLA-B*4402 and WT tapasin with or without ERp57 RNAi were incubated with mouse anti-HLA-A, B, and C directly coupled to APC or an APC-coupled non-binding isotype control for 30 minutes on ice.

5.4: Normal trafficking and maturation of HLA-B*4402 in ERp57-suppressed cells.

The composition of the loading complex is dramatically altered in cells expressing C95A mutant tapasin, but cell surface HLA-B*4402 expression is only slightly decreased in these cells compared to those expressing WT tapasin. It is not surprising, therefore, that cells with suppressed ERp57 expression but relatively normal PLC composition have normal surface HLA-B*4402 expression. The trafficking and maturation of HLA-B*4402 is dramatically impaired in C95A-expressing cells, however. Therefore, I wished to determine whether the decreased ERp57 expression and altered PLC composition in RVH1-ERp57 transduced cells affected HLA-B*4402 maturation.

Cells transduced with RVH1-ERp57 or RHV1-Ctrl were pulse-labeled for 15 minutes with [^{35}S]-methionine and cysteine and chased for different lengths of time in the presence of excess cold methionine and cysteine. Cell pellets were solubilized in digitonin to preserve MHC class I associations with tapasin and allow for immunoprecipitation of non-TAP-associated MHC class I/β_2m complexes with W6/32. Precipitated material was eluted and treated with EndoH overnight prior to reducing SDS-PAGE (**Figure 5.4**). The bands corresponding to EndoH resistant and sensitive MHC class I HC were quantitated, and the %EndoH resistant MHC class I HC was calculated. In contrast to what is seen in C95A-expressing cells (**Figure 4.2**), suppression of ERp57 expression and the resulting changes in the PLC are not sufficient to affect HLA-B*4402 trafficking through the Golgi. However, in RVH1-ERp57-transduced cells, the overall stability of W6/32 reactive complexes is reduced compared to RVH1-Ctrl or untransduced cells, including those that have passed through the Golgi

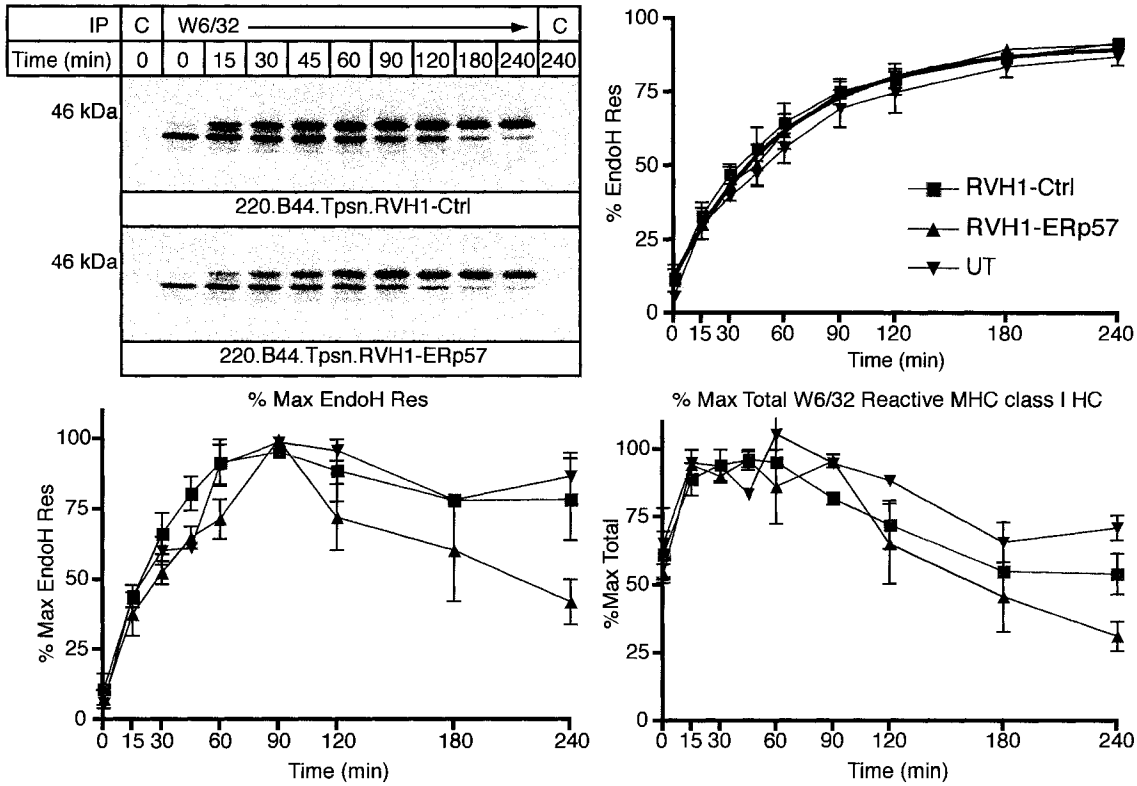

Figure 5.4: Normal trafficking of HLA-B*4402 assembled in ERp57-suppressed cells.

721.220 cells expressing HLA-B*4402 and WT tapasin with or without ERp57-specific RNAi were pulse-labeled with [^{35}S]-methionine and cysteine for 15 minutes and chased for the indicated periods of time. Frozen cell pellets were solubilized in 1% digitonin, and post-nuclear supernatants were immunoprecipitated with the anti-MHC class I HC/β_2m conformation specific antibody W6/32 or the CD1d specific antibody 51.1.3 as a control and protein A-sepharose. Samples were washed with 0.1% Triton X-100 in TBS, eluted in 2x EndoH buffer with heating to 95° C, and incubated with 1 mU EndoH overnight at 37° C. Digested material was then resolved by reducing SDS-PAGE. Bands corresponding to EndoH resistant (upper band) and sensitive (lower band) MHC class I HC were quantitated, and the % EndoH resistant MHC class I HC was calculated (upper right panel). Signals were further expressed as % Max EndoH Res MHC class I HC (lower left panel) and % Max Total W6/32 reactive MHC class I HC (lower right panel) as a measure of the overall stability of W6/32 reactive complexes throughout the chase period. The mean +/- SEM of two independent experiments is shown, and the comparalble data obtained from untransduced 721.220.B4402.WT-Tpsn (UT) cells from **Figure 4.2** is shown for reference.

(**Figure 5.4, lower panels**). These differences are not as great as those seen between cells expressing WT or C95A tapasin, and may reflect MHC class I complexes that were loaded with suboptimal peptides but were allowed to exit the ER.

5.5: Successful expression of FLAG-tagged mutant ERp57

Under ideal circumstances, the information regarding the function of ERp57 within the PLC that could be obtained from RNAi studies is likely not dissimilar from that based on the C95A mutant and ERp57 conditional knock-out. To fully define the mechanism of ERp57 action in peptide loading, the phenotype of cells expressing different ERp57 mutants should be examined. In particular, Dick et al. suggested that ERp57 could control the proper oxidation state of the MHC class I HC associated with the PLC (Dick et al., 2002). Indeed, when the presence of ERp57 in the PLC was first identified, three groups individually hypothesized that PLC-associated ERp57 could be redox active (Hughes and Cresswell, 1998; Lindquist et al., 1998; Morrice and Powis, 1998). The ability of tapasin to inactivate the escape pathway of the ERp57 *a* domain suggests that the *a'* domain would be responsible for any redox activity in the PLC. An ERp57 mutant in which only the active site cysteine residues of the *a'* domain were mutated to alanine (C406/409A) was not able to form the conjugate with tapasin. However, the inactivation of the *a* domain escape pathway in conjunction with this mutant (C60/406/409A) led to conjugate formation (Dick et al., 2002).

To determine if redox active sites of ERp57 are required for its function in the PLC, I transduced 721.220.B4402.WT-Tpsn cells stably suppressing endogenous ERp57 with retroviral vectors encoding FLAG-tagged WT, C60A, and C60/406/409A ERp57.

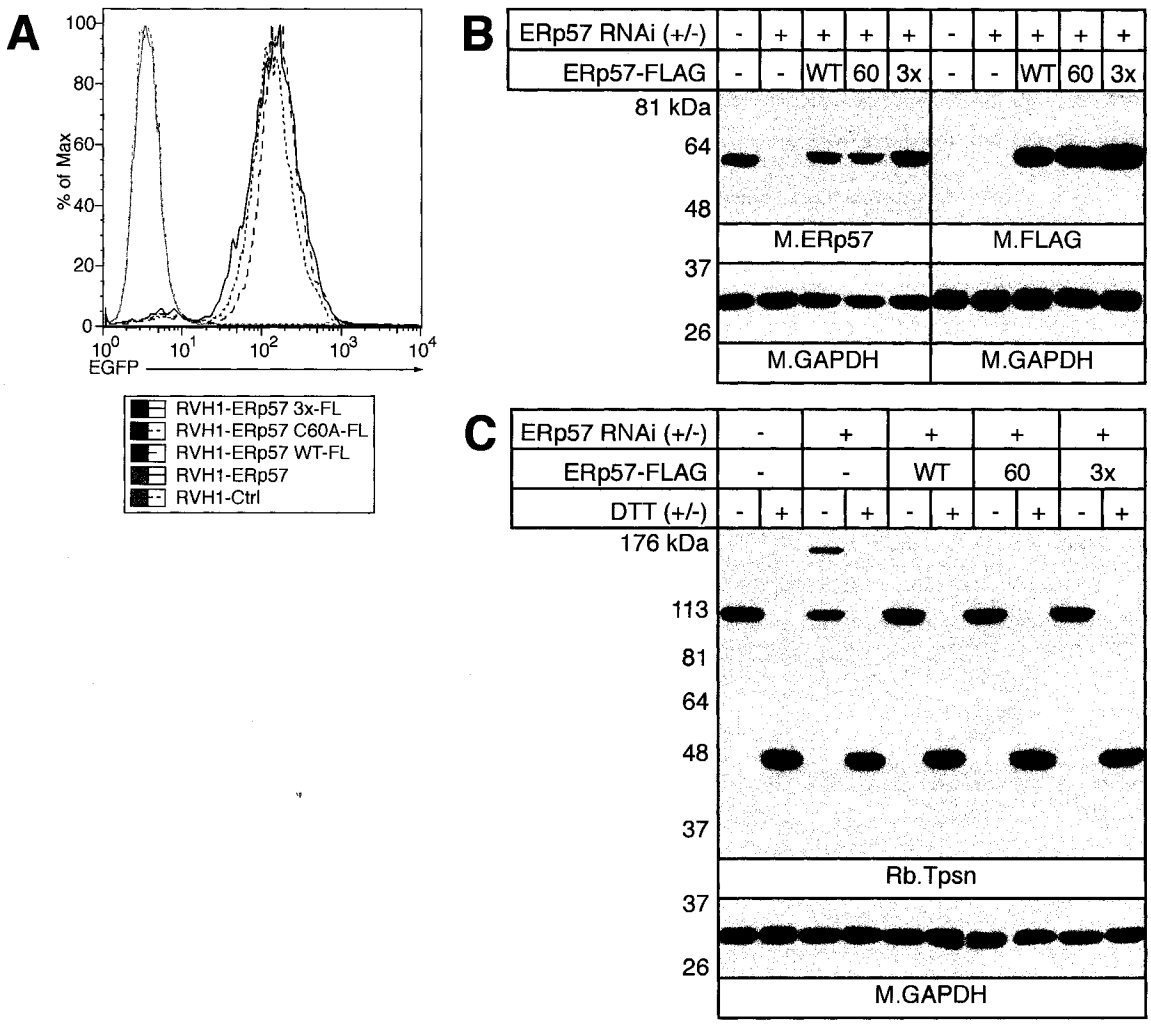

Figure 5.5: Successful re-expression of FLAG-tagged ERp57 mutants in ERp57-suppressed cells.

A) Generation of ERp57-FLAG expressing cells. 721.220 cells expressing HLA-B*4402 and WT tapasin with ERp57 RNAi were transduced with retroviruses encoding FLAG-tagged WT, C60A, or C60/406/409A ERp57 bicistronically with EGFP by "Spinfection". Cells were then FACS sorted for high EGFP expression.

B) Expression of FLAG-tagged ERp57 restores ERp57 expression levels. 721.220 cells expressing HLA-B*4402 and WT tapasin with or without ERp57 RNAi expressing FLAG-tagged WT, C60A, or C60/406/409A (3x) ERp57 were solubilized in 1% Triton X-100, and post-nuclear supernatants were resolved by reducing SDS-PAGE. Following transfer to PVDF membranes and blocking, membranes were cut and probed with mouse anti-ERp57 (MaP.ERp57), mouse anti-FLAG (M2), or mouse anti-GAPDH.

C) Expression of FLAG-tagged ERp57 constructs abrogates ERp72 conjugate formation. Cells from (B) were treated with 10 mM MMTS in PBS prior to solubilization in 1 % Triton X-100. Post-nuclear supernatants were resolved by reducing/non-reducing SDS-PAGE as indicated. Following transfer to PVDF membranes and blocking, membranes were cut and probed with rabbit anti-tapasin (R.SinE) or mouse anti-GAPDH.

In these cells, enhanced green fluorescent protein (EGFP) is expressed bicistronically with ERp57-FLAG allowing the sorting and isolation of transduced cells. Transduced cells were FACS sorted three times to obtain a population of cells expressing high levels of ERp57-FLAG (**Figure 5.5a** and **b**). After sorting, cells transduced with ERp57-FLAG encoding retroviruses were uniformly positive for EGFP, while RHV1-Ctrl and RVH1-ERp57 transduced cells were EGFP negative. The levels of ERp57-FLAG expression were comparable to levels of endogenous ERp57 expressed in RVH1-Ctrl cells, and no FLAG reactive material was present in untransduced cells. Additionally, there is a slight size difference (~1kDa) between FLAG-tagged and endogenous ERp57 that is clear in Figure 5.5b. Finally, expression of exogenous, FLAG-tagged ERp57 leads to the loss of the higher molecular weight conjugates seen in RVH1-ERp57-alone transduced cells (**Figure 5.5c**).

5.6: Incorporation of ERp57-FLAG into the PLC

The FLAG-tagged ERp57 constructs expressed in the absence of endogenous ERp57 were presumably able to form the conjugate with tapasin, and this is supported by the absence of higher molecular weight tapasin mixed disulfides in the transduced cells. However, the likelihood that a specific function associated with ERp57 would become apparent would be greater if the FLAG-tagged mutant proteins were the overwhelming majority of PLC-associated ERp57. To examine the extent of mutant ERp57 incorporation into the PLC, I immunoprecipitated the PLC using an anti-TAP1 rabbit antiserum from MMTS treated lysates. These samples were then resolved by SDS-PAGE under reducing conditions and probed with MaP.ERp57 and M.Tpsn-C, a

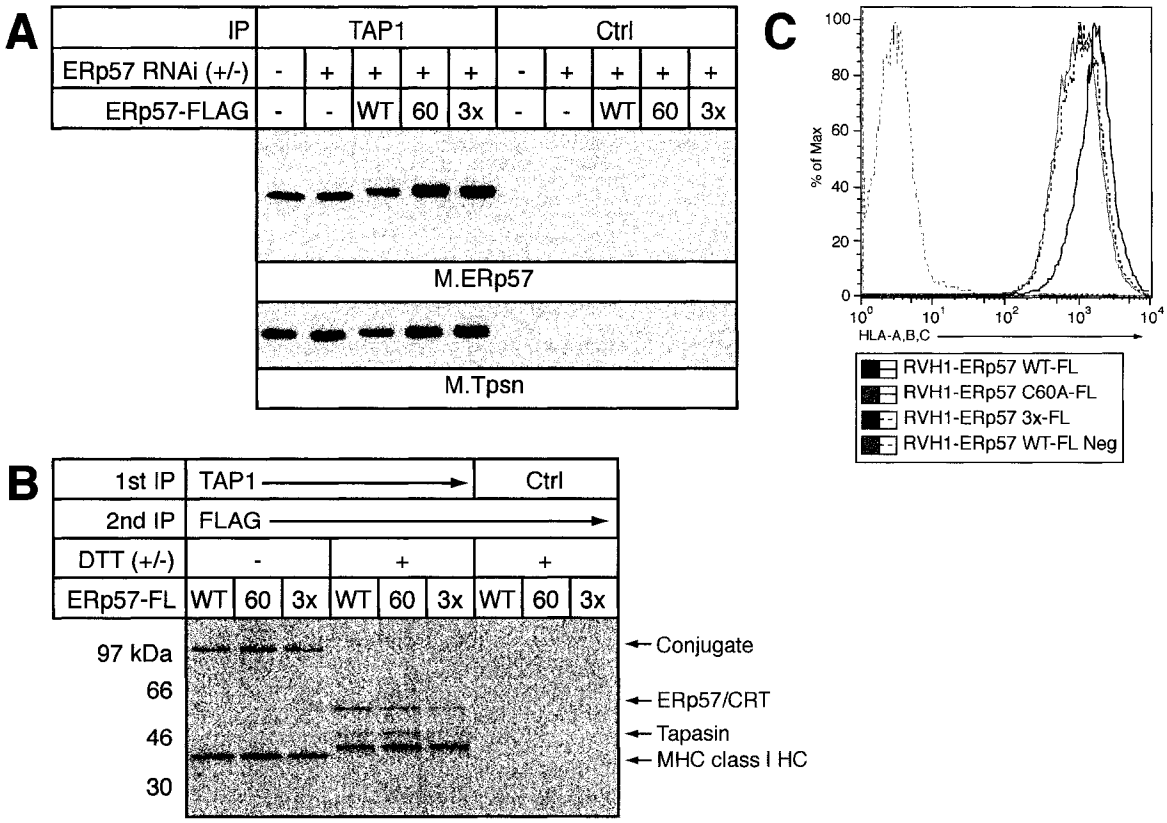

Figure 5.6: PLC incorporation of re-expressed FLAG-tagged ERp57 mutants

A) FLAG-tagged ERp57 is the predominant ERp57 form incorporated into the PLC. 721.220 cells expressing HLA-B*4402 and WT tapasin, with or without ERp57 RNAi, expressing FLAG-tagged WT, C60A, or C60/406/409A (3x) ERp57 were treated with 10 mM MMTS prior to solubilization in 1% digitonin. Precleared post-nuclear supernatants were immunoprecipitated with rabbit anti-TAP1 (RING.4C) or rabbit anti-HLA DR (R.DRAB) and protein A-sepharose. Immunoprecipitates were resolved by reducing SDS-PAGE and, following transfer and blocking, membranes were probed with mouse anti-ERp57 (MaP.ERp57). Membranes were then stripped in 1% SDS, washed, and re-probed for tapasin with mouse anti-tapasin (M.Tpsn-C) as an immunoprecipitation control.

B) FLAG-tagged ERp57 containing conjugates recruit MHC class I HC into the PLC. 721.220 cells expressing HLA-B*4402 and WT tapasin with suppressed endogenous ERp57 and re-expressed WT, C60A, or C60/406/409A (3x) FLAG-tagged ERp57 were pulse-labeled with [^{35}S]-methionine and cysteine for 45 minutes, treated with 10 mM MMTS, and solubilized in 1% digitonin. Post-nuclear supernatants were immunoprecipitated with rabbit anti-TAP1 (RING.4C) or NRS as a control and protein A-sepharose. Subcomplexes were eluted by incubating in 0.1% Triton X-100 for 5 min on ice. Eluted material was then re-precipitated with mouse anti-FLAG (M2) prior to resolution by reducing/non-reducing SDS-PAGE as indicated.

C) FLAG-tagged ERp57 supports normal cell surface MHC class I expression. 721.220 cells expressing HLA-B*4402 and WT tapasin with ERp57 RNAi expressing FLAG-tagged WT, C60A, or C60/406/409A (3x) ERp57 were stained with APC-coupled anti-HLA-A,B,C or an isotype control (Neg.). All steps were performed on ice, and only living cells are shown.

mAb raised against the C-terminal peptide of tapasin (**Figure 5.6a**). MaP.ERp57 should react equally well with endogenous and FLAG-tagged mutant ERp57. Under these conditions, PLC-associated ERp57 from RVH1-Ctrl and RVH1-ERp57 transduced cells ran as a single band, but a doublet was seen in TAP1 immunoprecipitates from cells expressing FLAG-tagged WT, C60A, and C60/406/409A ERp57. The lower molecular weight band was consistent in size with endogenous ERp57, and the higher molecular weight band most likely corresponds to the FLAG-tagged proteins. In all ERp57-FLAG transduced cells, the FLAG-tagged ERp57 appears to represent the majority of PLC-associated ERp57. Additionally, the efficiency of the TAP1 immunoprecipitation was comparable from all the cell lines as indicated by the tapasin blot.

The FLAG-tagged ERp57 mutants can associate with TAP, but they may not support full subcomplex formation. Additionally, the experiment in **Figure 5.6a** was performed using reducing conditions, and I wanted to examine the ability of the ERp57 mutants for form the conjugate with tapasin. To examine both conjugate formation and the association with MHC class I, I radio-labeled ERp57-FLAG transduced cells with [^{35}S]-methionine and cysteine for 45 minutes prior to MMTS treatment and digitonin solubilization. PLCs were precipitated with rabbit anti-TAP1, and subcomplexes were eluted with 0.1% Triton X-100. Samples were then immunoprecipitated with a mouse mAb targeting the FLAG tag and resolved by reducing/non-reducing SDS-PAGE. Using this approach, only proteins contained in specific subcomplexes with the FLAG-tagged mutants should be precipitated (**Figure 5.6b**). Based on the molecular weights of the co-precipitated proteins, all of the FLAG-tagged ERp57 constructs were able to form the conjugate with tapasin, and all recruited MHC class I HC. A band corresponding to CRT

is not seen in this experiment, but CRT labels poorly and/or it could be lost during the biochemical isolation. Additionally, the interaction of MHC class I with FLAG-tagged ERp57 containing PLCs supports a high level of HLA-B*4402 cell surface expression. The surface level of HLA-B*4402 in WT-FLAG expressing cells was somewhat higher than C60A or C60/406/409A expressing cells, however, suggesting that the redox activity of the ERp57 *a* domain may be important for peptide loading (**Figure 5.6c**). However, a biochemical analysis of MHC class I assembly is somewhat inconsistent with this conclusion (see below). A more detailed analysis of these discrepancies is ongoing.

5.7: The redox function of ERp57 is not required for MHC class I loading

ERp57 possesses several functional domains. It is unlikely that the *a* domain is involved in peptide loading beyond allowing for conjugate formation. The *bb'* domains interact with CRT and CNX, and the role of these domains will be investigated in the future. In contrast, a redox active *a'* domain could play an important role in controlling the loading and/or egress of peptide loaded MHC class I complexes from the PLC. Because a C406/409A mutant did not form the conjugate, I expressed a C60/406/409A mutant in ERp57-suppressed cells. The escape pathway of the *a* domain of this mutant is inactivated, and it is important to compare peptide loading and MHC class I trafficking in cells expressing this mutant to those expressing the C60A mutant.

I pulse-labeled cells expressing HLA-B*4402, WT tapasin, and WT, C60A, C60/406/409A FLAG-tagged ERp57 with [^{35}S]-methionine and cysteine for 15 minutes and chased these cells for different lengths of time up to four hours in an excess of cold methionine and cysteine. Cells were lysed in digitonin, and free MHC class I HC/β_2m

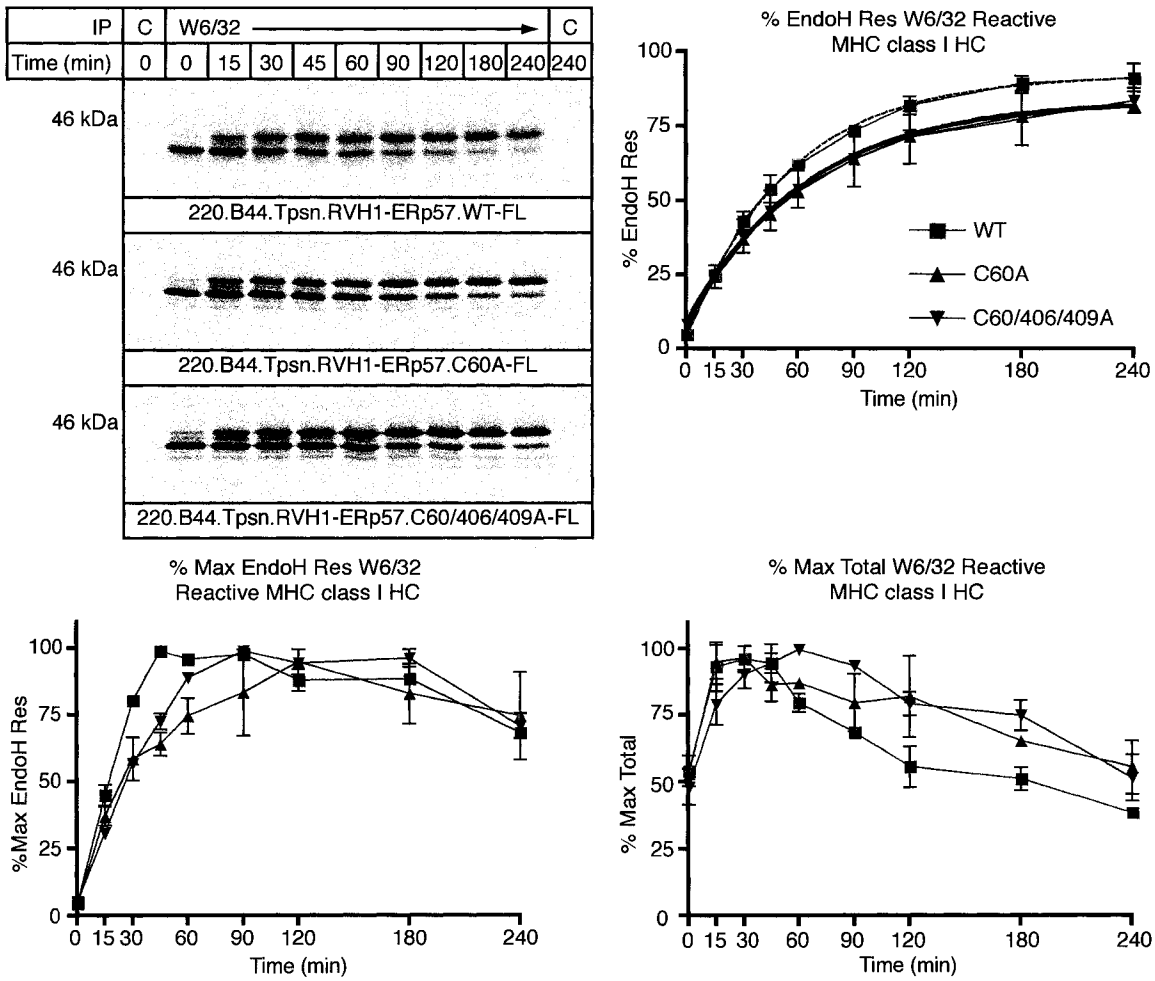

Figure 5.7: Normal trafficking and maturation of HLA-B*4402 in the presence of redox mutant conjugates.

721.220 cells expressing HLA-B*4402 and WT tapasin with suppressed endogenous ERp57 and re-expressed WT, C60A, or C60/406/409A FLAG-tagged ERp57 were pulse-labeled with [^{35}S]-methionine and cysteine for 15 minutes and chased for the indicated periods of time. Frozen cell pellets were solubilized in 1% digitonin, and post-nuclear supernatants were immunoprecipitated with the anti-MHC class I HC/β_2m conformation specific antibody W6/32 or the CD1d specific antibody 51.1.3 as a control and protein A-sepharose. Samples were washed with 0.1% Triton X-100 in TBS, eluted in 2x EndoH buffer with heating to 95° C, and incubated with 1 mU EndoH overnight at 37° C. Digested material was then resolved by reducing SDS-PAGE. Bands corresponding to EndoH resistant (upper band) and sensitive (lower band) MHC class I HC were quantitated, and the % EndoH resistant MHC class I HC was calculated (upper right panel). Signals were further expressed as % Max EndoH Res MHC class I HC (lower left panel) and % Max Total W6/32 reactive MHC class I HC (lower right panel) as a measure of the overall stability of W6/32 reactive complexes throughout the chase period. The mean +/- SEM of two independent experiments is shown.

dimers were precipitated with W6/32. After an overnight digestion with EndoH, samples were resolved by reducing SDS-PAGE. Bands corresponding to EndoH resistant and sensitive MHC class I HC were quantitated, and the rate of acquisition of EndoH resistance was calculated (**Figure 5.7**). The trafficking of HLA-B*4402 assembled in the presence of a redox inactive ERp57 mutant was the same as those assembled in cells expressing ERp57 with a functional *a'* domain. Additionally, the stability of W6/32 complexes was similar in all of these cells over the course of this four-hour experiment (**Figure 5.7, lower panels**). To examine the kinetics of MHC class I egress from PLCs containing mutant ERp57, I prepared cells as described above, but, at the indicated chase points, cells were treated with MMTS prior to digitonin lysis and immunoprecipitation with an anti-TAP1 antiserum. Precipitated material was eluted from the TAP heterodimer using 0.1% Triton X-100 prior to resolution by reducing SDS-PAGE (**Figure 5.8**). MHC class I HC appeared to transit through PLCs containing C60A mutant ERp57 more slowly than those containing WT or C60/406/409A ERp57, but these differences were not as pronounced as that seen with WT and C95A tapasin expressing cells. When **Figure 5.6**, **5.7**, and **5.8** are considered together, it is difficult to draw conclusions from these data. If the ERp57 *a* domain is essential for MHC class I loading, similar defects should be seen in C60A and C60/406/409A cells, but, if the *a'* domain functions in MHC class I loading, WT and C60A ERp57 should be comparable. The fact that WT and C60/406/409A are most similar with respect to MHC class I trafficking through the PLC is difficult to reconcile with a clear function for the redox domains of ERp57 in PLC action. However, the overall recruitment of MHC class I complexes into the PLC is not affected in these cells, as indicated by the MHC class I HC/tapasin ratio.

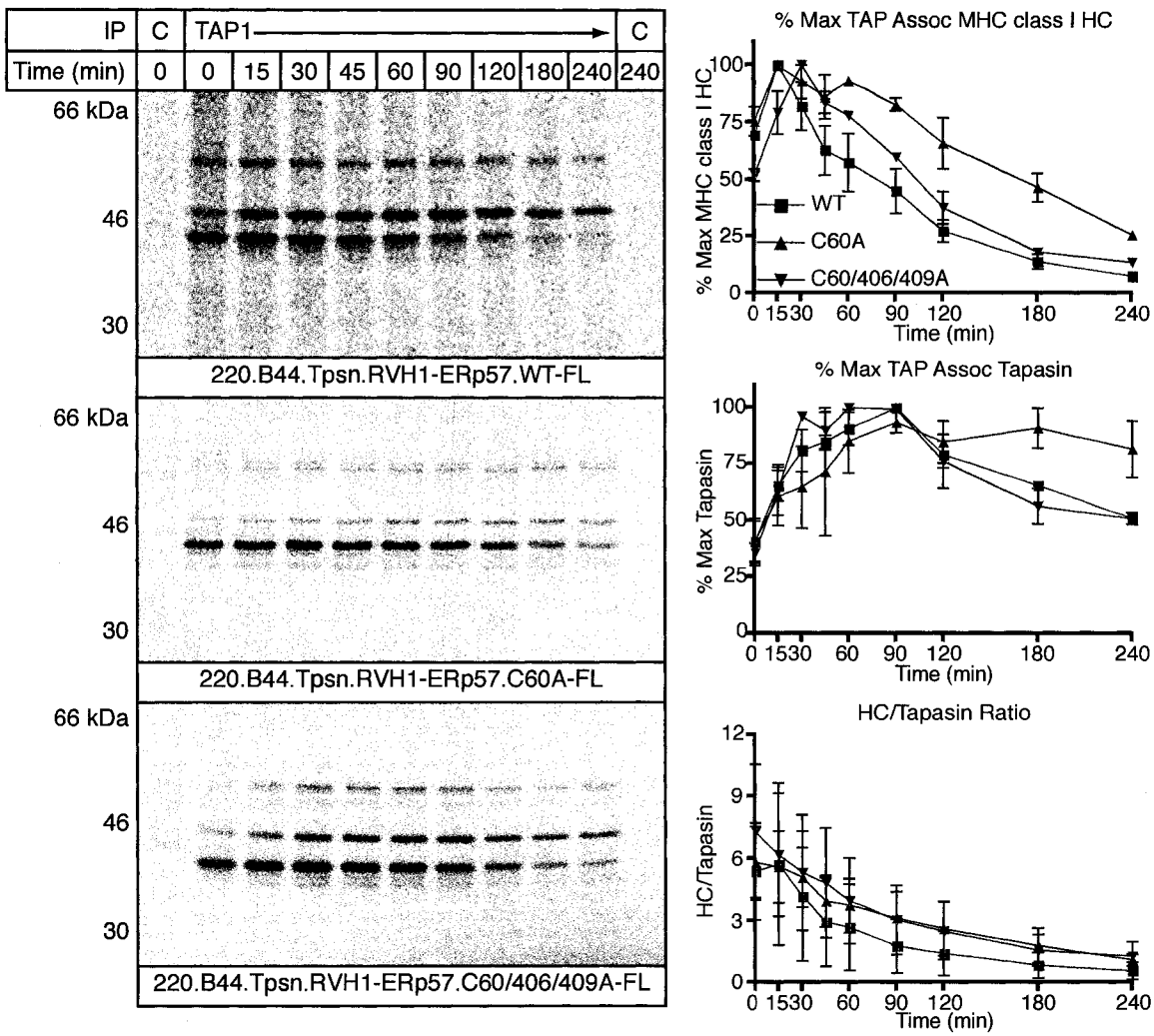

Figure 5.8: Altered HLA-B*4402 PLC recruitment and egress in the presence of redox mutant conjugates.

721.220 cells expressing HLA-B*4402 and WT tapasin with suppressed endogenous ERp57 and re-expressed WT, C60A, or C60/406/409A FLAG-tagged ERp57 were pulse-labeled with [^{35}S]-methionine and cysteine for 15 minutes and chased for the indicated periods of time. MMTS treated frozen cell pellets were solubilized in 1% digitonin, and post-nuclear supernatants were immunoprecipitated with either rabbit anti-TAP1 (RING.4C) or NRS as a control and protein A-sepharose. Precipitated material was washed with 0.1% digitonin in TBS prior to elution in 0.1% Triton X-100 in TBS for 5 min at 4° C. Eluted material was incubated with reducing sample buffer and resolved by SDS-PAGE. The bands corresponding to MHC class I HC and tapasin were quantitated and expressed as the % Maximum TAP associated MHC class I HC (upper right panel), the % Maximum TAP associated tapasin (middle right panel), and the MHC class I HC/tapasin ratio was also calculated (lower rightpanel). The mean +/- SEM of two independent experiments is shown.

Additionally, the stability of the TAP/tapasin interaction appears to be slightly greater for conjugates containing C60A ERp57. The relationship between the TAP/tapasin interaction and MHC class I association with the PLC could be inversely related. These differences will be further examined in the near future.

5.8: Normal redox state of MHC class I associated with ERp57-mutant PLCs

Dick et al. observed that PLC-associated HLA-B*4402 was partially reduced in cells expressing C95A tapasin, but Garbi et al. did not see any differences in the redox state of PLC-associated H2-K^b (Dick et al., 2002; Garbi et al., 2006). If ERp57 plays a direct role in maintaining the oxidation state of TAP-associated MHC class I HC, these effects are likely mediated by the *a'* domain. Thus, the redox state of PLC-associated HLA-B*4402 in C60/406/409A ERp57 expressing cells should be altered if this model is correct. However, the work of Dick et al. was performed prior to the use of MMTS for conjugate preservation, and the importance of cell pretreatment in maintaining PLC composition was not fully realized (Dick et al., 2002).

I first wished to confirm this key observation using MMTS. Cells expressing either C95A tapasin or WT tapasin were labeled with [^{35}S]-methionine and cysteine for 45 minutes prior to MMTS treatment and digitonin extraction. PLCs were isolated using an anti-TAP1 antiserum, and precipitated material was released by boiling in 1% SDS. Samples were then diluted into 1% Triton X-100, and MHC class I HCs were precipitated using the anti-MHC class I specific rat mAb 3B10.7 coupled to agarose beads. However, under these conditions, no redox differences were seen in HLA-B*4402 in C95A- and

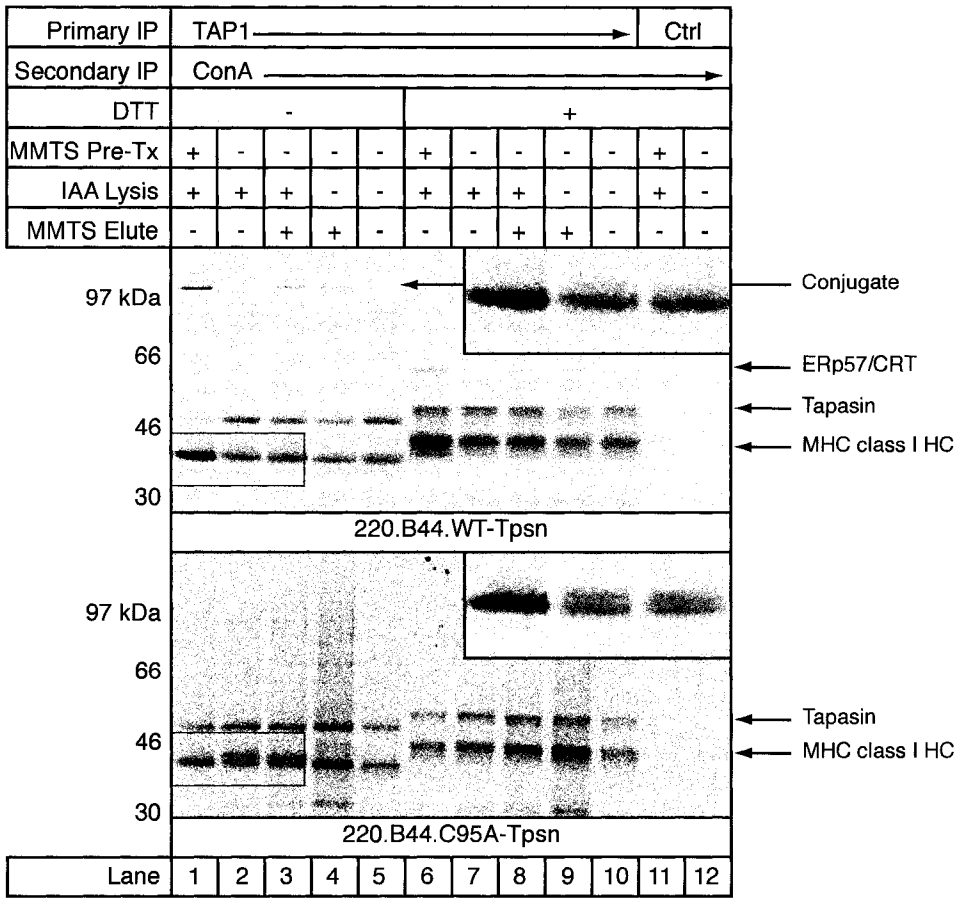

Figure 5.9: C95A-associated MHC class I HC reduction occurs post-solubilization in an IAA-dependent manner.

721.220 cells expressing HLA-B*4402 and WT or C95A tapasin were labeled with [^{35}S]-methionine and cysteine for 45 min and treated with MMTS as indicated (MMTS Pre-Tx). Cells were lysed in 1% digitonin in TBS with or without 10 mM IAA as indicated. Post-nuclear supernatants were immunoprecipitated with the anti-TAP1 antiserum RING.4C or NRS as a control and protein A-sepharose, and bound material was eluted in 0.1% Triton X-100 with MMTS as indicated. Samples were then immunoprecipitated with ConA-sepharose and resolved by reducing/non-reducing SDS-PAGE. Bands corresponding to the conjugate, ERp57/CRT, tapasin, and MHC class I HC are indicated. The inset boxes are 2x enlargements of the indicated regions corresponding to Lanes 1 – 3.

WT-tapasin expressing cells. All PLC-associated MHC class I HC was fully oxidized (data not shown).

The procedure used to demonstrate a redox difference in the presence of C95A tapasin was somewhat convoluted, but the data were very clear. Cells were solubilized in the presence of NEM and IAA, and subcomplexes were dissociated from TAP by eluting in 0.1% Triton X-100 with NEM. The NEM treatment was not very effective, however, because comparable amounts of free tapasin were seen in WT- and C95A-expressing cells under non-reducing conditions (Dick et al., 2002). Therefore, I wished to identify at which point during the experiment MHC class I HC reduction occurred. Cells expressing either WT or C95A mutant tapasin were labeled for 45 minutes with [^{35}S]-methionine and cysteine. Cells were then treated with MMTS or PBS alone prior to solubilization in digitonin with or without 20 mM IAA. TAP1 immunoprecipitates were then eluted with 0.1% Triton X-100 with or without 5 mM MMTS, and all samples were reprecipitated with Concanavalin A (ConA) sepharose. Samples were then resolved by reducing/non-reducing SDS-PAGE. ConA was used to precipitate all eluted MHC class I regardless of its association with tapasin, β_2m, and/or CRT. Under these conditions, only MHC class I HC isolated from C95A-expressing cells solubilized in the presence of IAA without prior MMTS treatment exhibited two redox forms (**Figure 5.9, Lanes 1 v. 2 v. 3**).

I next used these conditions to examine the redox state of HLA-B*4402 associated with WT tapasin in the presence or absence of different ERp57 mutants. As described above, cells were labeled for 45 minutes with [^{35}S]-methionine and cysteine and treated with or without MMTS prior to solubilization in digitonin with IAA. PLCs

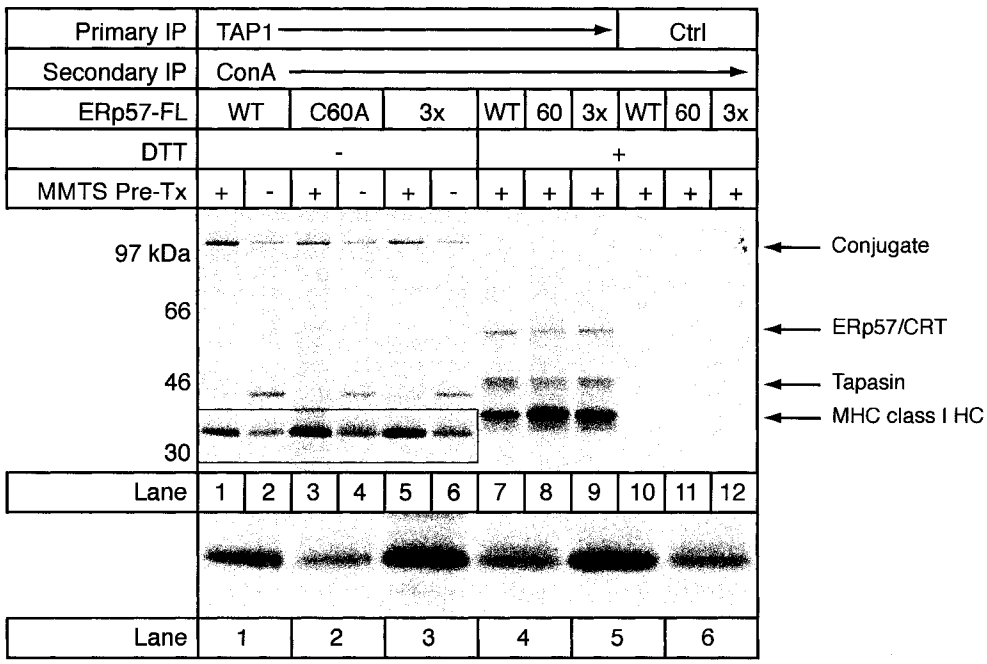

Figure 5.10: Normal MHC class I redox state in the presence of ERp57-redox mutants.

721.220 cells expressing HLA-B*4402 and WT tapasin with suppressed endogenous ERp57 and exogenously expressed FLAG-tagged WT, C60A, or C60/406/409A (3x) ERp57 were labeled with [^{35}S]-methionine and cysteine for 45 min and treated with MMTS as indicated (MMTS Pre-Tx). Cells were lysed in 1% digitonin in TBS with 10 mM IAA, and post-nuclear supernatants were immunoprecipitated with the anti-TAP1 antiserum RING.4C or NRS as a control and protein A-Sepharose. Bound material was eluted in 0.1% Triton X-100 with MMTS and reprecipitated with ConA-sepharose prior to resolution by reducing/non-reducing SDS-PAGE. Bands corresponding to the conjugate, ERp57/CRT, tapasin, and MHC class I HC are indicated. The lower panel is a 2x enlargements of the indicated region corresponding to Lanes 1 – 6.

were then isolated by immunoprecipitating for TAP1, and subcomplexes were released by incubating in 0.1% Triton X-100 with MMTS prior to precipitation with ConA-sepharose. Bound material was then resolved by reducing/non-reducing SDS-PAGE (**Figure 5.10**). Consistent with **Figure 5.9**, no redox differences were seen in HLA-B*4402 when cells were pretreated with MMTS prior to detergent lysis. Additionally, MHC class I HCs isolated from non-MMTS treated cells lysed in IAA were fully oxidized. While the mechanism by which HLA-B*4402 becomes reduced during solubilization of C95A-expressing cells is unclear, the *a'* domain of ERp57 does not play a role in maintaining the redox state of PLC-associated MHC class I.

5.9: Discussion

Over the past decade, RNAi has progressed from an interesting technique applicable to lower model organisms to a Nobel Prize winning discovery that has revolutionized many aspects of biology. Unfortunately, some of the conditions that could limit the suitability of RNAi to a particular system such as target stability, high expression, and strength of interaction all seem to apply the interaction of ERp57 with tapasin. Thus, despite achieving relatively high levels of ERp57 knock-down in a cell line that has traditionally been difficult to transfect, I observed no differences in HLA-B*4402 peptide loading. However, the cells I generated that stably suppress ERp57 expression allow for some conclusions about the nature of the conjugate to be made.

I previously showed that the amount of tapasin expressed controls the amount of free ERp57 available in cells (**Figure 2.1**). This experiment was still conducted under relatively physiologic conditions, and the amount of free ERp57 could still be sufficient

to meet the minimum requirements for glycoprotein folding. However, when I suppressed ERp57 expression using RNAi, all of the residual ERp57 was incorporated into the conjugate leaving no detectable free ERp57 in these cells (**Figure 5.1**). Thus, the recruitment of ERp57 into the conjugate is strongly preferred. In addition, the amount of unconjugated tapasin is further reduced in these cells due to the recruitment of PDI and ERp72 into mixed disulfides. These data also argue that when exposed to the ER lumen, Cys-95 of tapasin is very reactive, and maintaining this cysteine in reduced form is strongly disfavored.

The detection of mixed disulfides containing tapasin and PDI or ERp72 also argues that the ability of tapasin to inhibit the ERp57 escape pathway applies to other Trx-motif containing proteins. Admittedly, less tapasin is associated with PDI/ERp72 than ERp57, but this strongly suggests some degree of escape pathway inactivation for both PDI and ERp72. In the presence of MMTS, few if any mixed disulfides are seen for PDI and ERp72, consistent with the model of escape pathway activation discussed in Chapter 3 and proposed by Walker et al. (Walker and Gilbert, 1997). This is not surprising given the high degree of conservation surrounding the Trx active site in these oxidoreductases. I was unable to detect complexes of tapasin conjugated-PDI or -ERp72 with CRT or β_2m, but this does not eliminate the possibility that they associate *in vivo* (data not shown). The isolation conditions required for this experiment were somewhat harsh, and the interaction between ERp57 and CRT is relatively weak. The residues responsible for CRT binding are absent from PDI, and, while these residues are somewhat conserved in ERp72, the domain architecture of ERp72 differs from that of ERp57 (Kozlov et al., 2006). If the *a'* domain of ERp72 forms a mixed-disulfide with

tapasin, the *b'* domain would not be orientated properly to coordinate CRT binding. To fully assess the ability of PDI/ERp72 conjugated tapasin to recruit MHC class I/β_2m dimers and/or CRT, ERp57 expression should be knocked-down in cells unable to coordinate the 4:1 subcomplex:TAP stoichiometry seen in WT cells.

Given the only slight changes in conjugate level and PLC composition seen in cells stably suppressing ERp57, the lack of an effect on MHC class I surface expression, acquisition of EndoH resistance, and stability of MHC class I/β_2m complexes is not surprising. When these parameters are compared between WT- and C95A-tapasin expressing cells, differences in complex stability are the most striking. The fact that no differences were seen between cells expressing 100% conjugated tapasin and approximately 70% conjugated tapasin suggests that MHC class I molecules may undergo multiple rounds of PLC engagement. The "quality control" model of peptide loading predicts that MHC class I complexes interact with the PLC, bind peptide or undergo peptide exchange, and dissociate from the PLC. Once free in the ER, weakly bound peptides are lost triggering a conformational change in MHC class I that is sensed by UGGT leading to reglucosylation and reengagement with the PLC. Thus, the phenotype of cells containing a mixture of PLCs fully and partially competent for mediating peptide loading could be masked by the successive reengagement of poorly loaded MHC class I/β_2m dimers with fully functional subcomplexes containing both tapasin and ERp57. This model has yet to be proven, but, if correct, reengagement with the PLC must occur rapidly, however, as no differences in trafficking were seen between RVH1-Ctrl and –ERp57 transduced cells. Alternatively, the 30% unconjugated tapasin

present in RHV1-ERp57 transduced cells could support peptide loading sufficiently well as to be indistinguishable from fully conjugated tapasin.

The phenotypes of ERp57-deficient mouse B cells and human cells expressing HLA-B*4402 and C95A tapasin were very similar in most respects. Both suggest a role for ERp57 in recruiting and/or stabilizing MHC class I in the PLC, and this appears required for the acquisition of tightly bound peptide by a large population of MHC class I/β_2m dimers. Therefore, if ERp57 has a function in the PLC beyond forming the conjugate, the incorporation of different ERp57 mutants into the PLC should recapitulate the phenotype seen in these cells. However, when the redox activity of the ERp57 *a'* domain was completely eliminated, no differences in PLC association were seen compared to cells expressing WT ERp57. In contrast, MHC class I association with the PLC was prolonged in cells expressing predominantly C60A ERp57. These data are not straightforward, however, as the ratio of MHC class I HC to tapasin did not differ between any of these cell lines. There was an approximately 10-fold difference between the MHC class I HC to tapasin ratio in cells expressing WT and C95A tapasin. At best, the redox activity of the ERp57 *a'* domain only partially explains the role of ERp57 in the PLC. Thus, it is likely that the *bb'* domains are likely responsible for the function of ERp57 in peptide loading. Studies are ongoing to assess the role of these domains in recruiting CRT and MHC class I HC into the PLC.

It is possible that elimination of the redox activity of the ERp57 *a* domain while the activity of the *a'* domain is retained somehow affects the long-term association of tapasin with TAP. While ERp57 does not exhibit domain synergy comparable to PDI (Kulp et al., 2006), there is clearly some degree of functional interdependence for the *a*

and *a'* domains of ERp57 because, when the *a* domain is left intact, an *a'* domain redox mutant cannot form the conjugate (Dick et al., 2002). Additionally, a C406A mutant in which the N-terminal cysteine of the *a'* CXXC motif is replaced with alanine does not form the conjugate (data not shown). These observations suggest that the redox activity of the *a'* domain is somehow required for conjugate formation and/or preservation, but further studies are needed to clarify the potential redox mechanisms affecting this phenomena.

One of the most striking phenotypes observed in C95A-tapasin expressing cells was the altered redox state of PLC-associated HLA-B*4402. I have now shown that result is somewhat an artifact of solubilization conditions. The reactivity of MMTS is much greater than that of NEM or IAA, and proteins isolated from cells treated with MMTS most likely represent the true *in vivo* redox state. HLA-B*4402 associated with the PLC in C95A-tapasin expressing cells is fully oxidized following MMTS treatment, and only after solubilization in IAA does a redox difference appear. However, the absence of a redox difference in MHC class I HC in cells expressing WT tapasin under identical conditions suggests that the HLA-B*4402 associated with C95A tapasin is somehow more susceptible to reduction. Nevertheless, the presence of a redox inactive ERp57 mutant in the PLC does alter the redox state of HLA-B*4402 compared to WT-ERp57 containing conjugates. Park et al. recently identified a role for PDI in controlling the redox state and peptide loading of HLA-A*0201 exogenously expressed in HeLa cells. They did not pretreat cells with MMTS, but they followed a procedure similar to Dick et al. (Dick et al., 2002; Park et al., 2006). I have now shown that the redox state of MHC class I HCs in the ER is, under some conditions, exquisitely sensitive to the

biochemical isolation procedure. It is possible that PDI plays an indirect role in controlling the redox state of MHC class I HC, but this requires further clarification. NEM, IAA, and MMTS are generally considered interchangeable in their reactivity, but this is clearly not the case (Lundblad, 1995). Amongst these reagents, MMTS is the most specific for cysteine residues with the most rapid reaction kinetics. Additionally, IAA treatment does not preserve the conjugate, suggesting that ERp57 Cys-60 is not accessible to IAA *in vivo*. Differential Cys-60 accessibility may explain the differences in conjugate preservation seen with MMTS compared to NEM. For these reasons, the redox state of MHC class I isolated from cells pretreated with MMTS is likely the most representative of the *in vivo* redox state, and, under these conditions, I could detect no redox differences in PLC-associated HLA-B*4402. Taken together, my data argue against a role for the redox regulation of peptide loading.

Chapter 6: Conclusions and Future Directions

6.1: Peptide loading and PLC assembly

Peptide loading onto MHC class I complexes is a dynamic event involving multiple steps within the ER. There are three distinct phases of MHC class I assembly and peptide loading: events prior to PLC incorporation, events occurring in the PLC, and post-PLC events including ER egress and trafficking to the cell surface. The folding of MHC class I HC with β_2m prior to their PLC association is a classic case of glycoprotein folding involving glucosylation-dependent interactions of substrate (MHC class I HC) with CNX and ERp57-facilitated disulfide bond oxidation. Intermediates in this process can be detected using standard biochemical techniques, and the details of MHC class I HC folding and assembly with β_2m seem clear at the present time. In contrast, the assembly and mechanism of action of the PLC is less well studied.

To the best of our knowledge, a single PLC contains no less than 22 distinct polypeptide chains when the 4:1 tapasin:TAP stoichiometry is considered together with the composition of the tapasin-based subcomplexes. It is assumed that subcomplexes are functionally identical, and the factors regulating subcomplex assembly should not vary with the site of tapasin interaction with the TAP heterodimer. Despite involving well-characterized glycoprotein specific chaperones, I have now shown that the assembly of the core components of the PLC deviates substantially from models of glycoprotein quality control. In particular, ERp57 is specifically recruited to the PLC by glycan-independent interactions with tapasin alone. It remains in a mixed disulfide with tapasin despite tapasin having achieved all markers of a correctly folded, native protein. In

contrast, the interaction of CRT with the PLC appears to be entirely dependent upon the presence of monoglucosylated MHC class I HC, consistent with its role in glycoprotein folding.

The plethora of proteins and interactions within the PLC provides ample possible sources of variation that were hypothesized to be related to peptide loading. Most generally, the peptide loading status of MHC class I could affect the association of CRT or ERp57 with MHC class I/β_2m/tapasin subcomplexes. Additionally, the redox states of MHC class I, tapasin, and ERp57 could be modulated to correspond to different peptide loading states. Finally, the glucosylation state of the MHC class I N-linked glycan could indicate the quality of loaded peptide in the PLC. Standard biochemical techniques were used to address most of these possibilities, but, for all conditions examined, no variability was seen (this study and Pamela Wearsch, manuscript in preparation). All tapasin is conjugated to ERp57, and all subcomplexes contain monoglucosylated MHC class I HC and CRT. Additionally, I showed that variations in MHC class I HC redox state arise post-solubilization. It remains possible that the redox state of the Cys-7/Cys-71 disulfide bond in the N-terminus of tapasin and/or the *a'* domain of ERp57 are affected by peptide loading, but my studies suggest that this is not the case.

The function of ERp57 within the PLC remains unclear. The altered PLC composition seen in the absence of ERp57 clearly indicates that proper recruitment of MHC class I HC/β_2m dimers and CRT critically depend upon conjugate formation. This represents a classic "chicken and egg" puzzle. The lack of CRT recruitment could be secondary to the loss of ERp57-dependent interactions of MHC class I HC with tapasin.

Alternatively, the interaction of the CRT P-domain with ERp57 may be required for the full recruitment and/or stabilization of MHC class I complexes in the PLC.

The tapasin/ERp57 conjugate with the TAP heterodimer is the core of the PLC, and my data indicate that functional studies of tapasin that do not incorporate ERp57 likely do not reflect the state of tapasin *in vivo*. Within the cell, there is no unconjugated tapasin associated with the PLC, and this is the most functionally important tapasin population. While the phenotype of cells unable to form the conjugate is less pronounced than cells lacking tapasin altogether, tapasin has clearly evolved to specifically recruit and retain ERp57 within the PLC. Comparisons between tapasin-deficient and tapasin-sufficient cells are further complicated by the tapasin-mediated stabilization of the TAP heterodimer. Thus, the somewhat impaired peptide loading seen in cells expressing soluble tapasin could be related to decreased TAP-mediated peptide translocation. Finally, the conjugate appears able to enhance peptide loading *in vitro* to a much greater extent than tapasin alone (Pam Wearsch, manuscript in preparation).

The conjugate is preserved much more efficiently in cells treated with MMTS compared to NEM, but, in the absence of either reagent, no conjugate is seen after SDS-PAGE. For conjugates in which Cys-60 remains reactive, detergent solubilization leads to some degree of escape pathway activation and the release of non-covalently associated ERp57. The full extent of conjugate reduction is dependent on several factors including the detergent used, but it is likely that the non-covalently associated ERp57 immunoprecipitated with the PLC in early studies in the absence of NEM or MMTS was conjugated to tapasin immediately prior to the addition of SDS-PAGE sample buffer. The release of ERp57 in the absence of MMTS or NEM during solubilization and

biochemical isolation of the PLC could dramatically alter the quantity of co-precipitated PLC components. Specifically, less MHC class I and CRT are found associated with non-MMTS treated PLCs after digitonin lysis, preclear, and TAP1 immunoprecipitation (unpublished observations).

Conjugate preservation is especially essential for the proper assessment of interactions in the context of novel mutations in PLC components, and the duration of biochemical isolation could affect the observed phenotype of isolated PLCs. The lengths of time specified in Chapter 7 and the figure legends of this dissertation are accurate and reflect the shortest periods of time supporting a balance between signal sensitivity, specificity, and consistency. While not precisely empirically determined, preliminary results obtained following longer preclearing and immunoprecipitation steps were often inconsistent and exhibited variable amounts of non-specific background signals. Taken together, these observations suggest a series of critical steps that must be considered in future studies of MHC class I antigen loading. Inconsistencies between studies could be a reflection of the set of techniques used rather than the systems being studied. In particular, MMTS treatment should become standard practice in studies examining interactions within the PLC.

6.2: Future Studies

There are a number of questions surrounding MHC class I loading in the ER that remain unanswered. It is generally assumed that all MHC class I molecules interact with the PLC at some point, and poorly loaded MHC class I complexes are thought to undergo multiple rounds of PLC engagement. Inhibition of glucose trimming with CST prolongs

the interaction of MHC class I with the PLC (van Leeuwen and Kearse, 1996), but monoglucosylated MHC class I complexes could undergo multiple rounds of PLC binding in the absence of glucosidase activity. It remains to be determined where and when the final glucose trimming of MHC class I occurs. Additionally, UGGT presumably recognizes some aspect of peptide-free MHC class I complexes, but the role of reglucosylation and the structural aspects of UGGT recognition of MHC class I HC are entirely unknown.

Structural studies of the tapasin/ERp57 conjugate will greatly enhance our understanding of peptide loading. Tapasin alone has been refractory to crystallization, but I have shown that conjugation with ERp57 enhances the structural integrity of tapasin. Additionally, as stated above, conjugated tapasin is the most physiologically form. Current attempts at conjugate crystallization are encouraging (G. Dong and P. Wearsch, personal communication). A structure of the conjugate could provide valuable insight into the residues of both ERp57 and tapasin responsible for ERp57 recruitment and tapasin-mediated escape pathway inhibition. Furthermore, combining the structures of MHC class I/β_2m complexes with mutational analyses will allow the identification of the sites of interaction between MHC class I and tapasin. Taken together, these data will suggest a series of novel mutations in MHC class I HC, tapasin, and ERp57 to be generated and examined.

The changes that occur in MHC class I and the PLC during the course of peptide loading are not detectable given current techniques and reagents. It is likely that subtle conformation changes in MHC class I complexes correspond to the binding of high or low affinity peptides, and these changes dictate the recognition of MHC class I

complexes by tapasin. Additionally, tapasin binding could affect the conformation of MHC class I (Wright et al., 2004), and the converse cannot be excluded. These changes would likely take place on a very rapid time-scale, and their detection may require the application of advanced structural and biophysical techniques. In particular, NMR may be required to visualize changes in MHC class I and/or tapasin structure during their interaction in the presence and absence of peptide

There is a growing body of literature examining MHC class I antigen processing and presentation using confocal microscopy and related techniques (Neijssen et al., 2005; Pentcheva et al., 2002; Reits et al., 2000; Spiliotis et al., 2000). However, these studies largely exist independent of the biochemical literature making it difficult to fully incorporate these data into a comprehensive model of MHC class I trafficking. In particular, the cell lines that are amenable to examination by microscopy are not those that have been traditionally examined biochemically. Future studies should seek to combine these two spheres of study. Epstein Barr Virus transformed human B cell lines including 721 and its derivatives are the basis for much of our understanding of MHC class I biochemistry. Most if not all of the components of the MHC class I antigen processing pathway are constitutively upregulated in these cells lines, and greater insight into the factors regulating antigen presentation could be gained by examining epithelial and stromal cell lines under different conditions of immune stimulation such as by IFN-γ. Finally, primary human and mouse dendritic cells may be the most interesting and immunologically relevant cells for future studies.

Chapter 7: Materials and methods

7.1: Cell lines and antibodies

All cell lines used in these studies are listed in *Appendix II*. For experiments involving HeLa-M, FO-1, or FO-1.β_2m, the cells were treated with 200 U/mL human IFN-γ (R&D Systems) for two days prior to harvesting as indicated. HeLa-M, FO-1, FO-1.β_2m, CEM.NKR.A2, CEM.NKR.A2.CNX, and 293T were maintained in Iscove's modified Dulbecco's medium (IMDM) (Invitrogen) supplemented with 5% bovine calf serum (BCS) (Hyclone), GLUTAMAX (Invitrogen) and penicillin/streptomycin (Invitrogen), and C1R.A2.WT, C1R.A2.C60A, and all derivatives of 721 were grown in IMDM with 10% BCS, GLUTAMAX, and penicillin/streptomycin. All cells were grown in a humidified incubator with 6% CO_2 at 37°C.

Monoclonal antibodies and rabbit antisera used are listed in *Appendix III*. A new rabbit antiserum was raised against soluble, insect cell expressed tapasin (R.SinE) using conventional methods by a third party (Open Biosystems). Additionally, this is the first use of a mouse mAb raised against the C-terminal peptide of tapasin. Mice were immunized and hybridomas generated using conventional methods (Mary Pan, unpublished results).

7.2: Plasmids

Retroviral vectors encoding short-hairpin RNA (shRNA) constructs targeting ERp57 mRNA (RVH1-ERp57) or a non-targeting control (RVH1-Ctrl) were constructed using the RVH1 vector (Barton and Medzhitov, 2002). The RVH1 vector was digested

with BglII and XhoI and dephosphorylated by incubating with calf intestinal phosphatase (CIP) for 1 hr at 37°C. The digested vector was then gel purified. The following oligonucleotides were synthesized with 5' phosphates: ERp57-F 5'-gat ccc cGG ACT CTT CCA TCA GAG ATt tca aga gaA TCT CTG ATG GAA GAG TCC ttt ttg gaa c-3', ERp57-R 5'-tcg agt tcc aaa aaG GAC TCT TCC ATC AGA GAT tct ctt gaa ATC TCT GAT GGA AGA GTC Cgg g-3', Ctrl-F 5'-ga tcc ccG CTT CAA CAG CAG GCA CTC ttc aag aga GAG TGC CTG CTG TTG AAG Ctt ttt gga ac-3', Ctrl-R 5'-tcg agt tcc aaa aaG CTT CAA CAG CAG GCA CTC tct ctt gaa GAG TGC CTG CTG TTG AAG Cgg g-3'. Upper case letters indicate the complimentary regions giving rise to hairpin formation. Complimentary oligonucleotides were annealed by heating to 95°C for 4 min in annealing buffer (100 mM potassium acetate, 30 mM HEPES, 2 mM Mg-acetate, pH 7.4) followed by 10 min at 70°C with gentle cooling to 4°C. Annealed oligos were ligated into RVH1 using the rapid DNA ligation kit (Roche) according to the manufacturer's protocol. Following transformation and cloning, the constructs were confirmed by sequencing to generate RVH1-Ctrl and RVH1-ERp57.

Retroviral vectors encoding WT, C60A, and C60/406/409A FLAG-tagged ERp57 were generated by BamHI digestion and gel purification of ERp57-FLAG from pCDNA3.1-Puro (Dick et al., 2002). The retroviral vector pBMN-IRES-EGFP (a gift of A. Bothwell, Yale University) in which EGFP is expressed bicistronically with the gene of interest was digested with BamHI and dephosphorylated with CIP prior to gel purification. ERp57-FLAG was ligated into pBMN-IRES-EGFP as described above. Clones were screened for the correct insertion orientation by restriction digestion.

A glycan deficient tapasin mutant (N233A) was generated using the Quickchange Site Directed Mutagenesis kit (Stratagene) with primers N233A-S 5'-GCC CAT GGA CCG GAG CCG GGA CCT TCT GGC TG-3' and N233A-AS 5'-CAG CCA GAA GGT CCC GGC TCC GGT CCA TGG GC-3' with WT tapasin in pCR2.1 as a template according to the manufacturer's instructions (Ortmann et al., 1997). The mutation was confirmed by sequencing. WT tapasin in pBMN-IRES-Puro was digested with EcoRI prior to dephosphorylation and gel purification (Dick et al., 2002). N233A-tapasin in pCR2.1 was also digested with EcoRI and gel purified, and the region corresponding to the N-terminus of tapasin was extracted and ligated into pBMN-Tpsn-IRES-Puro using the rapid DNA ligation kit. Positive clones were screened for insert orientation by restriction digest.

7.3: Production of retrovirus and cell transduction

Infectious retrovirus was produced by the co-transfection of 12 μg retroviral vector with 12 μg pCL-Ampho (Imgenex) into 293T cells in 10 cm dishes using Lipofectamine 2000 (Invitrogen) following the manufacturer's protocol. Four hrs after transfection, the media was replaced and cells were shifted to a 32°C humidified incubator overnight. The following morning, 5 x 10^6 target cells were resuspended in harvested retrovirus containing media with 8 μg/mL polybrene. Cells were spun in 6-well plates for 90 min at 2500 RPM at 32°C ("spinfection"). Spinfected cells were then placed in a 32°C humidified incubator overnight. This process was repeated three times. For RVH1-Ctrl, RVH1-ERp57, and pBMN-ERp57-FLAG-IRES-EGFP transduced cells,

following the last spinfection, cells were resuspsended in fresh medium and placed at 37°C for two days prior to FACS to assess transduction efficiency.

For pBMN-N233A-IRES-Puro transduced cells, cells were placed in 1 μg/mL puromycin for selection. Cells growing after one week in selection were then cloned by limiting dilution, and cells were screened for tapasin expression by intracellular FACS using PaSta1. Clones with similar expression to 721.220.B4402 cells expressing WT tapasin were further screened by Western blotting.

7.4: Flow Cytometry and Sorting

All steps were performed at 4°C unless otherwise indicated, and all analysis was carried out using FlowJo software (Treestar Inc.). Cells were harvested and washed with FACS buffer (PBS with 0.05% BCS, 1 mM $CaCl_2$, and 0.1% Sodium Azide). Cells were then incubated with 100 μL of tissue culture supernatant, 1:100 dilutions of purified mouse mAbs, or 1:100 or 1:5 dilutions of directly coupled commercially available antibodies for 30 min. Cells were then washed with FACS buffer. Cells stained with uncoupled mAbs were then incubated with 1:100 dilutions of goat anti-mouse antiserum coupled to fluoroscein isothiocyanate (FITC) (Chemicon) or allophycocyanin (APC) (Caltag) for 30 min. After washing in FACS buffer, cells were analyzed using either a FACScan or FACScalibur (Becton Dickinson).

For isolation and sorting of RVH1-transduced cells, seven to ten days after the final spinfection, 10 x 10^6 cells were incubated with 1 mL of 1:200 dilution of mouse anti-CD4 directly coupled to APC (eBioscience), washed with FACS buffer, and sorted using a FACSvantage instrument. For sorting of cells transduced with pBMN-ERp57-

FLAG-IRES-EGFP, 10 x 10^6 cells were washed with FACS buffer before sorting. Cells highly expressing the CD4 or EGFP marker were isolated by three sorts.

For intracellular FACS, cells were washed with FACS buffer prior to fixation with 3.7% formaldehyde in serum free IMDM for 15 min at room temperature (RT). Fixation was stopped by washing cells in IMDM with 10 mM glycine, and cells were washed once in PBS. Fixed cells were then permeabilized in 0.1% Triton X-100 in FACS buffer with 10 mM glycine (permeabilization solution) for 15 min at RT followed by incubation in 1:100 dilutions of purified PaSta1 or BB7.2 in permeabilization solution for 30 min. Following washing in permeabilization solution, cells were incubated with a 1:100 dilution of goat anti-mouse antiserum coupled to FITC for 30 min at RT. After a final wash in FACS buffer, cells were analyzed using a FACScalibur.

7.5: Metabolic labeling and pulse chase analyses

For all metabolic labeling experiments, cells were harvested, washed with PBS, and resuspended in 3 mL of DMEM without methionine and cysteine with 3% dialyzed fetal bovine serum (Gibco) and penicillin/streptomycin (Invitrogen) for 1 hr in a 37°C standing incubator with rocking. Starved cells were then labeled with 1 mCi of [^{35}S]-methionine and cysteine labeling mix (ICN or Perkin Elmer) per 20 x 10^6 cells for the indicated period of time prior to harvesting or chase. For pulse-chase analyses, IMDM with 5% or 10% BCS, GLUTAMAX, penicillin/streptomycin, and 3 mM cold cysteine and methionine was added to the labeled cells, and aliquots were removed at the indicated times. During the chase period, cells were maintained in a standing 37°C incubator with rocking. Harvested, labeled cells were washed once with PBS with or

without 10 mM MMTS (Pierce) as indicated and frozen. Frozen cell pellets were handled as described below or membranes were prepared as described below. For experiments examining the glucosylation dependence of conjugate formation, cells were starved, labeled, and chased in the presence of 2 mM CST (Sigma) as indicated.

7.6: Detergent extraction of cells

Radio-labeled or unlabeled cells were washed in PBS with or without 10 mM MMTS as indicated. Either frozen or fresh cell pellets were solubilized in either 1% digitonin (EMD Biosciences) or Triton X-100 (American Bioanalytical) in 0.15M NaCl, 0.01M Tris-Cl, pH 7.4 (TBS) with 1 mM $CaCl_2$ and 500 μM phenyl-methylsulfonyl fluoride (PMSF) with or without 10 mM iodoacetamide (IAA) for 30 min on ice. Cell debris was removed by centrifugation at 14,000 RPM in a tabletop microcentrifuge at 4°C for 5 min.

For Western blotting, all cells were solubilized in 1% Triton X-100, and the protein content of the post-nuclear supernatants was quantitated by Bradford assay (Bio-Rad). For quantitative Western blots, three-fold serial dilutions were made in 1% Triton X-100 in TBS corresponding to the indicated amounts of loaded total protein, and for non-quantitative Western blots, 15 μg lysate was resolved by SDS-PAGE. For gels in which all samples were reduced, 10x SDS-PAGE sample buffer with 10% β-mercaptoethanol (β-ME) was added prior to heating to 95°C for 5 min. For gels containing both reduced and non-reduced samples, 50 mM dithiothreitol (DTT) (5 mM final concentration) (American Bioanalytical) was added to all samples as indicated prior

to heating at 95°C for 5 min. All samples were subsequently treated with IAA (15 mM final concentration) for 5 min at room temperature (RT) and resolved by SDS-PAGE.

7.7: Immunoprecipitations and EndoH digestion

For radio-labeled cells, post-nuclear supernatants were precleared with 7 μL NRS and 100 μL protein A-sepharose for 1 hr at 4°C with constant rotation. Precleared supernatants were then immunoprecipitated with specific rabbit antisera or NRS as a control and protein A-sepharose, mouse or rat mAbs or mIgG directly coupled to agarose beads, or mouse mAbs and protein G-sepharose or protein A-sepharose if an appropriate isotype for 1 hr at 4°C with constant rotation. Immunoprecipitated material was washed three times with 1 mL 0.1% detergent in TBS with 1 mM $CaCl_2$. For experiments involving only a single immunoprecipitation step without EndoH digestion, samples were eluted in 2x SDS-PAGE sample buffer with or without 2% β-ME for reducing or non-reducing gels, respectively, with heating to 95°C for 5 min. For gels containing both reduced and non-reduced samples, eluted material was incubated with or without 5 mM DTT at 95°C for 5 min, and IAA was added to all samples to a final concentration of 15 mM for 5 min at RT. Samples were then resolved by SDS-PAGE. For secondary immunoprecipitations, samples were eluted under non-denaturing conditions with 0.1% Triton X-100 in TBS with 1 mM $CaCl_2$ at 4°C, or samples were stripped by heating in 1% SDS in H_2O at 95°C for 5 min prior to 20-fold dilution into 1% Triton X-100 in TBS with 1 mM $CaCl_2$. Secondary immunoprecipitations and sample elution with or without reduction were performed as described above. For EndoH digestion, immunoprecipitates were eluted in 2x EndoH buffer (0.05M sodium phosphate, 0.25% SDS, pH6.5) by

heating to 95°C for five min. Samples were then incubated in 1 mU of EndoH (Roche) overnight at 37°C prior to reducing SDS-PAGE.

For unlabeled cells, $5x10^6$ cells per gel lane were treated with or without 10 mM MMTS in PBS and extracted as described above. Post nuclear supernatants were either immediately precipitated with directly coupled mAb or precleared with protein G-sepharose or protein A-sepharose for mouse or rabbit immunoprecipitations, respectively, rotating for 1 hr at 4°C. Precleared supernatants were specifically immunoprecipitated with mouse mAbs or rabbit antisera and protein G-sepharose or protein A-sepharose, respectively. Samples were then washed three times with 0.1% detergent in TBS with 1 mM $CaCl_2$. For gels containing all reduced samples, precipitated material was eluted in 2x reducing SDS-PAGE sample buffer with heating to 95°C for 5 min. For gels containing both reduced and non-reduced samples, material eluted in 2x NRSB with heating to 95°C for 5 min was incubated with or without 5 mM DTT at 95°C for 5 min. All samples were then incubated with 15 mM IAA for 5 min at RT prior to SDS-PAGE. Separated proteins were then transferred as described below.

7.8: Quantitative and non-quantitative immunoblotting

Non-radio-labeled samples separated by SDS-PAGE were transferred to Immobilon-P polyvinylidene fluoride (PVDF) membranes (Millipore) using a semi-dry method. Non-specific binding was then blocked by incubating membranes in 5% skim milk powder (Carnation) in PBS with 0.2% Tween-20 (Blotto) for either 30 min at RT or overnight at 4°C. Membranes were then cut or left intact and incubated with primary antibody in blotto for either 1 hr at RT or overnight at 4°C. Membranes were washed

once in PBS followed by two washes in PBS with 0.2% Tween-20 (PBS-T) for 5 min at RT. Membranes were then incubated with 1:5000 dilutions of species-specific, minimally cross-reactive goat antisera coupled to horseradish peroxidase (HRP) or alkaline phosphatase (AP) (Jackson Immunoresearch) for non-quantitative or quantitative blots, respectively, for 30 min at RT. Membranes were washed as above. Non-quantitative blots were visualized by incubation of membranes with enhanced chemiluminescent (ECL) substrate and exposure to film. Quantitative blots were incubated with enhanced chemifluorescent (ECF) substrate and visualized using a Storm 860 imaging system and ImageQuant software (GE Biosciences).

7.9: β_2m RNAi

The following β_2m specific and control siRNA oligonucleotides were obtained from Dharmacon: siβ_2m#1: 5'-AAG AGU AUG CCU GCC GUG UGA-3', siβ_2m#2: 5'-AAG CAA GGA CUG GUC UUU CUA-3', siCtrl: 5'-AAG CUU CAA CAG CAG GCA CUC-3'. 721.220 cells expressing HLA-B*0801 and WT tapasin were transfected using the Amaxa nucleofector device with program V01 and solution R (Amaxa) using a modified manufacturer's protocol. 20 x 10^6 cells were resuspended in 500 µL of solution R with 250 pmol siCtrl or 125 pmol each of siβ_2m#1 and siβ_2m#2. Five sets of 100 µL cell aliquots were transfected with program V01, and 500 µL of pre-warmed media was added to cells prior to transfer to T25 flasks with 9 mL of media equilibrated to 6% CO_2 at 37°C. Cells were harvested at 0, 3, 6, and 12 hrs after transfection, treated with 10 mM MMTS in PBS, and frozen. Frozen cell pellets were solubilized in 1% digitonin and processed as described above for quantitative immunoblotting.

7.10: Membrane preparation

Radio-labeled 721.221 or unlabeled FO-1.β_2m cells were harvested, washed in PBS with or without MMTS as indicated and frozen. Frozen cell pellets were resuspended in ice-cold TBS with 1 mM $CaCl_2$ and PMSF and centrifuged at 300xg at 4°C for 10 min. Supernatants were preserved on ice, and the pelleted material was resuspended in ice-cold 10 mM Tris-Cl, pH 7.4 and centrifuged at 300xg for 10 min. The pooled supernatants were pelleted at 100,000xg for 1 h at 4°C, and the membranes were treated as described in the figure legends. After the final addition of detergent, debris was removed by centrifugation at 14,000 RPM in a table-top microcentrifuge at 4°C for 10 min. Supernatants were then immunoprecipitated or directly resolved by SDS-PAGE for Western blotting.

7.11: Tapasin conformational stability

For the analysis of tapasin isolated from radio-labeled cells, TAP1 immunoprecipitates were incubated in 0.1% Triton X-100 in TBS with 1 mM $CaCl_2$ for 5 min on ice, and eluted material was incubated in heated water baths at the indicated temperatures for 30 min. Samples were placed on ice for 10 min followed by centrifugation at 14,000 RPM in a tabletop microcentrifuge for 10 min at 4°C. Supernatants were then precipitated with the conformation independent tapasin anti-serum gp48C or the conformation dependent mAb PaSta1 for 1 hr at 4°C with constant rotation. Immunoprecipitated material was washed with 0.1% Triton X-100 in TBS with 1 mM $CaCl_2$, eluted with 2x reducing or non-reducing sample buffer as indicated, and

resolved by SDS-PAGE. After exposure to phosphor screens, scanned images were analyzed with ImageQuant software.

Insect cell expressed, soluble recombinant free tapasin and the tapasin/ERp57 conjugate were obtained from Pamela Wearsch. 1.5 μg each of free tapasin and the conjugate per lane were diluted into 1 mL TBS with 1 mM $CaCl_2$. Samples were heated, cooled, centrifuged, immunoprecipitated, and washed as above. Heating and immunoprecipitation of recombinant tapasin was performed in the absence of detergent. Samples were eluted in 2x NRSB and separated by SDS-PAGE. Gels were then stained with Coomassie Brilliant Blue (0.025% Coomassie Brilliant Blue R, 40% methanol, 7% glacial acetic acid) overnight. Gels were destained with 40% methanol, 7% acetic acid and scanned using a G-box gel imaging system (Syngene) prior to quantitation. All samples were in the linear range of detection.

7.12: Software and analysis

Analysis of all radio-labeled data was performed using ImageQuant v5.2 for Windows 2000 (Molecular Dynamics/GE Biosciences). All charts were prepared using Graphpad Prizm software v4.0 for Macintosh (Graphpad software). The rates of acquisition of EndoH resistance and conjugate formation were compared using the "Bottom then increase to top" algorithm with post-test comparisons between fitted lines. $P < 0.05$ was considered significant.

References

Anderson, K. S., Alexander, J., Wei, M., and Cresswell, P. (1993). Intracellular transport of class I MHC molecules in antigen processing mutant cell lines. J Immunol *151*, 3407-3419.

Androlewicz, M. J., Anderson, K. S., and Cresswell, P. (1993). Evidence that transporters associated with antigen processing translocate a major histocompatibility complex class I-binding peptide into the endoplasmic reticulum in an ATP-dependent manner. Proc Natl Acad Sci U S A *90*, 9130-9134.

Androlewicz, M. J., and Cresswell, P. (1994). Human transporters associated with antigen processing possess a promiscuous peptide-binding site. Immunity *1*, 7-14.

Antoniou, A. N., and Powis, S. J. (2003). Characterization of the ERp57-Tapasin complex by rapid cellular acidification and thiol modification. Antioxid Redox Signal *5*, 375-379.

Antoniou, A. N., Powis, S. J., and Elliott, T. (2003). Assembly and export of MHC class I peptide ligands. Curr Opin Immunol *15*, 75-81.

Apweiler, R., Hermjakob, H., and Sharon, N. (1999). On the frequency of protein glycosylation, as deduced from analysis of the SWISS-PROT database. Biochim Biophys Acta *1473*, 4-8.

Argon, Y., and Simen, B. B. (1999). GRP94, an ER chaperone with protein and peptide binding properties. Semin Cell Dev Biol *10*, 495-505.

Bangia, N., Lehner, P. J., Hughes, E. A., Surman, M., and Cresswell, P. (1999). The N-terminal region of tapasin is required to stabilize the MHC class I loading complex. Eur J Immunol *29*, 1858-1870.

Barber, L. D., Howarth, M., Bowness, P., and Elliott, T. (2001). The quantity of naturally processed peptides stably bound by HLA-A*0201 is significantly reduced in the absence of tapasin. Tissue Antigens *58*, 363-368.

Barnden, M. J., Purcell, A. W., Gorman, J. J., and McCluskey, J. (2000). Tapasin-mediated retention and optimization of peptide ligands during the assembly of class I molecules. J Immunol *165*, 322-330.

Barnstable, C. J., Bodmer, W. F., Brown, G., Galfre, G., Milstein, C., Williams, A. F., and Ziegler, A. (1978). Production of monoclonal antibodies to group A erythrocytes, HLA and other human cell surface antigens-new tools for genetic analysis. Cell *14*, 9-20.

Barton, G. M., and Medzhitov, R. (2002). Retroviral delivery of small interfering RNA into primary cells. Proc Natl Acad Sci U S A *99*, 14943-14945.

Benham, A. M., Cabibbo, A., Fassio, A., Bulleid, N., Sitia, R., and Braakman, I. (2000). The CXXCXXC motif determines the folding, structure and stability of human Ero1-Lalpha. Embo J *19*, 4493-4502.

Bertolotti, A., Zhang, Y., Hendershot, L. M., Harding, H. P., and Ron, D. (2000). Dynamic interaction of BiP and ER stress transducers in the unfolded-protein response. Nat Cell Biol *2*, 326-332.

Bjorkman, P. J., Saper, M. A., Samraoui, B., Bennett, W. S., Strominger, J. L., and Wiley, D. C. (1987a). Structure of the human class I histocompatibility antigen, HLA-A2. Nature *329*, 506-512.

Bjorkman, P. J., Saper, M. A., Samraoui, B., Bennett, W. S., Strominger, J. L., and Wiley, D. C. (1987b). The foreign antigen binding site and T cell recognition regions of class I histocompatibility antigens. Nature *329*, 512-518.

Brocke, P., Garbi, N., Momburg, F., and Hammerling, G. J. (2002). HLA-DM, HLA-DO and tapasin: functional similarities and differences. Curr Opin Immunol *14*, 22-29.

Burda, P., and Aebi, M. (1999). The dolichol pathway of N-linked glycosylation. Biochim Biophys Acta *1426*, 239-257.

Cabibbo, A., Pagani, M., Fabbri, M., Rocchi, M., Farmery, M. R., Bulleid, N. J., and Sitia, R. (2000). ERO1-L, a human protein that favors disulfide bond formation in the endoplasmic reticulum. J Biol Chem *275*, 4827-4833.

Caramelo, J. J., Castro, O. A., Alonso, L. G., De Prat-Gay, G., and Parodi, A. J. (2003). UDP-Glc:glycoprotein glucosyltransferase recognizes structured and solvent accessible hydrophobic patches in molten globule-like folding intermediates. Proc Natl Acad Sci U S A *100*, 86-91.

Cascio, P., Hilton, C., Kisselev, A. F., Rock, K. L., and Goldberg, A. L. (2001). 26S proteasomes and immunoproteasomes produce mainly N-extended versions of an antigenic peptide. Embo J *20*, 2357-2366.

Chang, S. C., Momburg, F., Bhutani, N., and Goldberg, A. L. (2005). The ER aminopeptidase, ERAP1, trims precursors to lengths of MHC class I peptides by a "molecular ruler" mechanism. Proc Natl Acad Sci U S A *102*, 17107-17112.

Chen, M., Stafford, W. F., Diedrich, G., Khan, A., and Bouvier, M. (2002). A characterization of the lumenal region of human tapasin reveals the presence of two structural domains. Biochemistry *41*, 14539-14545.

Cresswell, P. (2000). Intracellular surveillance: controlling the assembly of MHC class I-peptide complexes. Traffic *1*, 301-305.

Cresswell, P., Arunachalam, B., Bangia, N., Dick, T., Diedrich, G., Hughes, E., and Maric, M. (1999a). Thiol oxidation and reduction in MHC-restricted antigen processing and presentation. Immunol Res *19*, 191-200.

Cresswell, P., Bangia, N., Dick, T., and Diedrich, G. (1999b). The nature of the MHC class I peptide loading complex. Immunol Rev *172*, 21-28.

Cuozzo, J. W., and Kaiser, C. A. (1999). Competition between glutathione and protein thiols for disulphide-bond formation. Nat Cell Biol *1*, 130-135.

D'Urso, C. M., Wang, Z. G., Cao, Y., Tatake, R., Zeff, R. A., and Ferrone, S. (1991). Lack of HLA class I antigen expression by cultured melanoma cells FO-1 due to a defect in B2m gene expression. J Clin Invest *87*, 284-292.

Daniels, R., Kurowski, B., Johnson, A. E., and Hebert, D. N. (2003). N-linked glycans direct the cotranslational folding pathway of influenza hemagglutinin. Mol Cell *11*, 79-90.

Danilczyk, U. G., and Williams, D. B. (2001). The lectin chaperone calnexin utilizes polypeptide-based associate with many of its substrates in vivo. J Biol Chem *276*, 25532-25540.

Darby, N. J., and Creighton, T. E. (1995). Characterization of the active site cysteine residues of the thioredoxin-like domains of protein disulfide isomerase. Biochemistry *34*, 16770-16780.

Darby, N. J., Morin, P. E., Talbo, G., and Creighton, T. E. (1995). Refolding of bovine pancreatic trypsin inhibitor via non-native disulphide intermediates. J Mol Biol *249*, 463-477.

DeMars, R., Chang, C. C., Shaw, S., Reitnauer, P. J., and Sondel, P. M. (1984). Homozygous deletions that simultaneously eliminate expressions of class I and class II

antigens of EBV-transformed B-lymphoblastoid cells. I. Reduced proliferative responses of autologous and allogeneic T cells to mutant cells that have decreased expression of class II antigens. Hum Immunol *11*, 77-97.

Denzin, L. K., Fallas, J. L., Prendes, M., and Yi, W. (2005). Right place, right time, right peptide: DO keeps DM focused. Immunol Rev *207*, 279-292.

Dick, T. B. (2004). Assembly of MHC class I peptide complexes from the perspective of disulfide bond formation. Cell Mol Life Sci *61*, 547-556.

Dick, T. P., Bangia, N., Peaper, D. R., and Cresswell, P. (2002). Disulfide bond isomerization and the assembly of MHC class I-peptide complexes. Immunity *16*, 87-98.

Dick, T. P., and Cresswell, P. (2002). Thiol oxidation and reduction in major histocompatibility complex class I-restricted antigen processing and presentation. Methods Enzymol *348*, 49-54.

Diedrich, G., Bangia, N., Pan, M., and Cresswell, P. (2001). A role for calnexin in the assembly of the MHC class I loading complex in the endoplasmic reticulum. J Immunol *166*, 1703-1709.

DuBridge, R. B., Tang, P., Hsia, H. C., Leong, P. M., Miller, J. H., and Calos, M. P. (1987). Analysis of mutation in human cells by using an Epstein-Barr virus shuttle system. Mol Cell Biol *7*, 379-387.

Edman, J. C., Ellis, L., Blacher, R. W., Roth, R. A., and Rutter, W. J. (1985). Sequence of protein disulphide isomerase and implications of its relationship to thioredoxin. Nature *317*, 267-270.

Ellgaard, L., Bettendorff, P., Braun, D., Herrmann, T., Fiorito, F., Jelesarov, I., Guntert, P., Helenius, A., and Wuthrich, K. (2002). NMR structures of 36 and 73-residue fragments of the calreticulin P-domain. J Mol Biol *322*, 773-784.

Ellgaard, L., and Frickel, E. M. (2003). Calnexin, calreticulin, and ERp57: teammates in glycoprotein folding. Cell Biochem Biophys *39*, 223-247.

Ellgaard, L., Riek, R., Braun, D., Herrmann, T., Helenius, A., and Wuthrich, K. (2001a). Three-dimensional structure topology of the calreticulin P-domain based on NMR assignment. FEBS Lett *488*, 69-73.

Ellgaard, L., Riek, R., Herrmann, T., Guntert, P., Braun, D., Helenius, A., and Wuthrich, K. (2001b). NMR structure of the calreticulin P-domain. Proc Natl Acad Sci U S A *98*, 3133-3138.

Ellgaard, L., and Ruddock, L. W. (2005). The human protein disulphide isomerase family: substrate interactions and functional properties. EMBO Rep *6*, 28-32.

Elliott, J. G., Oliver, J. D., and High, S. (1997). The thiol-dependent reductase ERp57 interacts specifically with N-glycosylated integral membrane proteins. J Biol Chem *272*, 13849-13855.

Exley, M., Garcia, J., Balk, S. P., and Porcelli, S. (1997). Requirements for CD1d recognition by human invariant Valpha24+ CD4-CD8- T cells. J Exp Med *186*, 109-120.

Fehling, H. J., Swat, W., Laplace, C., Kuhn, R., Rajewsky, K., Muller, U., and von Boehmer, H. (1994). MHC class I expression in mice lacking the proteasome subunit LMP-7. Science *265*, 1234-1237.

Ferrari, D. M., and Soling, H. D. (1999). The protein disulphide-isomerase family: unravelling a string of folds. Biochem J *339 (Pt 1)*, 1-10.

Fliegel, L., Burns, K., MacLennan, D. H., Reithmeier, R. A., and Michalak, M. (1989). Molecular cloning of the high affinity calcium-binding protein (calreticulin) of skeletal muscle sarcoplasmic reticulum. J Biol Chem *264*, 21522-21528.

Forster, M. L., Sivick, K., Park, Y. N., Arvan, P., Lencer, W. I., and Tsai, B. (2006). Protein disulfide isomerase-like proteins play opposing roles during retrotranslocation. J Cell Biol *173*, 853-859.

Frand, A. R., and Kaiser, C. A. (1998). The ERO1 gene of yeast is required for oxidation of protein dithiols in the endoplasmic reticulum. Mol Cell *1*, 161-170.

Frand, A. R., and Kaiser, C. A. (1999). Ero1p oxidizes protein disulfide isomerase in a pathway for disulfide bond formation in the endoplasmic reticulum. Mol Cell *4*, 469-477.

Frickel, E. M., Frei, P., Bouvier, M., Stafford, W. F., Helenius, A., Glockshuber, R., and Ellgaard, L. (2004). ERp57 is a multifunctional thiol-disulfide oxidoreductase. J Biol Chem *279*, 18277-18287.

Frickel, E. M., Riek, R., Jelesarov, I., Helenius, A., Wuthrich, K., and Ellgaard, L. (2002). TROSY-NMR reveals interaction between ERp57 and the tip of the calreticulin P-domain. Proc Natl Acad Sci U S A *99*, 1954-1959.

Gao, B., Adhikari, R., Howarth, M., Nakamura, K., Gold, M. C., Hill, A. B., Knee, R., Michalak, M., and Elliott, T. (2002). Assembly and antigen-presenting function of MHC class I molecules in cells lacking the ER chaperone calreticulin. Immunity *16*, 99-109.

Garbi, N., Tanaka, S., Momburg, F., and Hammerling, G. J. (2006). Impaired assembly of the major histocompatibility complex class I peptide-loading complex in mice deficient in the oxidoreductase ERp57. Nat Immunol *7*, 93-102.

Garbi, N., Tiwari, N., Momburg, F., and Hammerling, G. J. (2003). A major role for tapasin as a stabliizer of the TAP peptide transporter and consequences for MHC class I expression. Eur J Immunol *33*, 264-273.

Garboczi, D. N., Ghosh, P., Utz, U., Fan, Q. R., Biddison, W. E., and Wiley, D. C. (1996). Structure of the complex between human T-cell receptor, viral peptide and HLA-A2. Nature *384*, 134-141.

Germain, R. N. (1994). MHC-dependent antigen processing and peptide presentation: providing ligands for T lymphocyte activation. Cell *76*, 287-299.

Gething, M. J. (1999). Role and regulation of the ER chaperone BiP. Semin Cell Dev Biol *10*, 465-472.

Grandea, A. G., 3rd, Golovina, T. N., Hamilton, S. E., Sriram, V., Spies, T., Brutkiewicz, R. R., Harty, J. T., Eisenlohr, L. C., and Van Kaer, L. (2000). Impaired assembly yet normal trafficking of MHC class I molecules in Tapasin mutant mice. Immunity *13*, 213-222.

Greenwood, R., Shimizu, Y., Sekhon, G. S., and DeMars, R. (1994). Novel allele-specific, post-translational reduction in HLA class I expression in a mutant human B cell line. J Immunol *153*, 5525-5536.

Grusby, M. J., and Glimcher, L. H. (1995). Immune responses in MHC class II-deficient mice. Annu Rev Immunol *13*, 417-435.

Hammer, G. E., Gonzalez, F., Champsaur, M., Cado, D., and Shastri, N. (2006). The aminopeptidase ERAAP shapes the peptide repertoire displayed by major histocompatibility complex class I molecules. Nat Immunol *7*, 103-112.

Hammond, C., Braakman, I., and Helenius, A. (1994). Role of N-linked oligosaccharide recognition, glucose trimming, and calnexin in glycoprotein folding and quality control. Proc Natl Acad Sci U S A *91*, 913-917.

Hammond, C., and Helenius, A. (1994). Folding of VSV G protein: sequential interaction with BiP and calnexin. Science *266*, 456-458.

Harris, M. R., Lybarger, L., Yu, Y. Y., Myers, N. B., and Hansen, T. H. (2001). Association of ERp57 with mouse MHC class I molecules is tapasin dependent and mimics that of calreticulin and not calnexin. J Immunol *166*, 6686-6692.

Hebert, D. N., Foellmer, B., and Helenius, A. (1995). Glucose trimming and reglucosylation determine glycoprotein association with calnexin in the endoplasmic reticulum. Cell *81*, 425-433.

Hebert, D. N., Foellmer, B., and Helenius, A. (1996). Calnexin and calreticulin promote folding, delay oligomerization and suppress degradation of influenza hemagglutinin in microsomes. Embo J *15*, 2961-2968.

Helenius, A., and Aebi, M. (2004). Roles of N-linked glycans in the endoplasmic reticulum. Annu Rev Biochem *73*, 1019-1049.

Hirano, N., Shibasaki, F., Sakai, R., Tanaka, T., Nishida, J., Yazaki, Y., Takenawa, T., and Hirai, H. (1995). Molecular cloning of the human glucose-regulated protein ERp57/GRP58, a thiol-dependent reductase. Identification of its secretory form and inducible expression by the oncogenic transformation. Eur J Biochem *234*, 336-342.

Howarth, M., Williams, A., Tolstrup, A. B., and Elliott, T. (2004). Tapasin enhances MHC class I peptide presentation according to peptide half-life. Proc Natl Acad Sci U S A *101*, 11737-11742.

Hubbard, S. C., and Robbins, P. W. (1979). Synthesis and processing of protein-linked oligosaccharides in vivo. J Biol Chem *254*, 4568-4576.

Hughes, E. A., and Cresswell, P. (1998). The thiol oxidoreductase ERp57 is a component of the MHC class I peptide-loading complex. Curr Biol *8*, 709-712.

Hughes, E. A., Hammond, C., and Cresswell, P. (1997). Misfolded major histocompatibility complex class I heavy chains are translocated into the cytoplasm and degraded by the proteasome. Proc Natl Acad Sci U S A *94*, 1896-1901.

Hughes, E. A., Ortmann, B., Surman, M., and Cresswell, P. (1996). The protease inhibitor, N-acetyl-L-leucyl-L-leucyl-leucyl-L-norleucinal, decreases the pool of major histocompatibility complex class I-binding peptides and inhibits peptide trimming in the endoplasmic reticulum. J Exp Med *183*, 1569-1578.

Hwang, C., Sinskey, A. J., and Lodish, H. F. (1992). Oxidized redox state of glutathione in the endoplasmic reticulum. Science *257*, 1496-1502.

Isenman, D. E., Lancet, D., and Pecht, I. (1979). Folding pathways of immunoglobulin domains. The folding kinetics of the Cgamma3 domain of human IgG1. Biochemistry *18*, 3327-3336.

Jackson, M. R., Cohen-Doyle, M. F., Peterson, P. A., and Williams, D. B. (1994). Regulation of MHC class I transport by the molecular chaperone, calnexin (p88, IP90). Science *263*, 384-387.

Jessop, C. E., and Bulleid, N. J. (2004). Glutathione directly reduces an oxidoreductase in the endoplasmic reticulum of mammalian cells. J Biol Chem *279*, 55341-55347.

Kadokura, H., Katzen, F., and Beckwith, J. (2003). Protein disulfide bond formation in prokaryotes. Annu Rev Biochem *72*, 111-135.

Kang, S. J., and Cresswell, P. (2002). Calnexin, calreticulin, and ERp57 cooperate in disulfide bond formation in human CD1d heavy chain. J Biol Chem *277*, 44838-44844.

Keller, S. H., Lindstrom, J., and Taylor, P. (1998). Inhibition of glucose trimming with castanospermine reduces calnexin association and promotes proteasome degradation of the alpha-subunit of the nicotinic acetylcholine receptor. J Biol Chem *273*, 17064-17072.

Klappa, P., Ruddock, L. W., Darby, N. J., and Freedman, R. B. (1998). The b' domain provides the principal peptide-binding site of protein disulfide isomerase but all domains contribute to binding of misfolded proteins. Embo J *17*, 927-935.

Klein, J., and Sato, A. (2000). The HLA system. First of two parts. N Engl J Med *343*, 702-709.

Kleizen, B., and Braakman, I. (2004). Protein folding and quality control in the endoplasmic reticulum. Curr Opin Cell Biol *16*, 343-349.

Kowarik, M., Kung, S., Martoglio, B., and Helenius, A. (2002). Protein folding during cotranslational translocation in the endoplasmic reticulum. Mol Cell *10*, 769-778.

Kozlov, G., Maattanen, P., Schrag, J. D., Pollock, S., Cygler, M., Nagar, B., Thomas, D. Y., and Gehring, K. (2006). Crystal structure of the bb' domains of the protein disulfide isomerase ERp57. Structure *14*, 1331-1339.

Kulig, K., Nandi, D., Bacik, I., Monaco, J. J., and Vukmanovic, S. (1998). Physical and functional association of the major histocompatibility complex class I heavy chain alpha3 domain with the transporter associated with antigen processing. J Exp Med *187*, 865-874.

Kulp, M. S., Frickel, E. M., Ellgaard, L., and Weissman, J. S. (2006). Domain architecture of protein-disulfide isomerase facilitates its dual role as an oxidase and an isomerase in Ero1p-mediated disulfide formation. J Biol Chem *281*, 876-884.

Laboissiere, M. C., Sturley, S. L., and Raines, R. T. (1995). The essential function of protein-disulfide isomerase is to unscramble non-native disulfide bonds. J Biol Chem *270*, 28006-28009.

Labriola, C., Cazzulo, J. J., and Parodi, A. J. (1995). Retention of glucose units added by the UDP-GLC:glycoprotein glucosyltransferase delays exit of glycoproteins from the reticulum. J Cell Biol *130*, 771-779.

Ladasky, J. J., Boyle, S., Seth, M., Li, H., Pentcheva, T., Abe, F., Steinberg, S. J., and Edidin, M. (2006). Bap31 enhances the endoplasmic reticulum export and quality control of human class I MHC molecules. J Immunol *177*, 6172-6181.

Leach, M. R., Cohen-Doyle, M. F., Thomas, D. Y., and Williams, D. B. (2002). Localization of the lectin, ERp57 binding, and polypeptide binding sites of calnexin and calreticulin. J Biol Chem *277*, 29686-29697.

Lehner, P. J., Surman, M. J., and Cresswell, P. (1998). Soluble tapasin restores MHC class I expression and function in the tapasin-negative cell line .220. Immunity *8*, 221-231.

Lewis, J. W., and Elliott, T. (1998). Evidence for successive peptide binding and quality control stages during MHC class I assembly. Curr Biol *8*, 717-720.

Li, S. J., Hong, X. G., Shi, Y. Y., Li, H., and Wang, C. C. (2006). Annular arrangement and collaborative actions of four domains of protein-disulfide isomerase: a small angle X-ray scattering study in solution. J Biol Chem *281*, 6581-6588.

Lindquist, J. A., Jensen, O. N., Mann, M., and Hammerling, G. J. (1998). ER-60, a chaperone with thiol-dependent reductase activity involved in MHC class I assembly. Embo J *17*, 2186-2195.

Lundblad, R. L. (1995). Techniques in Protein Modification (Boca Raton: CRC Press).

Lutz, P. M., and Cresswell, P. (1987). An epitope common to HLA class I and class II antigens, Ig light chains, and beta 2-microglobulin. Immunogenetics *25*, 228-233.

Ma, Y., and Hendershot, L. M. (2004). ER chaperone functions during normal and stress conditions. J Chem Neuroanat *28*, 51-65.

Maio, M., Altomonte, M., Tatake, R., Zeff, R. A., and Ferrone, S. (1991). Reduction in susceptibility to natural killer cell-mediated lysis of human FO-1 melanoma cells after induction of HLA class I antigen expression by transfection with B2m gene. J Clin Invest *88*, 282-289.

Marks, M. S., Blum, J. S., and Cresswell, P. (1990). Invariant chain trimers are sequestered in the rough endoplasmic reticulum in the absence of association with HLA class II antigens. J Cell Biol *111*, 839-855.

Mazzarella, R. A., Marcus, N., Haugejorden, S. M., Balcarek, J. M., Baldassare, J. J., Roy, B., Li, L. J., Lee, A. S., and Green, M. (1994). Erp61 is GRP58, a stress-inducible luminal endoplasmic reticulum protein, but is devoid of phosphatidylinositide-specific phospholipase C activity. Arch Biochem Biophys *308*, 454-460.

Meunier, L., Usherwood, Y. K., Chung, K. T., and Hendershot, L. M. (2002). A subset of chaperones and folding enzymes form multiprotein complexes in endoplasmic reticulum to bind nascent proteins. Mol Biol Cell *13*, 4456-4469.

Meyer, T. H., van Endert, P. M., Uebel, S., Ehring, B., and Tampe, R. (1994). Functional expression and purification of the ABC transporter complex associated with antigen processing (TAP) in insect cells. FEBS Lett *351*, 443-447.

Mezghrani, A., Fassio, A., Benham, A., Simmen, T., Braakman, I., and Sitia, R. (2001). Manipulation of oxidative protein folding and PDI redox state in mammalian cells. Embo J *20*, 6288-6296.

Molinari, M., Calanca, V., Galli, C., Lucca, P., and Paganetti, P. (2003). Role of EDEM in the release of misfolded glycoproteins from the calnexin cycle. Science *299*, 1397-1400.

Molinari, M., Eriksson, K. K., Calanca, V., Galli, C., Cresswell, P., Michalak, M., and Helenius, A. (2004). Contrasting functions of calreticulin and calnexin in glycoprotein folding and ER quality control. Mol Cell *13*, 125-135.

Molinari, M., and Helenius, A. (1999). Glycoproteins form mixed disulphides with oxidoreductases during folding in living cells. Nature *402*, 90-93.

Molinari, M., and Helenius, A. (2000). Chaperone selection during glycoprotein translocation into the reticulum. Science *288*, 331-333.

Molteni, S. N., Fassio, A., Ciriolo, M. R., Filomeni, G., Pasqualetto, E., Fagioli, C., and Sitia, R. (2004). Glutathione limits Ero1-dependent oxidation in the endoplasmic reticulum. J Biol Chem *279*, 32667-32673.

Momburg, F., Roelse, J., Hammerling, G. J., and Neefjes, J. J. (1994). Peptide size selection by the major histocompatibility complex-encoded peptide transporter. J Exp Med *179*, 1613-1623.

Momburg, F., and Tan, P. (2002). Tapasin-the keystone of the loading complex optimizing peptide binding by MHC class I molecules in the endoplasmic reticulum. Mol Immunol *39*, 217-233.

Morrice, N. A., and Powis, S. J. (1998). A role for the thiol-dependent reductase ERp57 in the assembly of MHC class I molecules. Curr Biol *8*, 713-716.

Murthy, M. S., and Pande, S. V. (1994). A stress-regulated protein, GRP58, a member of thioredoxin superfamily, is a carnitine palmitoyltransferase isoenzyme. Biochem J *304 (Pt 1)*, 31-34.

Neefjes, J. J., Momburg, F., and Hammerling, G. J. (1993). Selective and ATP-dependent translocation of peptides by the MHC-encoded transporter. Science *261*, 769-771.

Neijssen, J., Herberts, C., Drijfhout, J. W., Reits, E., Janssen, L., and Neefjes, J. (2005). Cross-presentation by intercellular peptide transfer through gap junctions. Nature *434*, 83-88.

Nossner, E., and Parham, P. (1995). Species-specific differences in chaperone interaction of human and mouse major histocompatibility complex class I molecules. J Exp Med *181*, 327-337.

Oda, Y., Hosokawa, N., Wada, I., and Nagata, K. (2003). EDEM as an acceptor of terminally misfolded glycoproteins released from calnexin. Science *299*, 1394-1397.

Oliver, J. D., Roderick, H. L., Llewellyn, D. H., and High, S. (1999). ERp57 functions as a subunit of specific complexes formed with the ER lectins calreticulin and calnexin. Mol Biol Cell *10*, 2573-2582.

Oliver, J. D., van der Wal, F. J., Bulleid, N. J., and High, S. (1997). Interaction of the thiol-dependent reductase ERp57 with nascent glycoproteins. Science *275*, 86-88.

Ortmann, B., Copeman, J., Lehner, P. J., Sadasivan, B., Herberg, J. A., Grandea, A. G., Riddell, S. R., Tampe, R., Spies, T., Trowsdale, J., and Cresswell, P. (1997). A critical role for tapasin in the assembly and function of multimeric MHC class I-TAP complexes. Science *277*, 1306-1309.

Pagani, M., Fabbri, M., Benedetti, C., Fassio, A., Pilati, S., Bulleid, N. J., Cabibbo, A., and Sitia, R. (2000). Endoplasmic reticulum oxidoreductin 1-lbeta (ERO1-Lbeta), a

human gene induced in the course of the unfolded protein response. J Biol Chem *275*, 23685-23692.

Pamer, E., and Cresswell, P. (1998). Mechanisms of MHC class I--restricted antigen processing. Annu Rev Immunol *16*, 323-358.

Paquet, M. E., Cohen-Doyle, M., Shore, G. C., and Williams, D. B. (2004). Bap29/31 influences the intracellular traffic of MHC class I molecules. J Immunol *172*, 7548-7555.

Parham, P. (2005). Putting a face to MHC restriction. J Immunol *174*, 3-5.

Parham, P., and Brodsky, F. M. (1981). Partial purification and some properties of BB7.2. A cytotoxic monoclonal antibody with specificity for HLA-A2 and a variant of HLA-A28. Hum Immunol *3*, 277-299.

Park, B., Lee, S., Kim, E., and Ahn, K. (2003). A single polymorphic residue within the peptide-binding cleft of MHC class I molecules determines spectrum of tapasin dependence. J Immunol *170*, 961-968.

Park, B., Lee, S., Kim, E., Cho, K., Riddell, S. R., Cho, S., and Ahn, K. (2006). Redox Regulation Facilitates Optimal Peptide Selection by MHC Class I during Antigen Processing. Cell *127*, 369-382.

Peace-Brewer, A. L., Tussey, L. G., Matsui, M., Li, G., Quinn, D. G., and Frelinger, J. A. (1996). A point mutation in HLA-A*0201 results in failure to bind the TAP complex and to present virus-derived peptides to CTL. Immunity *4*, 505-514.

Peaper, D. R., Wearsch, P. A., and Cresswell, P. (2005). Tapasin and ERp57 form a stable disulfide-linked dimer within the MHC class I peptide-loading complex. Embo J *24*, 3613-3623.

Peh, C. A., Burrows, S. R., Barnden, M., Khanna, R., Cresswell, P., Moss, D. J., and McCluskey, J. (1998). HLA-B27-restricted antigen presentation in the absence of tapasin reveals polymorphism in mechanisms of HLA class I peptide loading. Immunity *8*, 531-542.

Pentcheva, T., Spiliotis, E. T., and Edidin, M. (2002). Cutting edge: Tapasin is retained in the endoplasmic reticulum by dynamic clustering and exclusion from endoplasmic reticulum exit sites. J Immunol *168*, 1538-1541.

Pirneskoski, A., Klappa, P., Lobell, M., Williamson, R. A., Byrne, L., Alanen, H. I., Salo, K. E., Kivirikko, K. I., Freedman, R. B., and Ruddock, L. W. (2004). Molecular

characterization of the principal substrate binding site of the ubiquitous folding catalyst protein disulfide isomerase. J Biol Chem *279*, 10374-10381.

Pollard, M. G., Travers, K. J., and Weissman, J. S. (1998). Ero1p: a novel and ubiquitous protein with an essential role in oxidative protein folding in the endoplasmic reticulum. Mol Cell *1*, 171-182.

Pollock, S., Kozlov, G., Pelletier, M. F., Trempe, J. F., Jansen, G., Sitnikov, D., Bergeron, J. J., Gehring, K., Ekiel, I., and Thomas, D. Y. (2004). Specific interaction of ERp57 and calnexin determined by NMR spectroscopy and an ER two-hybrid system. Embo J *23*, 1020-1029.

Purcell, A. W., Gorman, J. J., Garcia-Peydro, M., Paradela, A., Burrows, S. R., Talbo, G. H., Laham, N., Peh, C. A., Reynolds, E. C., Lopez De Castro, J. A., and McCluskey, J. (2001). Quantitative and qualitative influences of tapasin on the class I peptide repertoire. J Immunol *166*, 1016-1027.

Rammensee, H. G. (1995). Chemistry of peptides associated with MHC class I and class II molecules. Curr Opin Immunol *7*, 85-96.

Reits, E. A., Vos, J. C., Gromme, M., and Neefjes, J. (2000). The major substrates for TAP in vivo are derived from newly synthesized proteins. Nature *404*, 774-778.

Rizvi, S. M., Mancino, L., Thammavongsa, V., Cantley, R. L., and Raghavan, M. (2004). A polypeptide binding conformation of calreticulin is induced by heat shock, calcium depletion, or by deletion of the C-terminal acidic region. Mol Cell *15*, 913-923.

Rudd, P. M., Elliott, T., Cresswell, P., Wilson, I. A., and Dwek, R. A. (2001). Glycosylation and the immune system. Science *291*, 2370-2376.

Russell, S. J., Ruddock, L. W., Salo, K. E., Oliver, J. D., Roebuck, Q. P., Llewellyn, D. H., Roderick, H. L., Koivunen, P., Myllyharju, J., and High, S. (2004). The primary substrate binding site in the b' domain of ERp57 is adapted for endoplasmic reticulum lectin association. J Biol Chem *279*, 18861-18869.

Sadasivan, B., Lehner, P. J., Ortmann, B., Spies, T., and Cresswell, P. (1996). Roles for calreticulin and a novel glycoprotein, tapasin, in the interaction of MHC class I molecules with TAP. Immunity *5*, 103-114.

Sadasivan, B. K., Cariappa, A., Waneck, G. L., and Cresswell, P. (1995). Assembly, peptide loading, and transport of MHC class I molecules in a calnexin-negative cell line. Cold Spring Harb Symp Quant Biol *60*, 267-275.

Salter, R. D., and Cresswell, P. (1986). Impaired assembly and transport of HLA-A and -B antigens in a mutant TxB cell hybrid. Embo J *5*, 943-949.

Saric, T., Chang, S. C., Hattori, A., York, I. A., Markant, S., Rock, K. L., Tsujimoto, M., and Goldberg, A. L. (2002). An IFN-gamma-induced aminopeptidase in the ER, ERAP1, trims precursors to MHC class I-presented peptides. Nat Immunol *3*, 1169-1176.

Schrag, J. D., Bergeron, J. J., Li, Y., Borisova, S., Hahn, M., Thomas, D. Y., and Cygler, M. (2001). The Structure of calnexin, an ER chaperone involved in quality control of protein folding. Mol Cell *8*, 633-644.

Schroder, M., and Kaufman, R. J. (2005). The mammalian unfolded protein response. Annu Rev Biochem *74*, 739-789.

Sege, K., Rask, L., and Peterson, P. A. (1981). Role of beta2-microglobulin in the intracellular processing of HLA antigens. Biochemistry *20*, 4523-4530.

Serwold, T., Gonzalez, F., Kim, J., Jacob, R., and Shastri, N. (2002). ERAAP customizes peptides for MHC class I molecules in the endoplasmic reticulum. Nature *419*, 480-483.

Sevier, C. S., and Kaiser, C. A. (2002). Formation and transfer of disulphide bonds in living cells. Nat Rev Mol Cell Biol *3*, 836-847.

Shimizu, Y., Geraghty, D. E., Koller, B. H., Orr, H. T., and DeMars, R. (1988). Transfer and expression of three cloned human non-HLA-A,B,C class I major histocompatibility complex genes in mutant lymphoblastoid cells. Proc Natl Acad Sci U S A *85*, 227-231.

Silvennoinen, L., Myllyharju, J., Ruoppolo, M., Orru, S., Caterino, M., Kivirikko, K. I., and Koivunen, P. (2004). Identification and characterization of structural domains of human ERp57: association with calreticulin requires several domains. J Biol Chem *279*, 13607-13615.

Solda, T., Garbi, N., Hammerling, G. J., and Molinari, M. (2006). Consequences of ERp57 deletion on oxidative folding of obligate and facultative clients of the calnexin cycle. J Biol Chem *281*, 6219-6226.

Sousa, M., and Parodi, A. J. (1995). The molecular basis for the recognition of misfolded glycoproteins by the UDP-Glc:glycoprotein glucosyltransferase. Embo J *14*, 4196-4203.

Spies, T., Cerundolo, V., Colonna, M., Cresswell, P., Townsend, A., and DeMars, R. (1992). Presentation of viral antigen by MHC class I molecules is dependent on a putative peptide transporter heterodimer. Nature *355*, 644-646.

Spies, T., and DeMars, R. (1991). Restored expression of major histocompatibility class I molecules by gene transfer of a putative peptide transporter. Nature *351*, 323-324.

Spiliotis, E. T., Manley, H., Osorio, M., Zuniga, M. C., and Edidin, M. (2000). Selective export of MHC class I molecules from the ER after their dissociation from TAP. Immunity *13*, 841-851.

Stam, N. J., Vroom, T. M., Peters, P. J., Pastoors, E. B., and Ploegh, H. L. (1990). HLA-A- and HLA-B-specific monoclonal antibodies reactive with free heavy chains in western blots, in formalin-fixed, paraffin-embedded tissue sections and in cryo-immuno-electron microscopy. Int Immunol *2*, 113-125.

Strehl, B., Seifert, U., Kruger, E., Heink, S., Kuckelkorn, U., and Kloetzel, P. M. (2005). Interferon-gamma, the functional plasticity of the ubiquitin-proteasome system, and MHC class I antigen processing. Immunol Rev *207*, 19-30.

Suh, W. K., Derby, M. A., Cohen-Doyle, M. F., Schoenhals, G. J., Fruh, K., Berzofsky, J. A., and Williams, D. B. (1999). Interaction of murine MHC class I molecules with tapasin and TAP enhances peptide loading and involves the heavy chain alpha3 domain. J Immunol *162*, 1530-1540.

Suh, W. K., Mitchell, E. K., Yang, Y., Peterson, P. A., Waneck, G. L., and Williams, D. B. (1996). MHC class I molecules form ternary complexes with calnexin and TAP and undergo peptide-regulated interaction with TAP via their extracellular domains. J Exp Med *184*, 337-348.

Tan, P., Kropshofer, H., Mandelboim, O., Bulbuc, N., Hammerling, G. J., and Momburg, F. (2002). Recruitment of MHC class I molecules by tapasin into the transporter associated with antigen processing-associated complex is essential for optimal peptide loading. J Immunol *168*, 1950-1960.

Tector, M., Zhang, Q., and Salter, R. D. (1997). Beta 2-microglobulin and calnexin can independently promote disulfide bond formation in class I histocompatibility proteins. Mol Immunol *34*, 401-408.

Tian, G., Xiang, S., Noiva, R., Lennarz, W. J., and Schindelin, H. (2006). The crystal structure of yeast protein disulfide isomerase suggests cooperativity between its active sites. Cell *124*, 61-73.

Tiwari, R. K., Kusari, J., and Sen, G. C. (1987). Functional equivalents of interferon-mediated signals needed for induction of an mRNA can be generated by double-stranded RNA and growth factors. EMBO J *6*, 3373-3378.

Tjoelker, L. W., Seyfried, C. E., Eddy, R. L., Jr., Byers, M. G., Shows, T. B., Calderon, J., Schreiber, R. B., and Gray, P. W. (1994). Human, mouse, and rat calnexin cDNA cloning: identification of potential calcium binding motifs and gene localization to human chromosome 5. Biochemistry *33*, 3229-3236.

Turnquist, H. R., Petersen, J. L., Vargas, S. E., McIlhaney, M. M., Bedows, E., Mayer, W. E., Grandea, A. G., 3rd, Van Kaer, L., and Solheim, J. C. (2004). The Ig-like domain of tapasin influences intermolecular interactions. J Immunol *172*, 2976-2984.

Turnquist, H. R., Vargas, S. E., McIlhaney, M. M., Li, S., Wang, P., and Solheim, J. C. (2002). Calreticulin binds to the alpha1 domain of MHC class I independently of tapasin. Tissue Antigens *59*, 18-24.

Turnquist, H. R., Vargas, S. E., Reber, A. J., McIlhaney, M. M., Li, S., Wang, P., Sanderson, S. D., Gubler, B., van Endert, P., and Solheim, J. C. (2001). A region of tapasin that affects L(d) binding and assembly. J Immunol *167*, 4443-4449.

Van der Wal, F. J., Oliver, J. D., and High, S. (1998). The transient association of ERp57 with N-glycosylated proteins is regulated by glucose trimming. Eur J Biochem *256*, 51-59.

Van Kaer, L., Ashton-Rickardt, P. G., Eichelberger, M., Gaczynska, M., Nagashima, K., Rock, K. L., Goldberg, A. L., Doherty, P. C., and Tonegawa, S. (1994). Altered peptidase and viral-specific T cell response in LMP2 mutant mice. Immunity *1*, 533-541.

Van Kaer, L., Ashton-Rickardt, P. G., Ploegh, H. L., and Tonegawa, S. (1992). TAP1 mutant mice are deficient in antigen presentation, surface class I molecules, and CD4-8+ T cells. Cell *71*, 1205-1214.

van Leeuwen, J. E., and Kearse, K. P. (1996). Deglucosylation of N-linked glycans is an important step in the dissociation of calreticulin-class I-TAP complexes. Proc Natl Acad Sci U S A *93*, 13997-14001.

Van Leeuwen, J. E., and Kearse, K. P. (1997). Reglucosylation of N-linked glycans is critical for calnexin assembly with T cell receptor (TCR) alpha proteins but not TCRbeta proteins. J Biol Chem *272*, 4179-4186.

Vassilakos, A., Cohen-Doyle, M. F., Peterson, P. A., Jackson, M. R., and Williams, D. B. (1996). The molecular chaperone calnexin facilitates folding and assembly of class I histocompatibility molecules. Embo J *15*, 1495-1506.

Walker, K. W., and Gilbert, H. F. (1997). Scanning and escape during protein-disulfide isomerase-assisted folding. J Biol Chem *272*, 8845-8848.

Walker, K. W., Lyles, M. M., and Gilbert, H. F. (1996). Catalysis of oxidative protein folding by mutants of protein disulfide isomerase with a single active-site cysteine. Biochemistry *35*, 1972-1980.

Wang, N., Daniels, R., and Hebert, D. N. (2005). The cotranslational maturation of the type I membrane glycoprotein tyrosinase: the heat shock protein 70 system hands off to the lectin-based chaperone system. Mol Biol Cell *16*, 3740-3752.

Warburton, R. J., Matsui, M., Rowland-Jones, S. L., Gammon, M. C., Katzenstein, G. E., Wei, T., Edidin, M., Zweerink, H. J., McMichael, A. J., and Frelinger, J. A. (1994). Mutation of the alpha 2 domain disulfide bridge of the class I molecule HLA-A*0201. Effect on maturation and peptide presentation. Hum Immunol *39*, 261-271.

Ware, F. E., Vassilakos, A., Peterson, P. A., Jackson, M. R., Lehrman, M. A., and Williams, D. B. (1995). The molecular chaperone calnexin binds Glc1Man9GlcNAc2 oligosaccharide as an initial step in recognizing unfolded glycoproteins. J Biol Chem *270*, 4697-4704.

Watts, C. (2004). The exogenous pathway for antigen presentation on major histocompatibility complex class II and CD1 molecules. Nat Immunol *5*, 685-692.

Wearsch, P. A., Jakob, C. A., Vallin, A., Dwek, R. A., Rudd, P. M., and Cresswell, P. (2004). Major histocompatibility complex class I molecules expressed with monoglucosylated N-linked glycans bind calreticulin independently of their assembly status. J Biol Chem *279*, 25112-25121. Epub 22004 Mar 25131.

Wei, M. L., and Cresswell, P. (1992). HLA-A2 molecules in an antigen-processing mutant cell contain signal sequence-derived peptides. Nature *356*, 443-446.

Weissman, J. S., and Kim, P. S. (1993). Efficient catalysis of disulphide bond rearrangements by protein disulphide isomerase. Nature *365*, 185-188.

Wilkinson, B., and Gilbert, H. F. (2004). Protein disulfide isomerase. Biochim Biophys Acta *1699*, 35-44.

Williams, A. P., Peh, C. A., Purcell, A. W., McCluskey, J., and Elliott, T. (2002). Optimization of the MHC class I peptide cargo is dependent on tapasin. Immunity *16*, 509-520.

Williams, D. B., Barber, B. H., Flavell, R. A., and Allen, H. (1989). Role of beta 2-microglobulin in the intracellular transport and surface expression of murine class I histocompatibility molecules. J Immunol *142*, 2796-2806.

Wilson, C. M., Farmery, M. R., and Bulleid, N. J. (2000). Pivotal role of calnexin and mannose trimming in regulating the endoplasmic reticulum-associated degradation of major histocompatibility complex class I heavy chain. J Biol Chem *275*, 21224-21232.

Wright, C. A., Kozik, P., Zacharias, M., and Springer, S. (2004). Tapasin and other chaperones: models of the MHC class I loading complex. Biol Chem *385*, 763-778.

Yan, J., Parekh, V. V., Mendez-Fernandez, Y., Olivares-Villagomez, D., Dragovic, S., Hill, T., Roopenian, D. C., Joyce, S., and Van Kaer, L. (2006). In vivo role of ER-associated peptidase activity in tailoring peptides for presentation by MHC class Ia and class Ib molecules. J Exp Med *203*, 647-659.

Yang, S. Y., Morishima, Y., Collins, N. H., Alton, T., Pollack, M. S., Yunis, E. J., and Dupont, B. (1984). Comparison of one-dimensional IEF patterns for serologically detectable HLA-A and B allotypes. Immunogenetics *19*, 217-231.

Yewdell, J. W., and Nicchitta, C. V. (2006). The DRiP hypothesis decennial: support, controversy, refinement and extension. Trends Immunol *27*, 368-373.

York, I. A., Chang, S. C., Saric, T., Keys, J. A., Favreau, J. M., Goldberg, A. L., and Rock, K. L. (2002). The ER aminopeptidase ERAP1 enhances or limits antigen presentation by trimming epitopes to 8-9 residues. Nat Immunol *3*, 1177-1184.

Zapun, A., Darby, N. J., Tessier, D. C., Michalak, M., Bergeron, J. J., and Thomas, D. Y. (1998). Enhanced catalysis of ribonuclease B folding by the interaction of calnexin or calreticulin with ERp57. J Biol Chem *273*, 6009-6012.

Zarling, A. L., Luckey, C. J., Marto, J. A., White, F. M., Brame, C. J., Evans, A. M., Lehner, P. J., Cresswell, P., Shabanowitz, J., Hunt, D. F., and Engelhard, V. H. (2003). Tapasin is a facilitator, not an editor, of class I MHC peptide binding. J Immunol *171*, 5287-5295.

Zijlstra, M., Bix, M., Simister, N. E., Loring, J. M., Raulet, D. H., and Jaenisch, R. (1990). Beta 2-microglobulin deficient mice lack CD4-8+ cytolytic T cells. Nature *344*, 742-746.

Appendix I: Table of Abbreviations

ABC	ATPase binding cassette	Ig	Immunoglobulin
AP	Alkaline Phosphatase	IMDM	Iscove's Modified Dulbecco's Medium
APC	Allophycocyanin	mAb	Monoclonal Antibody
ATP	Adenosine Triphosphate	MEF	Mouse Embryonic Fibroblast
β_2m	β-2-microglobulin	MHC	Major Histocompatibility Complex
BCS	Bovine Calf Serum	min	Minutes
Blotto	PBS-T with 5% skim milk powder	MMTS	methyl methanethiosulfonate
β-ME	β-Mercaptoethanol	NB-DMJ	N-Butyldeoxynojirimycin
CIP	Calf Intestinal Phosphatase	NEM	N-ethylmaleimide
CNX	Calnexin	NRS	Normal Rabbit Serum
CRT	Calreticulin	NRSB	Non-reducing sample buffer
CST	Castanospermine	OST	Oligosaccharide transferase
DTT	Dithiothreitol	PBS	Phosphate Buffered Saline
ECF	Enhanced Chemifluorescent	PBS-T	Phosphate Buffered Saline with 0.2% Tween-20
ECL	Enhanced Chemiluminescent	PDI	Protein Disulfide Isomerase
EGFP	Enhanced Green Fluorescent Protein	PLC	Peptide Loading Complex
EndoH	Endoglycosidase H	PMSF	Phenyl-methylsulfonyl fluoride
ER	Endoplasmic Reticulum	PVDF	Polyvinylidene Fluoride
ERAP/ ERAAP	ER Aminopeptidase	RNAi	RNA-interference
Ero1 (hEro)	ER oxidoreductin	RT	Room Temperature
FACS	Fluorescence Assisted Cell Sorting	SDS	Sodium dodecyl sulfate
FITC	Fluoroscein Isothiocyanate	SDS-PAGE	Sodium dodecyl sulfate polyacrylamide gel electrophoresis
HA	Hemagglutinin	SEM	Standard Error of the Mean
HC	Heavy Chain	TAP	Transporter associated with antigen processing
HLA	Human Leukocyte Antigen	TBS	Tris Buffered Saline
hr(s)	Hour(s)	Tpsn	Tapasin
HRP	Horseradish Peroxidase	Trx	Thioredoxin
Hsp	Heat Shock Protein	UGGT	UDP-Glc:glycoprotein glucosyltransferase
IAA	Iodoacetamide	UTR	Untranslated region
IFN-γ	Interferon-gamma	WT	Wild-type

Appendix II: Table of Cell Lines

Cell Line	Parent cell Phenotype	Transfected	Ref
293T			(DuBridge et al., 1987)
K41 K42	WT MEF CRT -/- MEF		(Gao et al., 2002)
HeLa-M			(Tiwari et al., 1987)
CEM.NKR.A2 CEM.NKR.A2.CNX	Calnexin Negative	HLA-A*0201 HLA-A*0201, Calnexin	(Sadasivan et al., 1995)
FO-1 FO-1.β_2m	β_2m negative melanoma	 β_2m	(Maio et al., 1991)
C1R.A2.WT C1R.A2.C60A	MHC class I reduced	HLA-A*0201, WT-FLAG ERp57 HLA-A*0201, C60A-FLAG ERp57	(Dick et al., 2002)
721.221 721.174 721.45.1	MHC class I negative TAP negative Normal		(Shimizu et al., 1988) (DeMars et al., 1984)
721.220.B8.WT-Tpsn	MHC class I low, Tapasin negative	HLA-B*0801 and WT Tapasin	(Ortmann et al., 1997)
721.220.B44 B44.WT-Tpsn B44.C95A-Tpsn B44.N233A-Tpsn WT-Tpsn.RVH1-Ctrl WT-Tpsn.RVH1-ERp57 RVH1-ERp57.WT-FLAG-ERp57	MHC class I low, Tapasin negative	HLA-B*4402 HLA-B*4402, WT Tapasin HLA-B*4402, C95A Tapasin HLA-B*4402, N233A Tapasin HLA-B*4402, WT Tapasin, Ctrl shRNA HLA-B*4402, WT Tapasin, ERp57 specific shRNA HLA-B*4402, WT Tapasin, ERp57 specific shRNA, WT-FLAG ERp57	(Peh et al., 1998) (Dick et al., 2002) This Study This Study This Study

RVH1-ERp57.C60A-FLAG-ERp57		HLA-B*4402, WT Tapasin, ERp57 specific shRNA, C60A-FLAG ERp57	This Study
RVH1-ERp57.C60/406/409A-FLAG-ERp57		HLA-B*4402, WT Tapasin, ERp57 specific shRNA, C60/406/409A-FLAG ERp57	This Study

Appendix III: Table of Antibodies

Antibody/ Antiserum	Antigen	Notes	WB Dilution	Reference/Source
148.3	TAP1 C-terminal peptide		1:1000	(Meyer et al., 1994)
3B10.7	MHC class I HC	Free MHC class I HC	1:10,000	(Lutz and Cresswell, 1987)
4E	HLA-B and -C with β_2m	Conformation dependent epitope	N/A	(Yang et al., 1984)
51.1.3	CD1d/ β_2m complexes	Conformation dependent epitope	N/A	(Exley et al., 1997)
BB7.2	HLA-A*0201 with β_2m	Conformation dependent epitope	N/A	(Parham and Brodsky, 1981)
CD4		APC-coupled	N/A	eBioscience, L3T4
HC10		Free HLA-B, C HC only	1:1000	(Stam et al., 1990)
M.ERp72	ERp72	Denaturing only	1:100	BD Transduction Labs, 610970
M.GAPDH	GAPDH		1:20,000	RDI, 6C5
M.HLA-ABC-APC	MHC class I/ β_2m complexes	Directly coupled		BD Biosciences, G46-2.6
M.PDI	PDI		1:1000	ABR, MA3-018
M.Tpsn-C	Tapasin C-terminal peptide		1:100	This study
M2	FLAG-epitope tag		1:1000	Sigma, M2
MaP.ERp57	FL ERp57		1:1000	(Diedrich et al., 2001)
PaSta1	Soluble Tpsn	Conformation dependent epitope	N/A	(Dick et al., 2002)
R.DRAB	HLA-DR		N/A	(Marks et al., 1990)
R.ERp57-C	ERp57 C-terminal peptide		1:500	(Hughes and Cresswell, 1998)
R.ERp57-FL	Full Length ERp57		1:1000	(Diedrich et al., 2001)
R.gp48C	Tapasin C-terminal peptide		1:1000	(Bangia et al., 1999)
R.gp48N	Tapasin N-terminal peptide	Very redox sensitive	1:1000	(Lehner et al., 1998)
R.SinA	Soluble Tpsn		1:1000	(Ortmann et al., 1997)

R.SinE	Soluble Tpsn	Denaturing only	1:10,000	This study
Rb.CRT	Calreticulin		1:1000	ABR, PA3-900
Rb.ERp72			1:1000	Stressgen, SPA-720
Rb.PDI	Full Length PDI		1:1000	Stressgen, SPA-890
RING.4C	TAP1 C-terminal peptide		1:7,500	(Meyer et al., 1994)
Rt.Grp94	Grp94		1:40,000	Stressgen, SPA-850
W6/32	MHC class I/β_2m complexes	Conformation dependent epitope	N/A	(Barnstable et al., 1978)